



universität  
wien

# DIPLOMARBEIT

Titel der Diplomarbeit

Temperature dependence of the contact angle for 1-propanol on silver and  
on sodium chloride substrate

angestrebter akademischer Grad

Magister/Magistra der Naturwissenschaften (Mag. rer.nat)

Verfasserin / Verfasser:	Tamara Pinterich
Matrikel-Nummer:	0400152
Studienrichtung (lt. Studien- blatt):	A 411 Physik
Betreuerin / Betreuer:	Ao. Univ. Prof. Dr.h.c. Dr. Paul E. Wagner

Wien, am 25. Mai 2009

*Ich möchte mich herzlichst bei meinem Betreuer Prof. Paul Wagner für seine fachliche Unterstützung bedanken. Ebenso gilt mein Dank Dr. Paul Winkler, der mir bei den Experimenten jederzeit hilfreich zur Seite stand. Weiters bedanke ich mich bei Martina Rohrer, Mag. Michael Hindler, Mag. Christian Zafu und Josef Karoly für ihre Hilfe bei Probenpräparationen. Vor allem aber möchte ich meinen Eltern, Jeong-Suk und Hans Pinterich, danken, die mir mein Studium nicht nur ermöglicht sondern mich dabei auch in jeder Hinsicht stets unterstützt haben.*

### Abstract

The aim of the present thesis was to investigate the contact angle for 1-propanol on silver and on sodium chloride substrate as a function of temperature.

The interest in a potential temperature dependence of this special contact angles originates from the thesis of S. Schobesberger [33]. In the course of his study he measured the temperature dependence for heterogeneous nucleation of n-propanol vapour on NaCl-particles and on silver-particles. A strange temperature dependence for the nucleation process of n-propanol vapour on NaCl was found. This unexpected behavior could be explained by a certain temperature dependence of the contact angle.

In the present thesis contact angles and their temperature dependence are measured by independent methods.

Contact angle measurements in a temperature range from  $-7^{\circ}\text{C}$  to  $35^{\circ}\text{C}$  were performed using a modified Krüss K12 Tensiometer, featuring a refrigerated double-walled glass top. This allows a precise setting of the temperature of the probe, the surface of the observed liquid and thus the temperature both of the surrounding air and of the liquid is well defined. Within the above stated temperature range the *Dynamic Wilhelmy method* was applied to determine both the advancing as well as the receding angle whereas solely the advancing angle is of interest with respect to the influence on heterogeneous nucleation.

### Contact Angle between 1-propanol and silver as a function of temperature

Since contact angle measurements using the *Dynamic Wilhelmy method* require a uniform geometry of the analysed silver probes, multiple cutting and polishing stages were performed up to the accomplishment of a  $0.04\ \mu\text{m}$  grain size. The original probes were made out of a 925 sterling silver plate. Afterwards influences on measurements related to the 7.5% residual copper-content were additionally avoided by making use of 99.9% silver-powder evaporation process via Physical Vapour Deposition (PVD).

Results show that the influence of the above mentioned contamination by copper can not be neglected for a specification of contact angles. It turned out that the additional coating with silver p.A. not only changes the value of  $\theta_a$  but also its temperature dependence. The advancing angle between 1-propanol and the uncoated sterling silver plate turned out to be strong temperature dependent. Within the observed temperature range it increases from  $11.4^{\circ} \pm 0.5$  at  $T = -6.2 \pm 0.1^{\circ}\text{C}$  to  $31^{\circ} \pm 1$  at  $T = 24.7 \pm 0.1^{\circ}\text{C}$ . Results obtained with one time coated silver plates show a temperature dependence too, but not nearly as strongly as for the uncoated plate. Starting from  $22^{\circ} \pm 3$  at  $-6.2 \pm 0.1^{\circ}\text{C}$  the advancing angle rises up to  $25^{\circ} \pm 1$  at  $24.7 \pm 0.1^{\circ}\text{C}$ . This behavior of decreasing slope continues when coating the probe twice. In this case the contact angle only increased from  $17.1^{\circ} \pm 1$  at  $-6.2^{\circ}\text{C} \pm 0.1$  to  $18.0^{\circ} \pm 0.4$  at  $24.7 \pm 0.1^{\circ}\text{C}$ .

Since the above stated contact angles are advancing angles, the observed behavior can be referred to a decreasing copper content in the solid surface with increasing number of silver p.A. coats. Changes due to increasing surface roughness at plates with increasing number of coats can be excluded, because this would cause not only a decrease in  $\theta_a$  but also an increase in  $\theta_r$ . This latter behavior, however, has not been observed.

### Contact Angle between 1-propanol and sodium chloride as a function of temperature

Just as for the 1-propanol - silver measurements the *Dynamic Wilhelmy method* was used to determine the contact angle between sodium chloride and 1-propanol too. In addition to this measurement method the *Washburn method* was applied at a temperature of  $\approx 20^{\circ}\text{C}$ . This sorption method allows contact angle measurements between liquids and powder-form solids. Based on the experimental determination of the capillary climbing speed of the liquid the contact angle is calculated assuming the observed powder to be a bundle of capillaries. Thus the so determined contact angles are advancing angles and can therefore be compared with the  $\theta_a$  values obtained with the *Dynamic Wilhelmy method*.

Probes for the *Dynamic Wilhelmy method* were on the one hand made out of a sodium chloride crystal and on the other hand produced by coating glass plates with *NaCl* powder via PVD. All contact angle measurements within the observed temperature range ( $-7^{\circ}\text{C}; 35^{\circ}\text{C}$ ) resulted in an advancing angle of  $0^{\circ}$ . Comparative measurements with the *Washburn method* at  $T \approx 20^{\circ}\text{C}$  conform to this results. Thus it can be stated, that 1-propanol perfectly wets sodium chloride.

However contrary to expectations the receding angles obtained with the *Wilhelmy method* al-

most always exceeded the advancing angles, what might be referred to surface roughness and therewith associated adsorption of the liquid under study at the surface of the plates. Solely measurements using an untreated salt plate conform to the expected behavior that  $\theta_r$  amounts to  $0^\circ$  in agreement with  $\theta_a$ . Although both  $\cos\theta_a$  as well as  $\cos\theta_r$  data for the untreated salt plates always exceeded 1 what led to the just stated contact angles of  $0^\circ$  the  $\cos\theta$  values, which are proportional to the recorded force acting on the plates, were found to be bigger by withdrawing it from than by immersing the plate into the probational liquid.

In summary, it can be stated that the contact angle for 1-propanol on silver has a weak temperature dependence, if any. According to statistical errors of the single measurements it can not be excluded that the advancing angle for 1-propanol on silver remains  $17^\circ \pm 1^\circ$  within the observe temperature range. Further measurements with more often coated plates might indicate whether an influence of the copper content below the surface can already be excluded when the sterling silver is coated twice with silver p.A. or if additional coatings lead to a further decrease in contact angle.

The contact angle for 1-propanol on sodium chloride remains  $0^\circ$  from  $T \approx -7^\circ C$  to  $\approx 34^\circ C$  as it has been verified with two different methods. Thus a temperature dependence could not be determined.

Consequently the strange temperature dependence for the nucleation process of n-propanol vapour on NaCl can not be explained by a temperature dependent macroscopic contact.

# Contents

<b>Abstract</b>	<b>II</b>
<b>1 Theory of Surface Phenomena</b>	<b>1</b>
1.1 Surface Tension . . . . .	1
1.1.1 Introduction . . . . .	1
1.1.2 Thermodynamics of Surfaces . . . . .	3
1.1.3 Mechanics of Surfaces . . . . .	6
1.1.4 Effect of Curvature due to Surface Tension on Vapor Pressure . . . . .	9
1.1.5 Temperature Dependence of Surface Tension . . . . .	9
1.1.6 Forces between Atoms and Molecules . . . . .	10
1.2 Contact Angle . . . . .	12
1.2.1 Equation of Young . . . . .	12
1.2.2 Wetting as a Contact Angle Phenomenon . . . . .	13
1.2.3 Wetting as a Capillary Action Phenomenon . . . . .	14
1.3 Contact Angle Hysteresis . . . . .	16
1.3.1 Rough but Chemical Homogeneous Surface . . . . .	16
1.3.2 Smooth but Chemical Heterogeneous Surface . . . . .	18
1.4 Influence of Surface Properties on Nucleation Processes . . . . .	20
1.4.1 Classical Nucleation Theory - Homogeneous Nucleation . . . . .	20
1.4.2 Fletcher Theory - Heterogeneous Nucleation . . . . .	24
<b>2 Measurement Methods</b>	<b>27</b>
2.1 Determination of Surface Tension . . . . .	27
2.1.1 Introduction . . . . .	27
2.1.2 Wilhelmy Slide Method . . . . .	28
2.2 Determination of Contact Angle . . . . .	30
2.2.1 Sessile Drop Method . . . . .	30
2.2.2 Dynamic Wilhelmy Method . . . . .	31
2.2.3 Washburn Method . . . . .	34
<b>3 Experimental Setup</b>	<b>36</b>
3.1 Measurement procedure at temperatures $T_M$ different from room temperature $T_R \approx 26^\circ C$ . . . . .	37
<b>4 Preparation of the Probes</b>	<b>39</b>
4.1 Characterization of the Used Liquids . . . . .	39
4.1.1 Studied liquids . . . . .	39
4.1.2 Cleaning liquids . . . . .	39
4.2 Characterization of the Used Solids . . . . .	39
4.2.1 Silver plates . . . . .	39
4.2.2 Salt plates . . . . .	39
4.3 Preparation of the Silver Plates . . . . .	40
4.4 Preparation of the Salt Plates . . . . .	43
4.4.1 Polished salt crystals . . . . .	43
4.4.2 Untreated salt crystals . . . . .	44
4.4.3 Coated glass plates . . . . .	44

4.5	Cleansing of the Samples During Measurements . . . . .	45
<b>5</b>	<b>Temperature dependence of the contact angle for 1-propanol on silver</b>	<b>46</b>
5.1	Surface Tension during measurements (see appendix A.1) . . . . .	46
5.2	Not coated plates(0xPVD) (see appendix A.2) . . . . .	50
5.2.1	Contact Angles obtained with variously prepared but not coated 925 silver plates . . . . .	50
5.3	One time coated plates (1xPVD) (see appendix A.3) . . . . .	54
5.3.1	Temperature dependence of the contact angle for 1-propanol on one-time coated 925 silver . . . . .	54
5.4	Two times coated plates(2xPVD) (see appendix A.4) . . . . .	56
5.4.1	Temperature dependence of the contact angle for 1-propanol on two-times coated 925 silver . . . . .	56
5.5	Variously often coated silver plates by comparison . . . . .	57
<b>6</b>	<b>Temperature dependence of the contact angle for 1-propanol on NaCl</b>	<b>60</b>
6.1	Surface Tension during measurements (see appendix B.1) . . . . .	60
6.2	Dynamic Wilhelmy Method . . . . .	62
6.2.1	Uncoated glass plate (see appendix B.2.1) . . . . .	62
6.2.2	One-time coated glass plates (see appendix B.2.1) . . . . .	65
6.2.3	Two-times coated glass plates (see appendix B.2.1) . . . . .	68
6.2.4	Three-times coated glass plates (see appendix B.2.1) . . . . .	70
6.2.5	Polished Salt Crystals (see appendix B.2.2) . . . . .	73
6.2.6	Untreated salt plate (see appendix B.2.3) . . . . .	76
6.2.7	Variously prepared plates by comparison . . . . .	78
6.3	Washburn Method (see appendix B.3) . . . . .	83
6.3.1	Determination of the material constant $c$ . . . . .	83
6.3.2	Contact angle for 1-propanol on sodium chloride . . . . .	84
6.4	Errors of the measurement data . . . . .	87
<b>7</b>	<b>Conclusions</b>	<b>88</b>
	<b>Bibliography</b>	<b>90</b>

<b>List of Figures</b>	<b>93</b>
<b>Appendix</b>	<b>96</b>
<b>A Data for silver/1-propanol contact angle measurements</b>	<b>96</b>
A.1 Surface Tension during measurements . . . . .	96
A.2 Uncoated 925 sterling silver - 0xPVD . . . . .	97
A.3 One-time coated sterling silver - 1xPVD . . . . .	98
A.4 Two-times coated sterling silver - 2xPVD . . . . .	111
<b>B Data for NaCl/1-propanol contact angle measurements</b>	<b>116</b>
B.1 Surface tension during measurements . . . . .	116
B.2 Dynamic Wilhelmy method . . . . .	117
B.2.1 Coated glass plates . . . . .	117
B.2.2 Polished salt plates . . . . .	123
B.2.3 Naturally split salt plates . . . . .	126
B.3 Washburn method . . . . .	127

# 1 Theory of Surface Phenomena

## 1.1 Surface Tension

### 1.1.1 Introduction

If two bulk phases with at least one different physical property come in contact with each other an interface region is potentially formed in the region of contact. In the case of temperatures far away from the critical point this interface region does not extend beyond several molecular diameter into the bulk phases and therefore it is often considered to be a two dimensional boundary. However the interface formed between two bulk phases is a thin region in which physical properties, like e. g. the density, vary rapidly and continuously from the bulk properties of one phase to the bulk properties of the other phase [29]. The stable existence of such an interface depends on the free energy of formation of the interface. Only a positive free energy of formation allows the generation of a stable interface region. Looking at the interface region from one phase to the other in microscopic dimensions the transition becomes drastic but continuously as shown in figure 1 for a condensed phase in equilibrium with its coexistent gas:

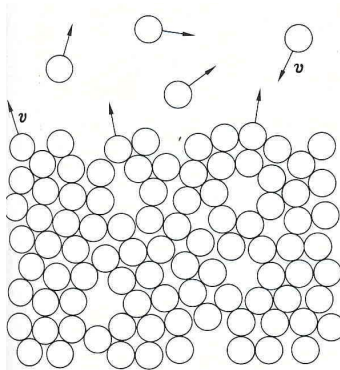


Figure 1: *Interfacial profile in molecular dimensions* [3]

The continuous change in density and concentration in the illustrated interface region causes the appearance of additional forces in this area. A molecule in the neighborhood of the interface between any two bulk phases will experience a different environment than if that some molecule were deep within a similar bulk phase [28]. This difference in intermolecular forces<sup>1</sup> is used for the definition of the term *surface tension* of *surface free energy*. Phenomena appearing in interfacial regions originate from the diverse energetic correlations between particles from the same phase and those interacting with neighboring molecules of another phase. Since the attractive forces between similar molecules are higher then between different ones only an addition of work to the “inner” particles will bring them into the interface region. Thus the work needed to modify the size and curvature of a phase boundary is supposed to be in proportion to the magnitude of the caused change in area. The differential form can be written as:

<sup>1</sup>The origin of intermolecular forces will be discussed later on in chapter 1.1.6



$$dw_A = \gamma dA \quad (1.1)$$

whereas  $w_A$  indicates the interface work and  $dA$  the interfacial area increment. The introduced proportional constant  $\gamma$  is the surface/interface free energy respectively surface/interface tension. Its common to use the term surface to describe the transition from solid to gas of liquid to gas whereas all other possible combination between the three matter of states form interfaces.

Surface	Interface
liquid-gas	liquid-liquid
solid-gas	solid-liquid
	solid-solid

Although surface free energy and surface tension express an equivalent phenomenon their derivations originate from different physical views. Thermodynamical considerations lead to the surface free energy in units  $[\frac{J}{m^2}]$  whereas the term surface tension in units  $[\frac{N}{m}]$  is based on mechanical reflections. In the following both views will be described in detail to finally show that they lead to the same prediction that is to say the formation of a minimal surface/interface.

### 1.1.2 Thermodynamics of Surfaces

Considering that the interfacial region has no sharply defined boundaries and its thickness only amount to a few Å a two dimensional mathematical boundary [1] can be used as an approximation for qualitative calculations [15] as shown in figure 2:

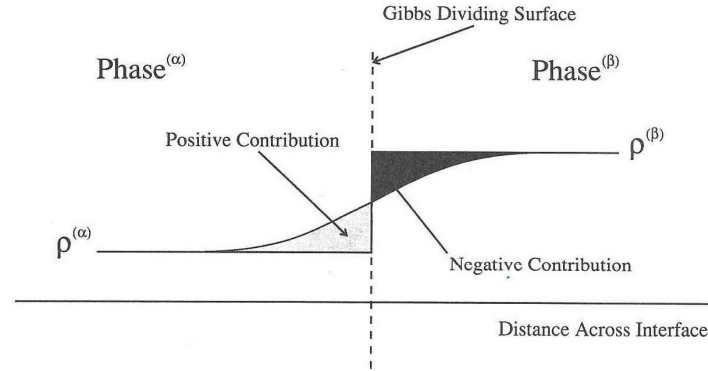


Figure 2: Density profile across a deformable liquid-vapor interface showing the placement of the dividing surface and the regions of the density profile which contribute to the final value of the surface density.[28]

Consequently the region over which the density and local pressure vary disappears and the extensive properties like  $G$ ,  $E$ ,  $S$ ,  $n$ , etc. pertaining to the bulk phases can be approximated to be constant up to this dividing surface. Therefore the bulk phases themselves extend uniformly right up to this boundary which is also known as the *Gibbs dividing surface*. However the assumption that the bulk phases continue unchanged to an assumed mathematical dividing surface will lead to a difference between the actual values for the real interface volume and the sum of the values for the two bulk phases by an excess or deficiency assigned to the surface region.

In the following the superscripts  $\alpha$  and  $\beta$  denote properties of the hypothetical bulk systems  $\alpha$  and  $\beta$  whereas  $\sigma$  indicates properties of the virtual surface. In addition to the already made simplification we will consider the case a curvature which is small compared to the thickness of the surface region or in other words we will assume a plane surface. In doing so curvature effects in the following calculations can be neglect.

$U'$  indicates the internal energy of the simplified system in which the concerned phases continue uniformly right up to the dividing surface. Since the internal energy is an extensive property it can be written as:

$$U' = U^\alpha + U^\beta \quad (1.2)$$

The value  $U$  of the real system with a nonzero interface volume will excess the hypothetical one by the internal energy of the surface phase  $U_\sigma$ :

$$U_\sigma = U - U_\alpha - U_\beta \quad (1.3)$$

Equally the number of moles  $n_{i\sigma}$  for the surface can be defined as:

$$n_{i\sigma} = n_i - n_{i\alpha} - n_{i\beta} \quad (1.4)$$

whereas  $n_i$  represents the real number of moles of molecular sort  $i$  in the whole interface area and  $n_{i\alpha}$  and  $n_{i\beta}$  indicate the amount of substance for bulk phase  $\alpha$  and  $\beta$  without a dividing interface region.

These thermodynamic properties of the surface can be used to determine the surface tension. It should be noted that, the following derivations assume a constant total energy, total entropy and total mass of the system. Fundamentally the internal energy  $U$  can be changed by transfer of mass and heat into and out of it. Therefore it can be written as a function of entropy  $S$  and number of moles  $n_i$  as follows:

$$dU = TdS + \sum_i \mu_i dn_i \quad (1.5)$$

where  $\mu_i$  indicates the chemical potential of the respective molecular sort  $i$ .

On the mentioned conditions this total differential has to disappear.

The same fundamental equation is true for the interface  $\sigma$ . Since the regarded system is the interfacial area  $\sigma$  instead of the volume, as in the case of the bulk phases, the work done in modifying an interfacial area increment  $dO$  has to be consult. Consequently the internal energy can be written as a function as follows:

$$dU_\sigma = TdS_\sigma + \sum_i \mu_i dni_\sigma + \gamma dO \quad (1.6)$$

with the surface tension  $\gamma$  as the change of internal energy  $U_\sigma$  with altering surface:

$$\gamma = \left( \frac{\partial U_\sigma}{\partial O} \right)_{S_\sigma, n_{i\sigma}} \quad (1.7)$$

Since the restriction to plane surfaces leads to wrong statements when treating small and therefore strongly curved droplets henceforward a pressure gradient between the two bulk phases ( $P_\alpha \neq P_\beta$ ) will be approved. Furthermore the inner energy  $U$  will be replaced by the Gibbs free energy  $G$  in what follows. Starting from the definition of the total Gibbs free energy:

$$G = U - TS + P^\alpha dV^\alpha + P^\beta dV^\beta \quad (1.8)$$

and assuming an isotherm process ( $dT = 0$ ) with a constant amount of substance ( $dn_i = 0$ ) at equilibrium the total differential...

$$dG = P^\alpha dV^\alpha + P^\beta dV^\beta + \gamma dA \quad (1.9)$$

... must disappear. The use of (1.6) for the derivation of  $dG$  entails the introduction of  $\gamma$ .

See that there is no change in total volume  $dV$  and therefore  $dV^\alpha + dV^\beta = 0$  the upper equation can be transformed to the expression:

$$(P^\alpha + P^\beta) dV^\alpha = \gamma dA \quad (1.10)$$

which describes the situation of two bulk phases separated by a membrane of infinitesimal thickness and of size  $A$  under tension  $\gamma$ .

Reintegrating now the three-dimensional surface region into our calculation and admitting curvatures of the bulk phases surfaces  $dA$  can be replaced by  $((c_1 + c_2) Adt)$ . Whereas  $c_1$  and  $c_2$  denote the reciprocals of the radii of curvature and  $dt$  is the change of the distance displacing the surface region. Since the change of bulk phase volume is equivalent to the alteration in  $Adt$  we can rewrite equation (1.17) to:

$$(P^\alpha + P^\beta) Adt = \gamma (c_1 + c_2) \quad (1.11)$$

or

$$\Delta P = \gamma (c_1 + c_2) \quad (1.12)$$

Equation 1.12 is the Young and Laplace equation.

### 1.1.3 Mechanics of Surfaces

The statistical mechanical theory of interfacial phenomena [21] relates surface tension to the potential of intermolecular force and molecular distribution functions. Instead of attempting to determine surface free energy as the isothermal work of formation of unit area of interface -  $\left[\frac{J}{m^2}\right]$  as in thermodynamic definition - a mechanical definition of surface tension in terms of the stress transmitted across a strip of unit width, normal to the local density respectively concentration gradient, offers the most direct approach to a molecular theory [kirkwood]. A schematic draft describing these forces is shown in figure 3

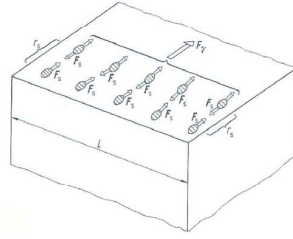


Figure 3: *Schematic diagram showing the intermolecular forces acting across the surface* [3]

For the mechanical derivation of surface tension we accept conditions as mentioned. The treated surface region shall be composed of two bulk phases, whereas one is the liquid and the other its coexistent gas, and a virtual dividing interface.

A statistical mechanical treatment assumes the kinetic effect of thermic motion. This requirement in combination with the profile of density (figure 2) concludes the isotropic pressure of gas in proportion to the local molecular density and thermodynamic temperature. The second influencing variable represents the attracting intermolecular correlation respectively its anisotropy in interface. The affected anisotropy is called forth by variable distribution and number of neighboring molecules. A net-stress exerted on a molecule in the surface results from the difference between local kinetic part and correlation part. Coming back to the simplified surface region we define surrounding region  $S_S$  all over normal to auxiliary areas  $S_\sigma$ ,  $S_\alpha$  and  $S_\beta$  whereas  $S_\alpha$  and  $S_\beta$  are virtual planes parallel to the interface  $S_\sigma$  and situated in bulk phase  $\alpha$  respectively  $\beta$  as shown figure 4:

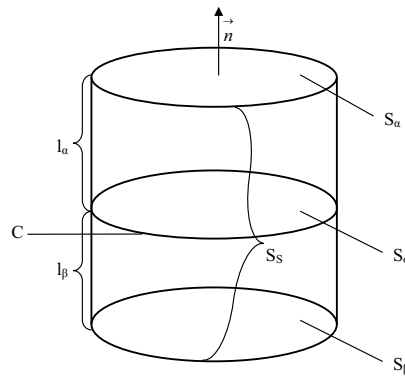


Figure 4: *Circumscription of the interface region -  $S_S$  is orthogonal to  $S_\sigma$ ,  $S_\alpha$  and  $S_\beta$*  [26]

Normal and tangential pressure components are similar as long as the pressure is isotrop as is the case with liquid and gas phase but not for  $S_\sigma$ . Studying all the forces exerted on the system in combination with Newtons second law we arrive to the formulas [26]:

$$\begin{aligned} \int_V \rho \vec{a} dV &= \int_V \rho \vec{g} dV + \int_{S_\alpha} p_\alpha \vec{n} dS - \\ &\quad \int_{S_\beta} p_\beta \vec{n} dS - \int_{S_S} p_T \vec{t} dS \end{aligned} \quad (1.13)$$

$$\begin{aligned} \int_{V_\alpha} \rho_\alpha \vec{a} dV &= \int_{V_\alpha} \rho_\alpha \vec{g} dV + \int_{S_\alpha} p_\alpha \vec{n} dS - \\ &\quad \int_{S_\sigma} p_\alpha \vec{n} dS - \int_{S_\alpha \cap S} p_\alpha \vec{t} dS \end{aligned} \quad (1.14)$$

$$\begin{aligned} \int_{V_\beta} \rho_\beta \vec{a} dV &= \int_{V_\beta} \rho_\beta \vec{g} dV + \int_{S_\beta} p_\beta \vec{n} dS - \\ &\quad \int_{S_\sigma} p_\beta \vec{n} dS - \int_{S_\beta \cap S} p_\beta \vec{t} dS \end{aligned} \quad (1.15)$$

$\vec{a}$  and  $\vec{g}$  signify on the one hand the local acceleration, on the other hand the acceleration of gravity.  $\vec{n}$  and  $\vec{t}$  identify the surface normal vector for areas  $S_\alpha$  and  $S_\beta$  respectively  $S$ .

Whereupon equation 1.13 is due to forces executed on the total system with interface  $\sigma$  and the sum of equations 1.13 and 1.14 results provided that the interface area is identically to phase  $\alpha$  (equ.1.13) respectively phase  $\beta$  (equ.1.14). As well as the approach in the thermodynamic treatment it can be concluded that the interface concerning part is the difference between equation 1.13 and the sum of 1.13 and 1.14.

$$\int_V \Delta \rho \vec{g} dV + \int_{S_\sigma} (p_\alpha - p_\beta) \vec{n} dS - \int_S \Delta p_T \vec{t} dS = \int_V \Delta \rho \vec{a} dV \quad (1.16)$$

whereas  $\Delta \rho$  respectively  $\Delta p_T$  relate to the density/pressure difference  $(\rho - \rho_i)$  resp.  $(p_T - p_i)$  ( $i = \alpha, \beta$ ) in volume  $V_\alpha$  or  $V_\beta$ . Approaching a constant gravitational acceleration all over the considered system and with the assumption of an extent  $l_\alpha$  and  $l_\beta$  for the two bulk phases we can rewrite the first part of equation 1.16 to:

$$\int_V \Delta \rho \vec{F} dV \cong \int_{S_\sigma} \left( \int_{l_\alpha}^{l_\beta} \Delta \rho dl \right) \vec{F} dS \quad (1.17)$$

In like manner the third part of equation 1.16 can be rewritten by using the closed bordering curve  $C$  of the interface area and the heights  $l_\alpha$  and  $l_\beta$  instead the bordering area  $S$ :

$$\int_S \Delta p_T \vec{t} dS \cong \oint_C \left( \int_{l_\alpha}^{l_\beta} \Delta p_T dl \right) \vec{t} ds \quad (1.18)$$

After a transformation of 1.18 with the area-divergence theorem [5] equation 1.16 can be rewritten with the redefined parts:

$$\begin{aligned} 0 &= \int_{S_\sigma} \left[ \left( \int_{l_\alpha}^{l_\beta} \Delta \rho (\vec{g} - \vec{a}) dl \right) + (p_\alpha - p_\beta) \right] dS + \\ &\quad \int_{S_\sigma} \left[ \vec{\nabla}_{S_\sigma} \left( - \int_{l_\alpha}^{l_\beta} \Delta p_T dl \right) + 2H \vec{n} \left( - \int_{l_\alpha}^{l_\beta} \delta p_T dl \right) \right] dS \end{aligned} \quad (1.19)$$

and by replacement of

$$\int_{l_\alpha}^{l_\beta} \Delta \rho dl = m_\sigma \quad \text{the surface mass} \quad (1.20)$$

$$- \int_{l_\alpha}^{l_\beta} \Delta p_T dl = \gamma \quad \text{the surface tension} \quad (1.21)$$

$$(1.22)$$

one achieves a differential equation for statics of fluids considering the independency of the surface form and thus the disappearance of the integrand:

$$m_\sigma \vec{g} - m_\sigma \vec{a} + (p_\alpha - p_\beta) \vec{n} + 2H\gamma \vec{n} + \vec{\nabla}_{s_\sigma} \gamma = 0 \quad (1.23)$$

This equation provided that the surface mass  $m_\sigma$  can be neglected inducts two conditions on the surface tension:

1.

$$\vec{\nabla}_{s_\sigma} \gamma = 0 \quad (1.24)$$

2.

$$p_\alpha - p_\beta = -2H\gamma = \gamma \left( \frac{1}{r_1} + \frac{1}{r_2} \right) \quad (1.25)$$

The first conditions predicates a constant surface tension along the surface. The second one is in strict conformity to the Young-Laplace equation deduced from thermodynamic considerations 1.12.

Finally the mechanic and thermodynamic definition of surface tension are identical [21].

The most phenomenons caused by surface tension and therefore the occurrence of an exerted force in some direction are reflected in the formation of an curved surface. Since in our case of interest the observed surfaces concern liquid - vapor interfaces a confinement on this special interface is usefull in deriving an equilibrium condition for surface curvature.

By modifying a the surface of a liquid in drawing out or pressing into a piece of it one must consider the hydrostatic pressure:

$$p = \rho gh \quad (1.26)$$

As on can infer from 1.26 this pressure changes for a liquid in proportion to the height  $h$ . This height indicates the distance between the plane surface and the displaced surface element. Its defined to be positive for exertion against the gravitation. In combination with the Laplace equation, which describes the form of a surface for a given pressure/pressure difference we arrive to:

$$\rho gh = \gamma \left( \frac{1}{r_1} + \frac{1}{r_2} \right) \quad (1.27)$$

The solution of this differential equation will specify the form of a liquid surface under gravitational influence. It shows that the curvature of a surface submits a force action against the gravitational field. Since a plane surface is not able to work against a force normal to it - like the gravitational force of an object placed on this surface - the item will sink in the liquid until the upwelling will compensate the gravity. See that the sinking object modifies the surface the caused curvature, the contact angle and the form of this body will influence the maximum upwelling. Figure 5 shows the equilibrium condition for a curved surface.

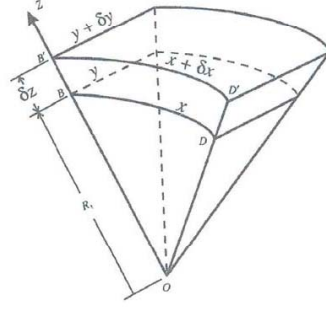


Figure 5: Condition for mechanical equilibrium for an arbitrarily curved surface [28]

#### 1.1.4 Effect of Curvature due to Surface Tension on Vapor Pressure

Since the surface curvature affects the molar free energy of a substance [1] and thus its vapor pressure it plays an important role in nucleation processes. As already derived the pressure difference  $\Delta p$  across an interface results in an interfacial curvature, which is described by the Young and Laplace equation. In the following this correlation will be used to relate the change in vapor pressure to the curvature of the surface.

If mechanical pressure is put onto a volume  $V$  by not changing temperature (i) and molar volume (ii) the amendment of molar free energy of a substance  $\Delta G$  is given by:

$$\Delta G =^{(i)} \int V dp =^{(ii) \& (14)} \gamma V \left( \frac{1}{r_1} + \frac{1}{r_2} \right) \quad (1.28)$$

It is convenient to relate the free energy of a substance to its vapor pressure [1]:

$$G = G^0 + RT \ln P \quad (1.29)$$

and consequently (1.40) can be written as:

$$RT \ln \frac{P}{P^0} = \gamma V \left( \frac{1}{r_1} + \frac{1}{r_2} \right) \quad (1.30)$$

$$= \left( \frac{2\gamma V}{r} \right) \quad (1.31)$$

where  $P^0$  is the normal vapor pressure of the liquid with plane surface and  $P$  the one observed over the curved surface. The last conversion part 1.31 describes the case of a spherical surface of radius  $r$ .

#### 1.1.5 Temperature Dependence of Surface Tension

Since the aim of this thesis was to measure the temperature dependence of the contact angle, which is mainly influenced by the surface tensions of the examined substances, the temperature on the surface tension itself should be treated too. Eötvös developed an equation describing the linear decrease of surface tension with increasing temperature for liquids [27]

$$\gamma V_M^{\frac{2}{3}} = k_e (T_{krit} - T_E - T) \quad (1.32)$$



whereas  $V_M$  is the volume of one mol of the liquid. As already implied in the introduction of this chapter the surface tension disappears at the critical temperature. By approaching this temperature the decreasing behavior differs from being linear. This fact is mirrored in the substance specific temperature  $T_E$ , which is about  $6K$ .  $k_\epsilon$  is an empirical constant - the *Eötvös-constant*. This constant states the association rate of a liquid ( $17.7K^{-1}\text{mol}^{-1}$  for non-associating liquids and e.g.  $7.5K^{-1}\text{mol}^{-1}$  for water).

### 1.1.6 Forces between Atoms and Molecules

So far surface phenomena have always been related to interaction forces between molecules in the liquid and air molecules at the interface. Thus a focus on the origin of them might be helpful. Basically the correlation between two molecules as a function of distance may be represented by the Lennard-Jones potential:

$$-\epsilon(r) = 4\epsilon_0 \left[ \left( \frac{\sigma}{r} \right)^{12} - \left( \frac{\sigma}{r} \right)^6 \right] \quad (1.33)$$

while  $\sigma$  terms an effective molecular diameter,  $\epsilon_0$  denotes the potential energy at the minimum and  $r$  is the distance of the molecule centers.

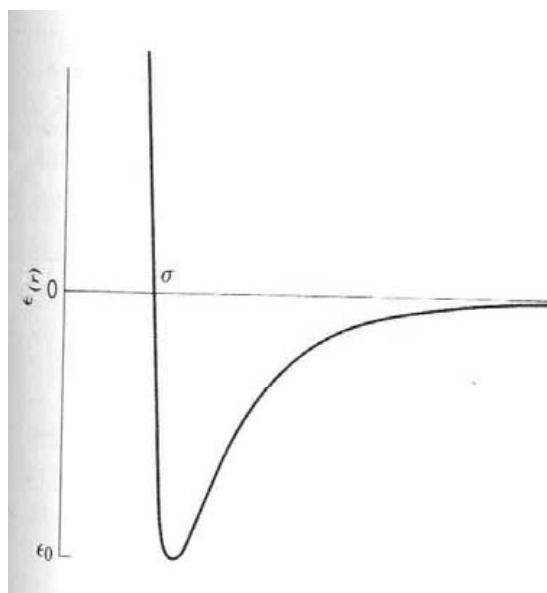


Figure 6: *Lennard-Jones potential showing the intermolecular correlation as a function of molecule distance*[1]

Though atoms respectively molecules can principally interact gravitationally, magnetically and electrically only the last that usually is of any importance in interfacial studies. Electrical forces may be separated up into those of repulsion and those of attraction according to the mentioned intermolecular potential.

First of all the repulsive ones again may be classified into coulomb repulsion between like-charged ions and general repulsion between two atoms brought too close together. While the coulomb repulsion has an infinite range the general atom-atom repulsion is very short range and rises rapidly as atoms or molecules come closer than a certain distance caused by the reluctance of the electron clouds for two atoms to overlap each other. This kind of repulsion is mathematically expressed in

the Lennard-Jones Potential by means of an inverse twelfth power of intermolecular distance.

For the description of the attractive forces causing surface phenomena the often called *van der Waals* forces play an important role. An important component of such forces is the *dispersion* force. Among the attraction between unlike-charged atoms resp. molecules:

$$\epsilon = -\frac{|q_1||q_2|}{x} \quad (1.34)$$

the interaction of dipoles (molecules having a dipole moment  $\mu$ ):

$$\bar{\epsilon} = -\frac{2\mu^4}{3kTx^6} \quad (1.35)$$

or the correlation between a dipoles and a polarizable molecule (field induces a dipole moment in a polarizable molecule  $\mu_{ind} = \alpha F$ ):

$$\epsilon = -\frac{\alpha\mu^2}{x^6} \quad (1.36)$$

London [25] showed the existence of an additional type of electrical force between atoms, which are known as *London-van der Waals* force. It is always attractive and originates through the fact that even neutral atoms constitute systems of oscillating charges because of the presence of a positive nucleus and negative electrons [1]. After detailed derivation [1] the corresponding form for two different atoms 1&2 is:

$$\epsilon(x) = -\frac{3}{2} \frac{\alpha_1\alpha_2}{x^6} \left[ \left( \frac{1}{h\mu_1} \right) + \left( \frac{1}{h\mu_2} \right) \right] \quad (1.37)$$

where  $\alpha_1$ & $\alpha_2$  denote the polarizability of the atoms;  $h\nu_1$ & $h\nu_2$  characteristic energies for the atoms and  $x$  the distance between them.

It is common to call intermolecular interactions that give rise to an attractive potential proportional to the inverse sixth power of molecule distance *van der Waals* forces. This dependence is also included in the van der Waals equation for nonideal gases by the  $\frac{a}{V^2}$  term:

$$(P + \frac{a}{V^2})(V - b) = RT \quad (1.38)$$

where  $V$  indicates the volume per mole and  $a$  and  $b$  are constants <sup>2</sup>. Although three different types of van der Waals interactions are given so far, which are  $\mu - \mu$ ,  $\mu - \alpha$  and  $\alpha - \alpha$  only the latter one is independent of structure <sup>3</sup>and therefore adapted for description of condensed systems. For that reason surface and colloide properties are generally attributed to the  $\alpha - \alpha$  dispersion force.

---

<sup>2</sup> $a$  gives the magnitude of attractive potential and  $b$  the actual volume of a mole of molecules

<sup>3</sup>at least in first order

## 1.2 Contact Angle

### 1.2.1 Equation of Young

If a drop is placed on a solid surface then two different possibilities concerning the spreading behavior of the liquid exist. Either the liquid placed on this solid surface will wet or remains as a drop having a definite angle of contact between the liquid and solid phases. The spreading behavior will on the one hand depend on the surface tensions of both liquid and solid phase and on the other hand on the interface tension between liquid and solid. To make the differentiation of surface and interface easier hereafter surface tension will be indicated with  $\sigma$  while  $\gamma$  denotes interface tensions. The change in surface free energy  $\Delta G^\sigma$  by placing a liquid drop on the solid surface can be written as:

$$\Delta G^\sigma = \Delta A(\gamma_{SL} - \sigma_S) + \Delta A \sigma_L \cos(\theta - \Delta\theta) \quad (1.39)$$

whereas  $S$  and  $L$  indicate surface properties of the solid respectively liquid phase.  $\Delta A$  is the change in area of solid covered by the droplet and  $\theta$  describes the angle formed by the contact of liquid and solid. Strictly speaking its the angle between liquid-vapor interface and solid.

Since all qualitative reflections mentioned are confined on systems in equilibrium the change in surface free energy with change in area of solid covered will disappear after a finite time  $\lim_{\Delta A \rightarrow 0} \frac{\Delta G^\sigma}{\Delta A} = 0$  and 1.39 can be rewritten to:

$$\gamma_{SL} - \sigma_S + \sigma_L \cos\theta = 0 \quad (1.40)$$

the Young equation. Combining Fig. 7 and the mechanical definition of surface tension as the force working across a surface per unit length it can be concluded that all the Young Equation does is to constitute a equilibrium condition for the forces acting on the three-phases contact line. At this point it should be noted that

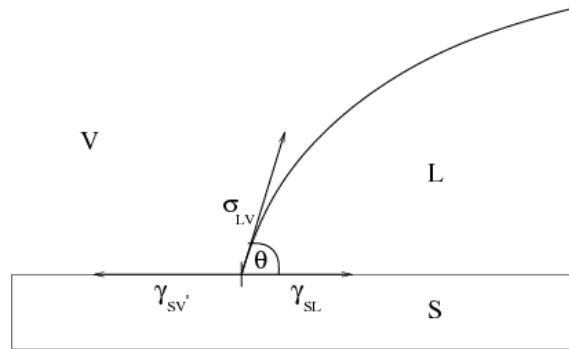


Figure 7: Draft of the 3 forces action on the contact line[36]

it is important that the phases are mutually in equilibrium. That is to say that  $\sigma_S$  is supposed to describe the surface tension of the solid in equilibrium with the saturated vapor pressure  $P^0$ . Thus its better to replace  $\sigma_S$  by  $\gamma_{SV^0}$ . The distinction between  $\sigma_S$  and  $\gamma_{SV^0}$  have been made Bangham and Razouk in [2] and was also stressed by Harkins and Livingstone in [18]. It arises from adsorption of a gas or vapor at the solid gas interface. For vapors at pressures approaching the saturation pressure, the amount of adsorption can be large and might approach or exceed the point of monolayer formation on the solid surface [1]. The degree of the so called *physical adsorption* caused by “van der Waals” forces influences the solid-gas interfacial free

energy respectively the change in surface free energy of a solid.

The amount of absorbed vapor molecules depends on the ratio  $\frac{P}{P^0}$  whereas  $P$  is the pressure of the adsorbate vapor and  $P^0$  the one of the pure liquid adsorbate. Consequently the adsorption will decrease the surface tension of the solid by the film pressure  $\pi^0$ . That's why the Young equation should rather contain  $\gamma_{SV^0} = \sigma_S - \pi^0$  instead of  $\sigma_S$  :

$$\sigma_L \cos \theta = \gamma_{SV^0} - \gamma_{SL} \quad (1.41)$$

### 1.2.2 Wetting as a Contact Angle Phenomenon

As already mentioned there exist approximately two possibilities how a liquid drop can react by bringing in contact with a solid surface. Either the drop will spread easily over the solid and therefor the liquid will be called wetting or it will tend to ball up and run off the surface easily what is named nonwetting. The first case means that the contact angle between a liquid and a solid is zero or very close to zero and the second arrives for an angle greater than  $90^\circ$ . A useful parameter to predict the wetting behavior of a liquid is the spreading coefficient  $S_{L/S}$ . It gives the free energy change for the spreading of a liquid film on the solid. Since spreading is always related to a zero contact angle the spreading coefficient follows from the Young Equation:

$$S_{L/V} = \gamma_{SV^0} - \sigma_L - \gamma_{SL} \quad (1.42)$$

Qualitatively spoken,  $\sigma_L$  and  $\gamma_{SL}$  should be made as small as possible if spreading is to occur. In this case the wetting process will be spontaneous and initial since  $S_{L/S}$  is positive and therefore accompanied by a decrease in free energy. Or in other words to follow Dupre - if the work of adhesion  $w_{L/S}$  between liquid and solid molecules is bigger then the work of cohesion  $w_{LL}$  between liquid molecules:

$$w_{L/S} \geq w_{LL} \quad (1.43)$$

Figure 8 clarifies the difference between  $w_{L/S}$  and  $w_{L/L}$ : As one can clearly see the

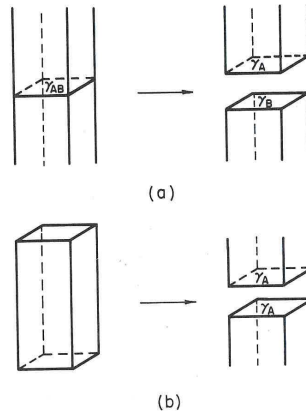


Figure 8: *Work of adhesion and work of cohesion*[1]

work of adhesion

$$w_{L/S} = \sigma_L + \gamma_{SV^0} - \gamma_{SL} \quad (1.44)$$

gives the work necessary to separate one square centimeter of interface in to liquid-vapor and solid-vapor surfaces. The work of cohesion again defined as:

$$w_{LL} = 2\sigma_L \quad (1.45)$$

correspond to the reversible work to pull apart a column of liquid. [1]

### 1.2.3 Wetting as a Capillary Action Phenomenon

For some types of wetting not only the contact angle is involved in the basic mechanism of the action but also a phenomenon related to that of capillary rise. As already deduced in the previous chapter every curved surface and thus the curved surface of a meniscus too is related to a pressure difference across it respectively to a force action normal to the surface. For any contact angle  $\theta$  and a spherical curvature of the surface the equation of Young and Laplace can be rewritten in:

$$\Delta P = \sigma_L \cos\theta \left( \frac{2}{r} \right) \quad (1.46)$$

where  $r$  denotes the equivalent radius of the capillary [1]. According to this equation the pressure  $P_i$  causing a spontaneous capillary adhesion is defined by the advancing contact angle  $\theta_a$ . Otherwise  $P_0$  is required for the desorption of liquid out of the capillary and therefore given by the receding contact angle  $\theta_r$ . Since  $\theta_a$  is always larger than  $\theta_r$  the needed pressure  $P_0$  to get the liquid out of the capillary is always bigger than the so called *penetration pressure*  $P_i$  [19].

More specifically detailed in the case of a finite contact angle equation 1.46 can be rewritten:

$$\Delta P = (\gamma_{SV^0} - \gamma_{SL}) \left( \frac{2}{r} \right) \quad (1.47)$$

so that the principal requirement for a large pressure difference is that the interfacial tension  $\gamma_{SL}$  is made as small as possible since for practical reasons  $\gamma_{SV^0}$  can not be varied that easily.

In the case of a zero contact angle 1.46 becomes

$$\Delta P = \sigma_L \left( \frac{2}{r} \right) \quad (1.48)$$

and the determining parameter for a large  $\Delta P$  is therefore a large surface tension  $\sigma_L$ .

Another factor next to a large pressure difference in promoting capillary penetration is the *rate* of entry  $v$ . Supposing that gravity can be neglected Washburn *et al.* [37] developed the Lucas-Washburn equation for the rate of entry of a liquid into a capillary displacing air:

$$v = \frac{r\sigma_L \cos\theta}{2\eta l} \quad (1.49)$$

where  $l$  is the length of the liquid column entering into the capillary of radius  $r$  and  $\eta$  is viscosity of the liquid. In the described case of a liquid displacing air the rate  $v$  has the dimension of velocity and thus gives a measure of the penetrating power of the liquid in a given situation.

By replacing the length  $l$  with the mass  $m$  of the lifted liquid the equation serves as a

basis for contact angle measurements between liquids and powder-form solids<sup>4</sup>. The basic principal is to approach a powder as a bundle of random arranged capillaries. Since neither the radius nor the orientation of each capillary will always be the same the implemented solid material constant  $c$  replaces  $r$  in equation 1.49.

The lifted mass of each liquid column arises from:

$$m_L = lr^2\pi\rho_L \quad (1.50)$$

By plugging this term in the Lucas-Washburn equation the received equation can be written as:

$$\cos\theta = \frac{m^2}{t} \frac{\eta_L}{\rho_L\sigma_L c} \quad (1.51)$$

---

<sup>4</sup>A more detailed description of this measurement method follows in chapter *Measurement Methods*

### 1.3 Contact Angle Hysteresis

As a matter of fact the solid surfaces never keeps the strict conditions required by the validity of the Young equation and therefore an experimental determination of the predicted equilibrium contact angle seems to be impossible. Performing dynamic contact angle measurements the state of the observed solid surface will influence the contact angle and cause the contact angle hysteresis  $\theta_{hyst}$ , which is the difference between advancing contact angle  $\theta_a$  and receding contact angle  $\theta_r$ . A detailed description of the experimental implementation of such dynamic measurements will follow in the next chapter. At the moment I will only write down that such dynamic cycles always include a constant replacement of the three-phases contact line. In combination with the surface inhomogeneity the shift of the contact line will cause a deviation of the experimentally determined contact angle from the predicted equilibrium contact angle. In order to get a clearer understanding for the causes and consequences of  $\theta_{hyst}$  I will hereafter present various types of surface inhomogeneities, their influences on the apparent contact angle and different explanation attempts.

#### 1.3.1 Rough but Chemical Homogeneous Surface

First of all we will draw up the case of a rough solid surface and the roughness impact on the measured contact angle. Although the observed surface is constituted of only one chemical substance and therefore the contact angle should be set by the constant surface tensions of the solid and the liquid <sup>5</sup> experimental observations show the measured value never accords to the predicted equilibrium contact angle. On the one hand the experimental determined value depends on the shift direction. Whereas a distinction is made between the advance of the contact line toward solid-vapor region and the recess of it in direction of the liquid-solid region according to which one differs between advancing contact angle  $\theta_a$  and receding contact angle  $\theta_r$ . A schematic draft of the different cases is shown in figure 9. One recognizes that the

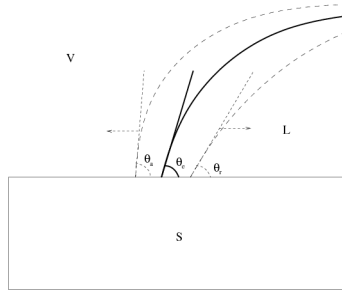


Figure 9: Illustration of the difference between  $\theta_a$ ,  $\theta_e$  and  $\theta_r$

advancing angle will always be bigger than the equilibrium one and  $\theta_e$  again will exceed the receding contact angle :  $\theta_a > \theta_e > \theta_r$ . And on the other hand even a static analysis of the contact angle by placing a drop of fixed volume on a rough surface <sup>6</sup> will yield to a value different from the predicted equilibrium contact angle. To start with an explanation of the second phenomenon - the change in dropshape

<sup>5</sup>In what follows we will exclude the influence of the vapor phase on the solid surface assuming the system to be in equilibrium

<sup>6</sup>The so called *Sessile drop method*

by surface roughness - Wenzel's treatment of rough surfaces [41];[42] result in the following consequences for the measured contact angle. The surface may be rough

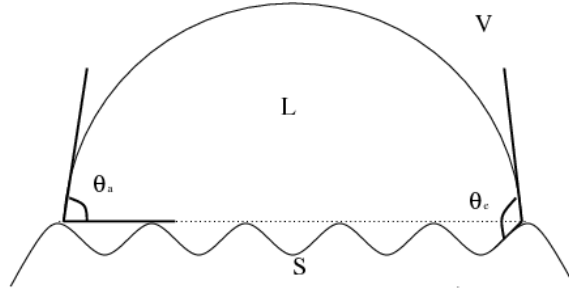


Figure 10: Idealized rough surface showing the difference between apparent and real contact angle[19]

as shown in figure 10 with a coefficient  $r$  giving the ratio of actual to apparent of projected area [1]. Whereas  $\Delta A_{SL(true)} = r\Delta A_{SL(apparent)}$  and similarly  $\Delta A_{SV(true)} = r\Delta A_{SV(apparent)}$ . Consequently the apparent contact angle  $\theta_a$  will differ from  $\theta_e$ :

$$\cos\theta_a = r\cos\theta_e \quad (1.52)$$

As we can conclude from this equation: An equilibrium contact angle of less than  $90^\circ$  will decrease by roughness, while an angle greater than  $90^\circ$  will increase - see figure 11 Dynamic cycling contact angle measurements performed by Lam *et al* indicated

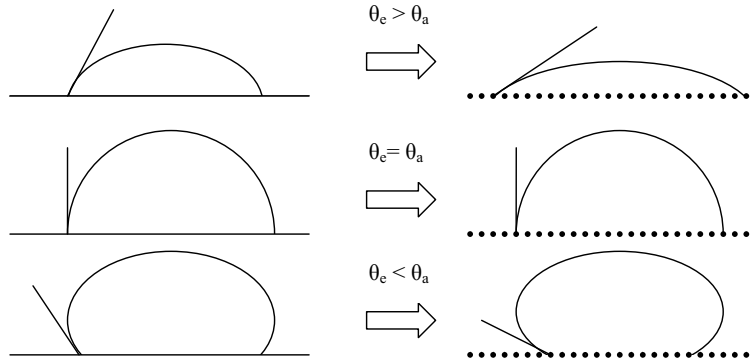


Figure 11: Change of the contact angle on a rough surface[22]

again that all  $\theta_a$  data obtained beyond the first cycle and all  $\theta_r$  values reflect liquid sorption and/or retention by the solid and are therefore not a property of the solid alone [24]. Experimentally observations by increasing and decreasing the volume of a drop placed on a solid showed that the contact angle hysteresis depends on the chain length of the liquids tested and therefore increased with decreasing chain length. In addition to this result not only the receding contact angle was found to decrease with time, suggesting liquid sorption and surface swelling, but also  $\theta_a$  turned out to be time-dependent. Allegeable by increasing solid surface modification by the liquid with longer solid-liquid contact. Moreover  $\theta_{hyst}$  was found on the one hand to decrease with increasing chain length of the liquid molecules and vanish when the chain length was extrapolated to infinity and on the other hand to increase initially and then level off with increasing number of cycles ( $\equiv$  increasing time) by using the very same liquid. This result suggests that processes which occurred on the solid surface during the experiment will eventually approach a steady state



and hence lead to constant hysteresis.

Before coming to the case of chemical surface heterogeneity i would like to note the influence of mechanical deformation on the solid surface tension. Since principally experiments are out to comply with the theoretical stated premises in order to declare the predicted contact angle one strives always to prepare the observed substances optimally. As a consequence solid surfaces are mostly polished and heated in order to get them as smooth and clear as possible. Since the immobility, at least the large-scale immobility, of the surface atoms of a refractory solid has the consequence that the surface energy quantities and other physical properties of the surface depend greatly on the immediate history of the material different mechanical procedures will affect their nature and therefore the contact angle as well.

A clean cleavage surface of a crystal <sup>7</sup> will have a different surface energy than a ground or abraded surface of the same material what turned out to be measurable by sodium chloride crystals.

Furthermore the mechanical procedure involved in a polishing operation differs considerably from that used in grinding [1]. Polishing on the one hand is performed with a relatively soft and high melting material, e.g. rouge or iron oxide, which is best held by a backing of soft material [1]. In contrary to grinding where a material as hard as or harder than the surface to be abraded must be employed. However, electron diffraction studies of the surface region indicated that whereas grinding leads usually just to a mechanical attrition of the surface without greatly changing its molecular crystallinity, polishing leaves a fairly deep and nearly amorphous surface layer <sup>8</sup> [14].

Finally it must be concluded that even the effort of forming the solid surface as smooth as possible will cause a change in surface properties and therefor a distortion of contact angle measurements

### 1.3.2 Smooth but Chemical Heterogeneous Surface

Another possibility for nonideal surface is the chemical surface heterogeneity as illustrated in figure 12 The observed surface may be consist of small patches of

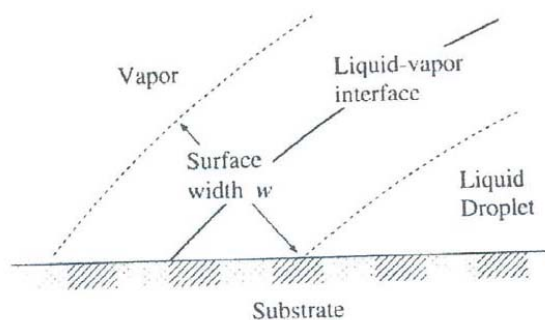


Figure 12: *Illustration of an idealized heterogeneous surface* [19]

various kinds. Cassie [6] extended Wenzel's treatment of rough surfaces to chemical

<sup>7</sup> A general, quasi-geometric solution to the question how to construct a shape of specified volume such that the total surface free energy is a minimum has been given by Wulff [43]

<sup>8</sup> This surface layer resulting from polishing is generally known as the *Beilby* layer [45] and amounts to a depth of  $20 - 100 \times 10^{-10} m$

heterogeneous but smooth ones. By restricting the heterogeneity to a solid surface having two fractions  $\sigma_1$  and  $\sigma_2$  with the intrinsic contact angles  $\theta_1$  and  $\theta_2$  he derived an important equation for heterogeneous surfaces [6]:

$$\cos\theta_a = \sigma_1\cos\theta_1 + \sigma_2\cos\theta_2 \quad (1.53)$$

As we can deduce from this equation he predicted the appearance of an average contact angle  $\theta_A$  for experimental investigation on a heterogeneous surface.

In the case of porous material the solid is treated like a two component surface consisting of a solid surface area  $\delta_1$  and a vapor area  $\delta_2$ . Consequently the contact angle becomes:

$$\cos\theta_A = \delta_1\cos\theta_1 - \delta_2 \quad (1.54)$$

A quasi-steady-state computer simulation of contact angle hysteresis on a heterogeneous surface has been presented by Brandon and Marmur [4]. They performed contact angle measurements on a smooth planar solid with periodic chemical heterogeneity by changing the drop volume slowly. However they came to the conclusion that for most drop volumes the contact angle and the base of the drop change continuously, but, when an inflection point on the free energy curve is reached, irreversible jumps in the contact angle and the size of the base occur. The extent of the continuous change in the base of the drop is in general, small and decreases with increasing drop volume. Thus, the base of the drop appears stationary in between the irreversible jumps. This simulated behavior is very similar to the experimentally observed “stick-slip” behavior.

Later some papers like for example the one of Cubaud and Fermigier [8] try to explain  $\theta_{hyst}$  with metastable states in the sense of the presence of multiple local minima of the total free energy of the system.

In more recent studies the patch structure of the surface [13], molecular mobility and packing as well as roughness of the surface in molecular dimensions [7]; [10]; [44] have been found to be a possible solution. Another newish approach to the problem of hysteresis has been developed by Lam *et al* [24]. They extended the link of contact angle hysteresis to liquid penetration and surface swelling made by Sedev *et al* [34] to a dependence on the chain length of the liquids tested. They determined an increasing hysteresis with decreasing chain length of the liquid and mathematically predicted a vanishing  $\theta_{hyst}$  when the chain length was extrapolated to infinity. Consequently they came to the conclusion that all  $\theta_a$  values obtained beyond the first cycle and all  $\theta_r$  data reflect liquid sorption and/or retention by the solid and are therefore not a property of the solid alone.

The mentioned results confirm the common practice of using advancing contact angles in surface energetic calculations and disregarding the receding contact angles.

## 1.4 Influence of Surface Properties on Nucleation Processes

The formation and growth of aerosol particles by condensation plays an important part in a wide range of natural mass transfer processes, e. g. the formation of clouds, and thus greatly influences the climate. Since the formation of a new phase as it is the case for condensation of vapor includes the generation of a participating surface I will in the following elaborate on the influence of surface tension and contact angle on condensation processes. The nucleation theory primarily in terms of situations involving the liquid-vapor interface - homogeneous nucleation - has been extended in consideration of the estimation of solid-liquid interfacial free energies - heterogeneous nucleation.

Recognizing that in the absence of participating foreign surfaces the general sequence of events is that small clusters of molecules form and that these grow by accretion to the point of grow to yield massive amounts of the new phase I will firstly approach the conditions for the taking place of nucleation.

### 1.4.1 Classical Nucleation Theory - Homogeneous Nucleation

Homogeneous nucleation is the formation of particles from a supersaturated vapor without the assistance of condensation nuclei or ions. The term *supersaturated* refers to a saturation ratio  $S$  greater than 1:

$$S = \frac{p}{p_s} \quad (1.55)$$

where  $p$  indicates the actual *partial pressure*<sup>9</sup> of vapor and  $p_s$  the *saturation vapor pressure*<sup>10</sup> at the temperature of the system.

Consequently a mixture is saturated for  $S = 1$  and unsaturated for a saturation ratio less than one.

### *Kelvin Effect*

If the liquid surface is sharply curved such as the surface of a small droplet, the saturation vapor pressure initially defined as the equilibrium partial pressure for a plane surface at a given temperature must be redefined for sharply curved surfaces. As already mentioned in chapter 1.1.4 the curvature of a surface modifies the attractive forces between surface molecules and leads therefor to a greater partial pressure required to maintain equilibrium. In other words one can reason that the smaller the droplet the easier it is for molecules to leave the droplet surface. Consequently the saturation ratio required for a stable droplet is related to the droplet size and their relationship is given by the *Kelvin* or *Thomson-Gibbs* equation<sup>11</sup>[20]:

$$S = \frac{p}{p_s} = e^{\frac{2\sigma_L M}{\rho_L R T r^*}} \quad (1.56)$$

<sup>9</sup>The pressure that a gas in a mixture of gases would exert if it were to occupy the entire volume occupied by the mixture. According to *Dalton's law* the sum of the partial pressures of the components equals the total pressure of a mixture.

<sup>10</sup>The pressure required to maintain a vapor in mass equilibrium with its condensed phase at a specified temperature and therefore a fixed property of a bulk material. In the case of aerosol condensation  $p_s$  is always related to a plane liquid surface.

<sup>11</sup>This equation remains valid as long as the observed liquid is pure. Since in the context of my measurements I solely applied pure liquids and insoluble solids this restriction is appropriate

whereas  $M$  indicates the molecular weight ( $[\frac{g}{mol}]$ ),  $\rho_L$  the density ( $[\frac{kg}{m^3}]$ ) and  $\sigma_L$  the surface tension ( $[\frac{mN}{m}]$ ) of the liquid.  $r^*$  is the *Kelvin* radius of a stable droplet that will neither grow nor evaporate at the associated saturation ratio. Any deviation from either the saturation ratio related to a fixed drop size or the drop radius corresponding to a given saturation ratio will lead to drop evaporation or growth. The so called *Kelvin effect* does not matter until particle diameters less than  $0.1\mu m$ . Since the arguments of the exponential function are positive per definition one will always require to a supersaturation in order to prevent droplets from evaporating.

Coming back to the behavior of a supersaturated system one observes that the sequence of formation of a new phase does not take place if the vapor pressure is only just slightly over the saturation value. Instead, the vapor pressure usually can be increased considerably over the equilibrium value without anything happening, until, at some fairly sharp limit, general condensation takes place. This impedance to the forming of a new phase clearly is associated with the extra surface energy of small clusters that make their formation difficult. Considering the process of nucleation qualitatively the free energy of nucleation  $\Delta G$  results out of the energy required for transferring vapor molecules into liquid phase<sup>12</sup> On the supposition that the formed cluster is spherical<sup>13</sup> one finds the following expression for  $\Delta G$ :

$$\Delta G = -nkT \ln S + 4\pi r_L^2 \quad (1.57)$$

where the first term indicates the change in free energy by transferring  $n$  moles from the vapor phase at pressure  $p$  to the liquid phase at pressure  $p_S$  seeing that the change in free energy per molecule for the transfer from vapor to liquid phase is given by:

$$\mu_V - \mu_L = kT \ln S \quad (1.58)$$

Since the observed system is supersaturated  $S$  is always bigger than 1 and  $n$ ,  $k$ ,  $T$  are in any case positive per definition the first term will support the formation of a spherical assumed droplet. In contrast the second term including the surface energy  $4\pi r^2 \sigma_L$  possessed of the formed drop retards its formation. By replacing the number of moles  $n$  with:

$$n = \frac{4}{3}\pi r^3 \frac{\rho_L}{M} \quad (1.59)$$

equation 1.57 can be rewritten as:

$$\Delta G = -\frac{4}{3}\pi r^3 \frac{\rho_L}{M} RT \ln S + 4\pi r_L^2 \quad (1.60)$$

By setting  $\frac{d\Delta G}{dr} = 0$  one obtains that the maximum positive value  $\Delta G_{max}$  required to form a drop is related to the critical radius  $r^*$ :

$$r^* = \frac{2\sigma_L}{n_L kT \ln S} \quad (1.61)$$

<sup>12</sup>The so formed droplet obviously posses a surface and the associated surface molecules have a higher free energy then those of the inner drop.

<sup>13</sup>Next to this assumption the classical nucleation theory includes additional simplifications which are just valid for a cluster size up to  $1nm$ . The effect of curvature is neither consider for the surface tension nor for pressure change in the inner of the the droplet

In other words for a given saturation ratio greater then one a particle must initially reach a *critical* radius  $r^*$  to grow and become a stable droplet because the homogeneous nucleation process does not start with individual molecules. If  $S \leq 1$  the free energy of nucleation will always be positive and therefor the growth process of a droplet will never appear spontaneously  $(\frac{\partial \Delta G}{\partial r})$ .

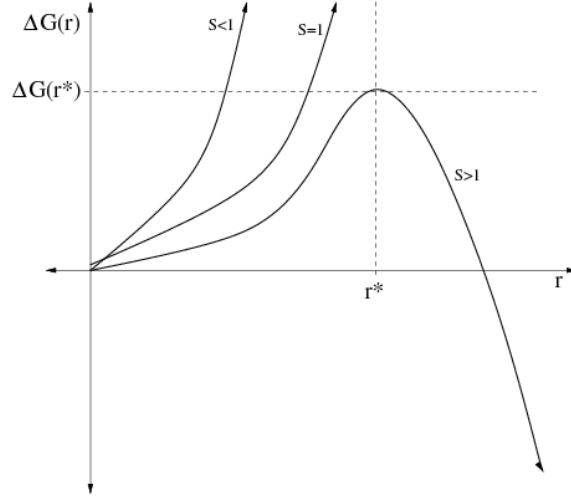


Figure 13: Free energy  $\Delta G$  as a function of droplet radius  $r$  at different saturation ratios  $S = \frac{p}{p_s(T)}$  [36]

The conclusion that this maximum change in free energy:

$$\Delta G_{max} = \frac{4\pi r^{*2} \sigma_L}{3} \quad (1.62)$$

is equal to one-third of the surface free energy for the whole nucleus was given by Gibbs [15] and illustrates the importance of surface properties for homogeneous nucleation [1].

As we can conclude from the previous illustration the critical drop radius is related to a certain supersaturation - the *critical supersaturation*. According to the *classical gas theory* even in an unsaturated vapor all sizes may exist even, because the kinetic energy of a molecule caused by the attractive forces between molecules comply with the *Boltzmann* distribution. Consequently their numbers would be subject to random fluctuations proportional to  $e^{-\frac{\Delta G}{kT}}$  with the result that clusters are in principle formed continuously but unstable and continuously disintegrate [20]. The number concentration  $n(r)$  of cluster with radius  $r$  as a function of the mentioned thermic fluctuation can be written as:

$$n(r) \approx n(1)e^{-\frac{\Delta G(r)}{kT}} \quad (1.63)$$

where  $n(1)$  indicates the number concentration of individual molecules. This relation will be valid as long as the number of cluster is negligible compared with the number of individual molecules. It shows that, since  $\Delta G$  for a cluster increases steadily with size although in principle all sizes would exist.

However with increasing saturation ratio the number concentration of clusters increases and therefor the probability for the formation of transient agglomerates having

a size that exceeds  $r^*$  will increase too. Similar to the relation for  $n(r)$  the number concentration of stable clusters can be defined as

$$n(r^*) \approx n(1)e^{-\frac{\Delta G(r^*)}{kT}} \quad (1.64)$$

by applying the critical radius  $r^*$  given by the *Kelvin* equation and the related free energy  $\Delta G^*$ . Once such an *agglomerate* exceeds the critical radius it becomes stable and grows by condensation to form a large particle.

Finally the main object is to estimate the rate of formation of nuclei of critical size. Under the simplifications of considering the case of a steady-state situation in terms of supersaturation preservation<sup>14</sup> the flux  $J$  of cluster passing the state of critical size can be defined as:

$$J \approx Zcn(1)e^{-\frac{\Delta G^*}{kT}} \quad (1.65)$$

where  $\Delta G^*$  denotes the free energy required to form a nuclei with critical radius  $r^*$ . The *Zeldoviche* factor  $Z = \frac{1}{n_c}(\frac{\Delta G^*}{3\pi kT})$  including the number of molecules in the critical nucleus  $n_C$  [1] describes the kinetics of the nucleation process [36].  $c$  indicates the capture rate - the number of adsorbed vapor molecules per unit time and  $n(1)$  is the number of individual molecules according to the ideal gas law  $n(1) = \frac{pV}{kT}$ . Thus the full equation of the flux  $J$  reads as follows [20]:

$$J = 2n^2 A_C^2 \sqrt{\frac{RT}{M}} e^{-\frac{\Delta G^*}{kT}} \quad (1.66)$$

---

<sup>14</sup>Actually the growth of droplets will destroy the initial conditions and therefor the saturation ratio will decrease.

### 1.4.2 Fletcher Theory - Heterogeneous Nucleation

Compared with the homogeneous nucleation the heterogeneous nucleation is a process of particle formation and growth assuming the presence of condensation nuclei or ions. The availability of such a condensation nuclei relieves the formation of clusters with critical size (the so called *germs*). While homogeneous nucleation usually requires saturation ratios of 2 – 10, heterogeneous nucleation can occur at supersaturations of only a few percent[20]. Initially confining to insoluble nuclei obviously the interfacial free energy between cluster and particle is smaller than between vapor and cluster. Consequently the total energy needed for the formation of a droplet of critical size is smaller than in the event of homogeneous nucleation although the critical radius remains the same [11].

As contrasted with the free energy  $\Delta G_{hom}$  required for drop formation in homogeneous nucleation

$$\Delta G_{hom} = n_L(\mu_L - \mu_V)V + \sigma_L A \quad (1.67)$$

in the case of heterogeneous nucleation the needed energy  $\Delta G_{het}$  becomes:

$$\Delta G_{het} = n_L(\mu_L - \mu_V)V_L + \sigma_L A_{LV} + (\gamma_{SL} - \sigma_S)A_{SL} \quad (1.68)$$

Since  $\gamma_{SL}$  is always smaller than  $\sigma_L$  and the volume including liquid molecules and therefor the number of liquid molecules required  $n_L$  decreases equal to the condensation nucleus volume it follows that  $\Delta G_{het} < \Delta G_{hom}$ . Regarding figure 14 one can geometrically deduce the newly introduced quantities as a function of particle radius  $R$  and contact angle  $\theta$ :

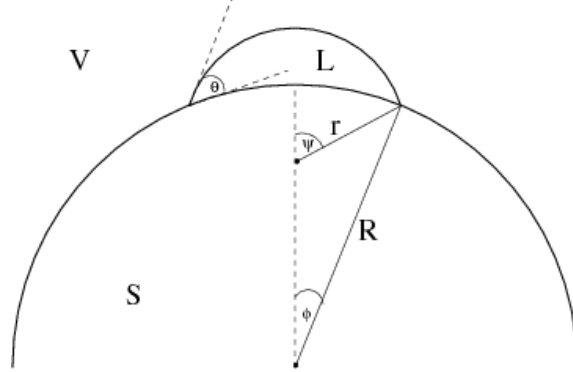


Figure 14: Draft of a cluster on the surface of an insoluble solid particle[32]

$$A_{LV} = 2\pi r^2 (1 - \cos\psi) \quad (1.69)$$

where  $\cos\psi$  is a function of the contact angle  $\theta$  the particle radius  $R$  and the germ radius  $r$ :

$$\cos\psi = -\frac{r - R\cos\theta}{\sqrt{R^2 + r^2 - 2Rr\cos\theta}} \quad (1.70)$$

and

$$A_{SL} = 2\pi R^2 (1 - \cos\phi) \quad (1.71)$$

including  $\cos\phi$  as a function of  $R$ ,  $r$  and  $\theta$

$$\cos\phi = \frac{R - r\cos\theta}{\sqrt{R^2 + r^2 - 2Rr\cos\theta}} \quad (1.72)$$

Since the steady state condition for the droplet refers only to an equilibrium with the surrounding vapor phase the critical radius  $r^*$  remains the same as for homogeneous nucleation. By plugging the terms  $r^*$ ,  $A_{SL}$  and  $A_{LV}$  in equation 1.68 one receives the free energy required to form a stable droplet:

$$\Delta G^* = \frac{16\pi\sigma_L^3}{3 \left[ n_L k T \ln \left( \frac{p}{p_0} \right) \right]^2} f(\cos\theta, x) \quad (1.73)$$

with

$$\begin{aligned} 2f(\cos\theta, x) = & 1 + \left[ \frac{1 - x\cos\theta}{g} \right]^3 + x^3 \left[ 2 - 3 \left( \frac{x - \cos\theta}{g} \right) + \left( \frac{x - \cos\theta}{g} \right)^3 \right] + \\ & + 3x^2\cos\theta \left[ \frac{x - \cos\theta}{g} - 1 \right] \end{aligned} \quad (1.74)$$

,

$$x = \frac{r^*}{r} = \frac{r n_L k T \ln \left( \frac{p}{p_0} \right)}{2\sigma_L} \quad (1.75)$$

and

$$g = \sqrt{1 + x^2 - 2x\cos\theta} \quad (1.76)$$

Obviously  $\Delta G^*$  strongly depends on the surface tension  $\sigma_L$  and the contact angle  $\theta$  (both parameter influence the free energy in the third power). The critical free energy again influences the nucleation rate exponentially. Consequently an accurate determination of the surface tension and the contact angle is essential for any prognoses concerning nucleation rates.

Compared with the nucleation rate derivated for homogeneous nucleation the formation of particles in the case of heterogeneous nucleation can not explained by random fluctuations. Since the now observed system originally includes condensation nuclei the vapor molecules will most notably conglomerate on surface of the already existing surfaces. Therefor the determining physical process will be molecule adsorption and diffusion on the nucleus surface. Consequently the number concentration of particles having critical size must be redefined as follows:

$$n(r^*) = n'(1)4\pi R^2 e^{-\frac{\Delta G^*}{kT}} \quad (1.77)$$

the number of germs  $n(r^*)$  having critical size and including a condensation nucleus of radius  $R$  may be Boltzmann distributed, but has to be modified by  $n'(1)4\pi R^2$  the number of adsorbed molecules on the surface of the condensation nucleus. Thus the nucleation rate  $J_P$  of germs per particle is given by:

$$J_P = B4\pi^2 R^2 r^{*2} n'(1) e^{-\frac{\Delta G^*}{kT}} \quad (1.78)$$

assuming a germ surface of  $r^{*2}\pi$  and an impaction rate  $B$  per unit area for individual molecules. In order to get the nucleation rate per aerosol one assumes that the nucleation rate per particle is small compared to the growth velocity of a droplet. In other words one excludes the case of multiple germ formation on a single condensation nucleus.



After several calculations including the time development of activated particles  $N(t)$ <sup>15</sup> one results in the following expression for the “real” nucleation rate of heterogeneous nucleation:

$$J = N_0 B 4\pi^2 R^2 r^{*2} n'(1) e^{-\frac{\Delta G^*}{kT}} e^{-B 4\pi^2 R^2 r^{*2} n'(1) e^{-\frac{\Delta G^*}{kT}} t} \quad (1.79)$$

As one can clearly see the so derived expression for the heterogeneous nucleation rate differs from the one found for the homogeneous case. Obviously the heterogeneous nucleation rate is time dependent and includes the particle concentration. Although both the homogeneous as well as the heterogeneous nucleation rates bear the same meaning they can not be compared due to the different dependencies occurring. E. g. plugging in a contact angle of  $180^\circ$  in equation 1.79 what corresponds to the case of homogeneous nucleation the so calculated nucleation rate will differ from the one resulting from equation (1.66).

---

<sup>15</sup>In aerosol physics activated particles are those droplets including a condensation nucleus and exceeding the critical size

## 2 Measurement Methods

### 2.1 Determination of Surface Tension

#### 2.1.1 Introduction

In the past decades a wide range of measurement methods have been developed to determine surface tension. First of all they can be distinguished in investigations of the equilibrium between surface forces and other mechanical forces and observations of dynamic surface phenomena. Hereafter a distinction is made between static and dynamic measurements. While static methods principally leave the observed surface as it is dynamic measurements are based on a continuous surface deformation. As a consequence static methods can be used to determine appropriate absolute resp. equilibrium values whereas dynamic ones are rather proper for studies of dynamic resp. time dependent surface properties, e. g. the time dependent influence of surfactants on surface tension [22]. In the following i am giving a general overview of the most common measurement methods, their applications and their pros and cons. From a historical viewpoint Du Noüy developed in 1919 the first surface tension measurement instrument [31]. Although originally intended for the determination of absolute time independent values and therefore principally a static method nevertheless the *Du Noüy Ring method* is based on a surface modification. In the ring method the liquid is raised until contact between a thin metal ring suspended from a balance and the liquid surface is registered. The sample liquid is then lowered again so that the film produced beneath the ring is stretched. At the same time the change in force as the distance of the ring from the surface increases is recorded. As the film is stretched before it is snapped off the maximum force can be determined and afterwards used to calculate the surface tension. Provided that:

- the ring was adjusted parallel to the liquid,
- the contact angle between liquid and ring was zero when the maximum force was recorded and
- the density of the liquid under study was known and remained constant during measurements

the calculated value is trustable.

Another static method is the *Pendant Drop method*. Based on the geometrical drop shape analysis the pendant drop method applies the Young-Laplace equation  $\sigma_L = \frac{\Delta P}{\frac{1}{r_1} + \frac{1}{r_2}}$  to calculate the surface tension. Generally performed by producing a drop surrounded by air this method can also be applied for the determination of interfacial tensions. In doing so the drop under study is placed into another liquid which has to have a lower density in order to eliminate buoyancy effects.

So, too, the *Spinning Drop method* applies the drop geometry to calculate the desired value. Unlike the pendant drop method the diameter of a drop within a heavy phase is measured while both are rotated and therefore the spinning drop method is “just” qualified for measurements of low interfacial tensions.

An example for dynamic surface tension measurements is the *Maximum Bubble Pressure method* - a measurement technique developed for the determination of “short age” surface tensions. By producing gas bubbles through a capillary which

is immersed into the sample liquid, the pressure of each bubble is recorded. In the course of this the maximum bubble pressure ( $\leftrightarrow r_{capillary} \equiv r_{bubble}$ ) can be determined and the surface tension can be calculated out of it.

Depending on the desired surface property - high or low surface/interface tension, time dependent or static value - one must choose the appropriate method out of the wide range of options. In the case of surface tension and contact angle determination as a function of temperature the Wilhelmy Slide method turned out to be the most practical one. On the one hand the very same experimental setup can be used to obtain both the surface tension as well as the contact angle and on the other hand the simple geometric assumptions on the samples facilitate repeatable measurements.

### 2.1.2 Wilhelmy Slide Method

The most significant advantage of the Wilhelmy Slide method is to require no corrections for the measurement values. That is to say, that the measured value can be directly converted to the desired result. E.g. by applying the already mentioned du Noüy ring method [31] one must know the liquids density to subtract the weight of the volume of liquid lifted beneath the ring from the measured maximum force as it also affects the balance. In addition to this complication measurements with the ring method include a permanent reformation of the surface or interface due to the movement of the ring. If the ring is moving with high velocity, but also if solutions of large molecules or with high viscosities are to be studied, the maximum force is obtained when the diffusion equilibrium at the surface or interface may still not be reached. The problem caused by this dynamic effect does not occur with the plate method. Another advantage of the plate method as compared to is that it is not restricted to static surface tensions but also dynamic contact angles and wetted lengths can be measured by simply modifying the test sequence as compared to all other surface tension measurement methods mentioned.

The Wilhelmy method is based on the measurement of the force acting on a roughened platinum-iridium plate in contact with the liquid under study. Suspended from a balance the plate is firstly immersed into the probational liquid until a preassigned depth of immersion is reached. Subsequently the now wetted plate is withdrawn until the bottom edge of the plate is at the level of the undisturbed liquid surface (see Fig. 15).

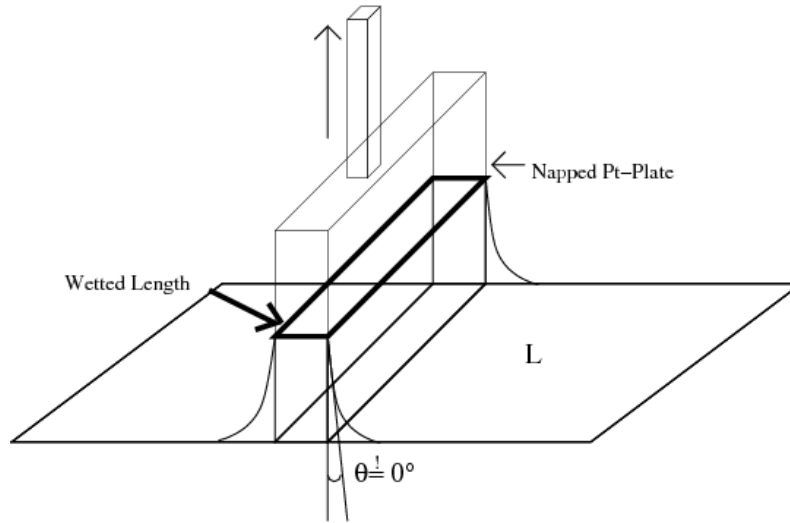
Based on the mechanical interpretation of surface tension as a force acting along the borderline of the surface per unit length  $[\frac{mN}{m}]$  one can calculate the surface tension by knowing the perimeter  $l$  of the immersed plate and providing that the contact angle between plate and liquid is zero. A schematic diagram of the experimental setup with the force compensated by the balance is shown in the following figure 15:

Since we assume perfect wetting by the liquid the measured force acting on the plate is solely caused by the liquid's surface tension  $\sigma_L$  can be used to calculate  $\sigma_L$  in the following way:

$$\sigma_L = \frac{|\vec{F}|}{l} \quad (2.1)$$

whereas  $l$  is the wetted length i.e. the perimeter of the plate and  $|\vec{F}|$  is the force measured by the balance.

In order to satisfy the criteria of zero contact angle the plate is made of a substance with high surface tension  $\sigma_S$  and additionally napped to take advantage of the

Figure 15: *Schematic profile of the slide method*[22]

mentioned capillary adhesion effect (figure 11). Furthermore in order to guarantee an optimal wetting the depth of immersion has to be adjusted to the magnitude of surface tension<sup>16</sup>. By taring the balance at the beginning of every measurement the influence of the weight of the plate on the measured force is excluded and by suspending the plate parallel to the liquid surface also the required perimeter is given by the geometry of the plate.

- Determination of wetted lengths

Performing the same test sequence one can besides surface tension determinations also obtain the wetted length  $l$  of a probational plate. The only variation is to use a liquid with known surface tension which has a contact angle of zero on any solid surface. Once these conditions are met the wetted length of the plate can be determined from the following equation:

$$l = \frac{|\vec{F}|}{\sigma_L} \quad (2.2)$$

For its low surface tension ( $\sigma_L = 18.4 \frac{mN}{m}$  at  $T = 20^\circ C$ ) usually n-hexan is used as probational liquid.

Compared to the conventional determination using a gauge the mentioned method is more time-consuming without leading to more precise values. Thus its application is not generally advisable.

However the adaption of the *Wilhelmy slide method* provides an opportunity to check the correct suspension of plate. As will become apparent in chapter 4 an alignment of the plate in parallel with the liquid surface becomes difficult at low temperatures. In this case a correspondence between the wetted length determined with the Wilhelmy method and the previously gauged perimeter confirms a correct suspension of the plate.

<sup>16</sup>Experimental experience showed that the necessary depth of immersion increases with increasing value of the surface tension of the liquid (see chapter 5.1.1).

## 2.2 Determination of Contact Angle

Principally contact angles are measured in order to determine the surface tension of solids. According to the immobility of the surface atoms of a refractory solid a distinction between static and dynamic measurement methods can not be made. However depending on the used method resp. sequence of measurement different contact angles (see chapter 1.3) that are either  $\theta_e$ ,  $\theta_a$  or  $\theta_{hyst} = \theta_a - \theta_r$  can be measured. The various techniques for measuring contact angles have been reviewed in detail by Neumann and Good [17]. In the following just the methods applied in the present study will be described.

### 2.2.1 Sessile Drop Method

The most commonly used method is that measuring  $\theta$  directly from a liquid drop resting on a flat solid surface. By simply viewing a sessile drop through a comparator microscope fitted with a goniometer scale the angle can be read off immediately. On the one hand this method allows the determination of the “equilibrium” contact angle by stabilizing the volume of the drop and on the other hand by increasing/decreasing the volume the advancing/receding angle can be measured too. Since the drop volume has to be small<sup>17</sup> in order to exclude gravitational influences on the drop shape the sessile drop method is inappropriate for not thermostated measurements with low boiling point liquids.

As well as for the *Pendant Drop method* the surrounding air can be replaced by another liquid (see Fig. 16) and therefore the interfacial tension between solid and liquid can be calculated from contact angle measurements.

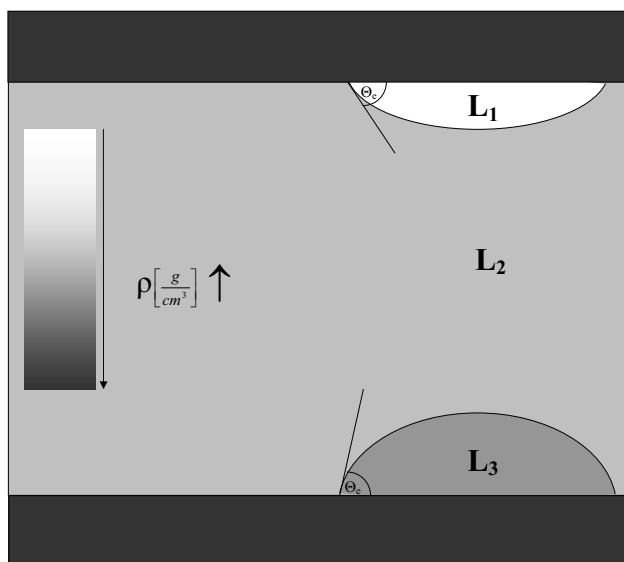


Figure 16: Illustration of both applicabilities by performing the sessile drop method - liquid density decreases with increasing lightness

<sup>17</sup>Usually the drop volume amounts to some microliter

### 2.2.2 Dynamic Wilhelmy Method

Neumann *et al.* [29], [30] have developed the Wilhelmy slide technique into a method capable of providing contact angles to high precision. As shown in figure 17 the meniscus at partially immersed plate rises to a definite height  $h$  if  $\theta$  is finite.

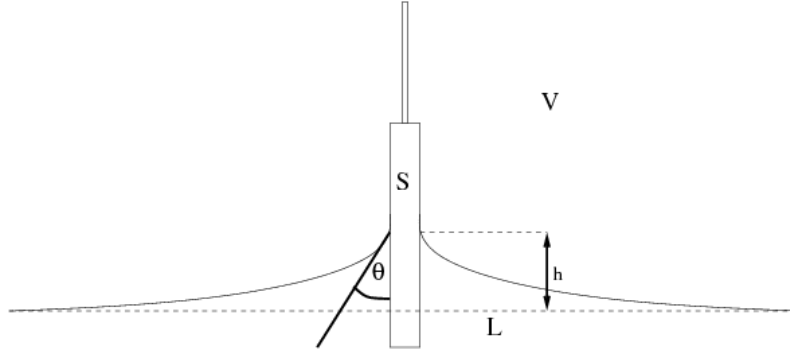


Figure 17: *Neumann's method for contact angle measurement* [1]

Unless the contact angle is small the termination of the meniscus and therefore the height of capillary rise  $h$  is sharp under proper illumination. By applying the experimentally determined property  $h$  in the following equation the desired contact angle can be given to  $0.1^\circ$  precision [1].

$$\sin\theta = 1 - \left(\frac{h}{a}\right)^2 \quad (2.3)$$

where  $a$  is the capillarity constant of the liquid defined by:

$$a^2 = \frac{2\sigma_L}{\Delta\rho g} = rh \quad (2.4)$$

Since this technique assumes a not too small contact angle as a consequence of the optical analysis it is unsuitable for the posed problem.

In contrast to the restrictions by performing the *Neumann method* the *Dynamic Wilhelmy Method* affords the opportunity to measure a wide range of contact angles applying principally the same experimental setup. By merely modifying the measurement cycle a calculation of average advancing and receding contact angles is possible. The sole variation is to immerse the sample plate first into the liquid reaching a fixed depth  $d$  and then withdrawing the plate from the liquid until the lifted liquid film is snapped off. During the cycle the force acting on the plate suspended from a balance is recorded and afterwards evaluated to get the desired contact angles. As already mentioned the measured contact angles are no equilibrium values since by immersing the advancing angle  $\theta_a$  and by withdrawing the receding angle  $\theta_r$  appears. Figure 18 illustrates the occurring angles as a function of the direction of motion.

In addition to wetting force the buoyant force caused by the immersion of the plate into the liquid occurs. However, using an appropriate experimental procedure, as described below, an explicit determination of the buoyant force can be avoided.

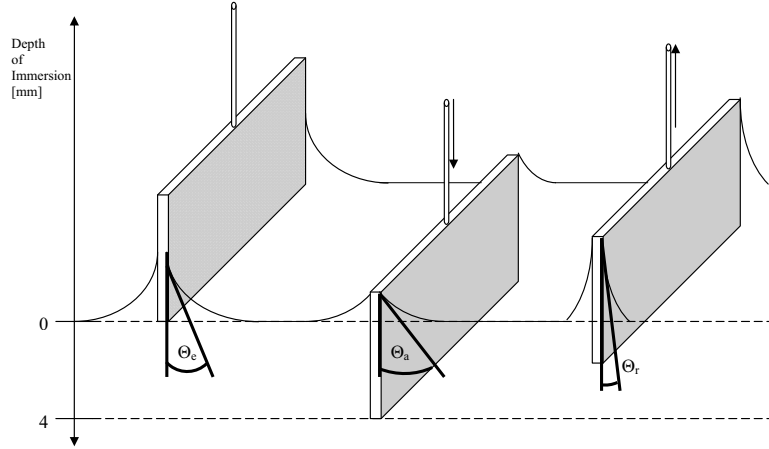


Figure 18: *Illustration of the occurring contact angles as a function of the plate's direction of movement in comparison with the contact angle occurring by holding the plate constant on liquid surface level*

For the cuboid shaped geometry of the plate the buoyant force increases linearly<sup>18</sup> with increasing depth of immersion. Since all sides of the solid must have the same properties the constant wetting force on the solid can be determined by fitting and extrapolating the measured points using a linear regression. An example for the described analysis is illustrated in figure 19:

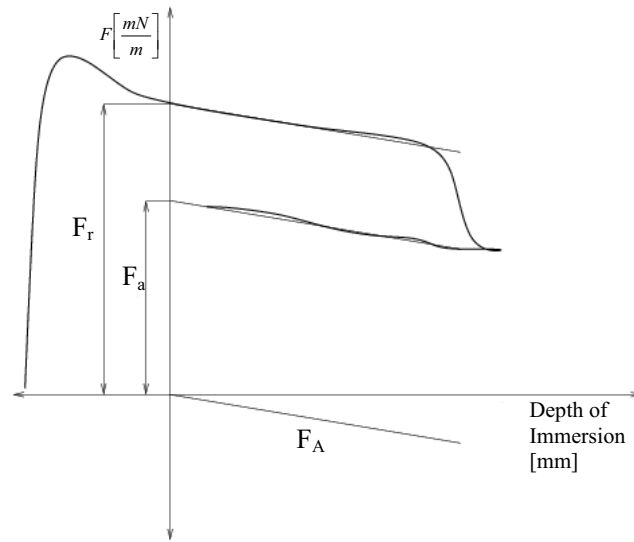


Figure 19: *Idealized measurement log of the dynamic Wilhelmy method [22]*

where the curve  $F_A$  illustrates the buoyant force caused by the suppression of liquid. As we can see the force acting on the plate decreases until the turning point is reached. Hereafter by withdrawing the plate the force curve initially jumps up which indicates the change from  $\theta_a$  to  $\theta_r$  and then with decreasing depth of immersion the

<sup>18</sup>For rectangular and cylindric solids the buoyant force increases linearly

measured points increase parallel to the buoyant force curve. Since the depth of immersion is zero for the marked values  $F_a$  and  $F_r$  any buoyant force influence is excluded. Consequently the marked forces are solely caused by wetting and therefore the contact angles  $\theta_a$  and  $\theta_r$  can be calculated from them as described below:

The total force acting on the plate  $F_{tot}$  is given by:

$$F_{tot} = \begin{cases} F_a - F_A \\ F_r - F_A \end{cases} \quad (2.5)$$

where the upper line of the second part describes the immersing process and the lower line the withdrawing one. For a depth of immersion of zero the buoyant force disappears in both terms:

$$\lim_{d \rightarrow 0} F_{tot} = \begin{cases} F_a \\ F_r \end{cases} \quad (2.6)$$

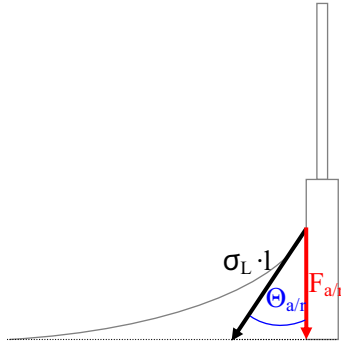


Figure 20: Illustration of the forces acting on a plate by performing the dynamic Wilhelmy method

according to Fig. 20 both the receding and the advancing contact angle can be calculated by knowing the surface tension of the liquid  $\sigma_L$  and plate perimeter  $l$  as follows:

$$\cos\theta_a = \frac{F_a}{\sigma_L l} \quad (2.7)$$

$$\cos\theta_r = \frac{F_r}{\sigma_L l} \quad (2.8)$$

Finally it should be mentioned that the velocity the plate is immersed and withdrawn might possibly influence the measured contact angles. As stated in [?] former investigations resulted in an increase in contact angle hysteresis ( $\theta_a - \theta_r$  with increasing velocity).



### 2.2.3 Washburn Method

If the analysed solid is available just in powder form the Washburn method provides an opportunity for determinations of contact angle between liquids and powders by sorption. The powder to be measured is filled into a glass tube with a filter base and this is suspended from the balance. After the vessel has contacted the liquid the speed at which the liquid rises through the bulk powder is measured by recording the increase in weight as a function of time.

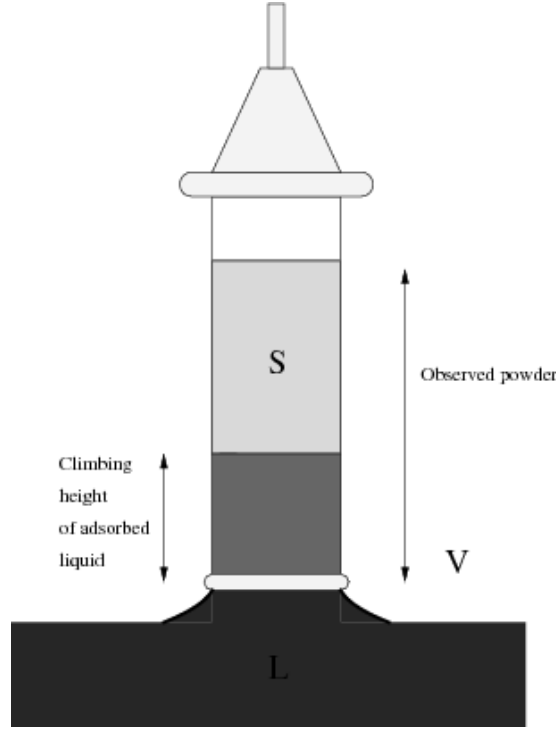


Figure 21: *Scheme of the Washburn method*[22]

Performing the capillary rise method the powdery solid is assumed to be a bundle of capillaries as the name implies. According to the Washburn theory [38] the rise of liquid into the pores of the solid due to capillary action will be governed by the following equation:

$$\cos\theta_a = \frac{1}{c} \frac{m^2}{t} \frac{\eta}{\rho^2 \sigma_L} \quad (2.9)$$

whereas  $\eta$ ,  $\rho$  and  $\sigma_L$  indicate the known viscosity, density and surface tension of the observed liquid. Before being able to calculate the contact angle by monitoring the mass of liquid which rises into the porous solid as a function of time the material constant  $c$  has to be determined. By performing the experiment with a liquid which is known to have a contact angle of zero<sup>19</sup> on the solid the solid material constant is the only remaining unknown in the above equation and can thus be specified. This constant contains information regarding the pore structure, pore size, and number of pores in the solid sample and will therefore remain constant during an experiment for the resulting contact angle measurements to be correct. Once  $c$  has been determined for a analysed solid, a second sample of the solid can be tested for wettability

<sup>19</sup>Due to its low surface tension of  $18.4 \frac{\text{mN}}{\text{m}}$  typically n-hexan is used

by another liquid. The material constant determined by the n-hexane test is simply used in the Washburn equation, in combination with  $\frac{m^2}{t}$  data obtained during testing with the second liquid. This allows calculation of the contact angle between the second liquid and the solid and the capillary climbing velocity of the liquid. Since the reproducibility of the mentioned material constant is rather low the Washburn is not suited as a method to determine absolute values but quite helpful to get a qualitative information concerning for the behavior of the liquid<sup>20</sup>.

---

<sup>20</sup>In the chapter *Results and Discussions* i will go more in detail with this estimations

### 3 Experimental Setup

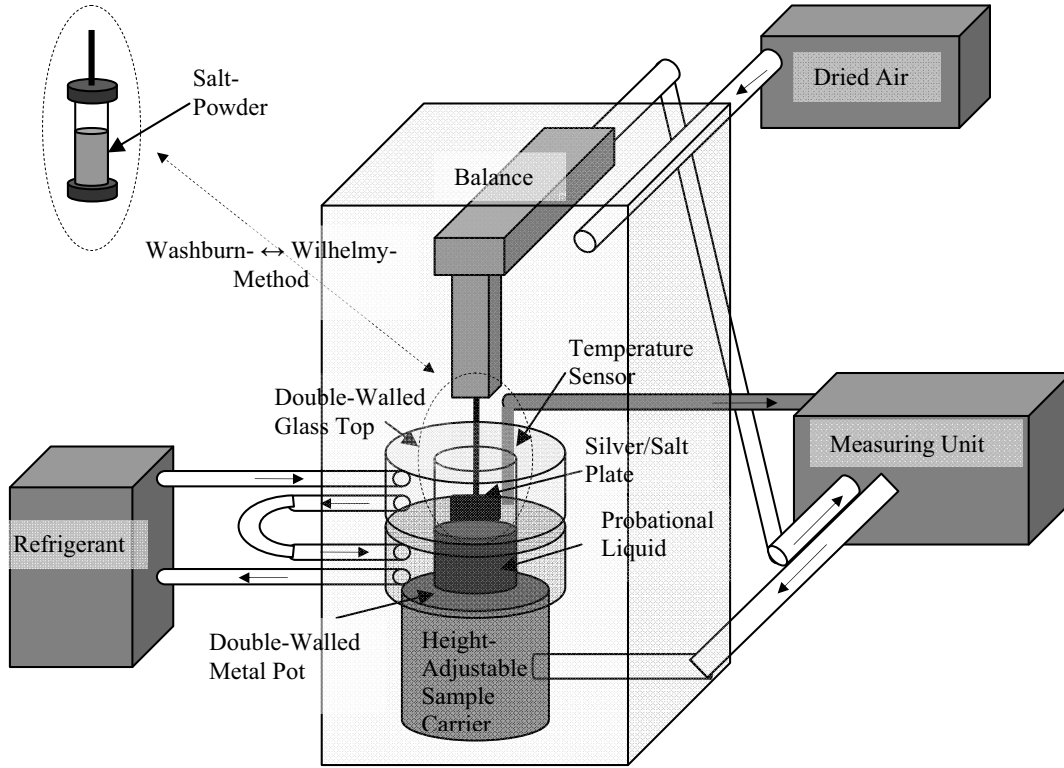


Figure 22: Draft of the measuring setup

All measurements (surface tensions, wetted lengths, material constants, contact angles) were performed using a *Company KRÜSS K12/3* tensiometer. A process-controlled measurement instrument to determine surface properties with the aid of a probe suspended from a precision balance. A height-adjustable sample carrier is used to bring the probational liquid into contact with the probe. As soon as the probe touches the surface the force acting on the balance is recorded and can be used to calculate surface tension, contact angle etc. from it. Application units such as the cooling attachment, the dry-air supply and the double-walled glass top were integrated in the course of the present study to create optimal conditions for measurements at low temperatures.

Measuring instructions given in [23] can be applied for measurements at room temperature as there is no need to apply the above mentioned applications.

### 3.1 Measurement procedure at temperatures $T_M$ different from room temperature $T_R \approx 26^\circ C$

First and foremost the highly sensitive balance must be immovably fixed.

As the process to equilibrate the temperature for the system (liquid, solid and surrounding air) is the most time-consuming one during the whole measurement, the supplies of refrigerant and dried air were started before the probes were installed.

Enroute from the refrigerant box to the tensiometer (stretch of way amounts to  $\approx 260cm$ ) the temperature of the coolant raises as a function of the temperature difference between refrigerant  $T_C$  and room temperature  $T_R \dots$

$$\Delta T = T_M - T_C \longrightarrow \begin{cases} 0^\circ C & \text{if } T_C \rightarrow T_R \\ 3^\circ C & \text{if } T_C \rightarrow -10^\circ C \end{cases} \quad (3.1)$$

Thus a temperature sensor with a measuring accuracy of  $\pm 0.1^\circ C$  was placed next to the probes to define the process temperature  $T_M$ , (see Fig. 23).

In order to avoid contaminations of the probe-surfaces (liquid and solid) due to condensation of water vapor at low temperatures a dry-air supply was installed. The flow rate ( $\approx 3 \frac{l}{min}$ ) was chosen so that measurements were thereby not disturbed. The dry-air purging of the measurement chamber proved to be necessary for temperatures  $T_M$  lower than  $10^\circ C$ .

Subsequently the cleaned probes (plate<sub>Wilhelmy</sub>/filled glass tube<sub>Washburn</sub> and liquid) were applied to the tensiometer like shown in Fig. 22 and 23. Then the stage bearing the probational liquid was manually turned upwards to position the liquid surface as close as possible to the lower edge of the hanged plate. At the same time one must pay attention that on the one hand the plate does not touch the liquid and on the other hand its lower edge is parallel to the liquid surface. Not until everything was correctly adjusted the balance was disengaged from the fixation. After reaching a steady

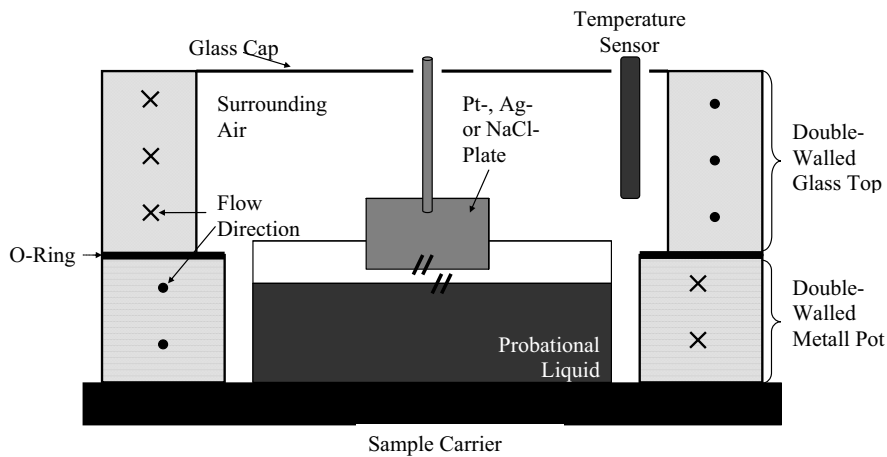


Figure 23: Profile of the measurement chamber

temperature <sup>21</sup> the required parameters such as depth of immersion, sensibility of the balance, number of recorded data etc. were finally entered into the measuring program.

By starting the measurement initially the balance was tarred and thereafter the cycle started considering previously entered parameters.

---

<sup>21</sup>... which was fixed after the temperature remained stationary for at least 5 minutes

## 4 Preparation of the Probes

### 4.1 Characterization of the Used Liquids

#### 4.1.1 Studied liquids

	<b>1-Propanol.</b> $CH_3CH_2CH_2OH$	<b>N-Hexan</b> $CH_3(CH_2)_4CH_3$	<b>Water</b> $H_2O$
<b>Surface Tension</b> $[\frac{mN}{m}]$	23.7	18.4	72.75
<b>Density</b> $[\frac{g}{ml}]$	0.802 – 0.802	0.695 – 0.661	0.998203
<b>Assay [%]</b>	> 99.5	> 99.5	> 99.9
<b>Viscosity</b> $[mPas]$	2.2227	0.68	1.0
<b>Ignition point</b> [46] $[^{\circ}C]$	385		

#### 4.1.2 Cleaning liquids

	<b>Propan-2-ol.</b> $(CH_3)_2CHOH$	<b>Propan-2-on (Aceton)</b> $(CH_3)_2OH$	<b>Toluol</b> $C_7H_8$
<b>Assay [%]</b>	> 99.8	> 99.5	> 99.5

### 4.2 Characterization of the Used Solids

#### 4.2.1 Silver plates

	<b>Sterling Silver Plate</b>	<b>Silver Powder p.A.</b>
<b>Assay [%]</b>	92.5	> 99.9
<b>Dimensions</b>	Thickness $\approx 0.5mm$	Grainsize $0.6 - 2\mu m$
<b>Density</b> $[\frac{g}{cm^3}]$	10.37	10.49
<b>Boiling point</b> $[^{\circ}C]$		2162
<b>Mohs hardness</b>	4 [47]	2.5

#### 4.2.2 Salt plates

	<b>NaCl Crystal</b> resp. <b>NaCl Powder</b>	<b>Glass Plate</b>
<b>Assay [%]</b>	99.9 <sup>22</sup> resp. > 99.5	$SiO_2 \approx 72$ $Al_2O_3 \approx 2$ $Na_2O \approx 14$ $CaO \approx 10$
<b>Density</b> $[\frac{g}{cm^3}]$	2.16	2.5
<b>Boiling point</b> $[^{\circ}C]$	1465	2230???
<b>Mohs hardness</b>	2.5 [48]	6-7

### 4.3 Preparation of the Silver Plates

For the first contact angle measurements the silver plates used in former experiments [32], [19] were applied. The obvious surface discoloration by oxidation was removed by polishing like described in [32]. After greasing a polishing application for the drill with fat-bounded aluminum oxide polishing paste and attaching the silver plates to a plane wooden board with double-sided tape the cleansing process was performed by gently pressing the fixed plates against the rotating drill attachment. In order to prevent stick and slip behavior of the contact line attention was payed that the polishing direction was perpendicular to the contact line as demonstrated in Fig. 24:

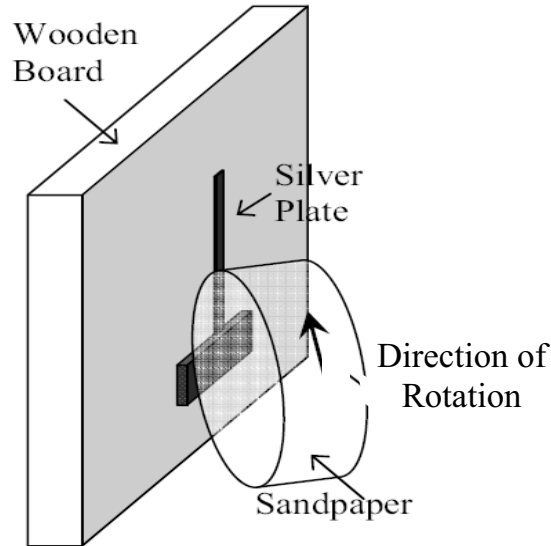


Figure 24: *Illustration of the polishing procedure showing the position of the plate in right coordination with the direction of rotation*

After removing the plates from the board they took a multi-stage cleaning in an ultrasonic bath. First of all they were cleaned 15 minutes in Toluol, afterwards another 15 minutes in Aceton to solubilize paste residuals and finally 15 minutes in high-purity water. Since water has a high contact angle on silver the liquid residuals dripped off and the plate were clean, dry and ready to get applied.

Unfortunately this polishing procedure caused not only visible scratches on the plate but also bends and thus the measured contact angles were not reproducible.

Consequently new probes were produced out of a 925 sterling silver plate (see table 3, column 2). After cutting the plate into small pieces ( $2 \times 1\text{cm}$ ) a goldsmith<sup>23</sup>

<sup>23</sup>Mr. Josef Karoly; Deutsch Wagram

polished the probes in order to get them as smooth as possible. Following polishing and cleaning steps were performed . . .

1. Grinding with an 800-grit sandpaper (*Company Norton*)
2. Polishing with an 1000-grit polishing paper (*Company Rusch*)
3. Soldering on copper wire for the suspension on the balance with a hard solder:
  - (a) 600 Silver solder L2 (*Company ÖGUSSA*); melting point at  $T \approx 700^\circ\text{C}$
  - (b) Borax(Natriumcarbonat flux)
  - (c) Boric acid in powder form to prevent the plates from discoloration caused by soldering
4. Pickling with diluted sulfuric acid to eliminate the oxide film at  $T \approx 60 - 70^\circ\text{C}$ <sup>24</sup> in an ultra sonic bath.
5. Cleaning with pumic powder (powdered volcanic rock) and commercially available soap under tap water.

In order to remove contaminations due to transport<sup>25</sup> an ultra sonic cleansing as mentioned before was performed.

Although no visible scratches remained measurements were still not reproducible and therefore another polishing procedure permitting more fine-grained steps was performed. Again it was stressed that the polishing direction parallels the afterwards during measurements occurring liquid/solid contact line (see Fig. 25).

1. Pre polishing with . . .
  - (a) 1000-grit polishing paper (*Company Kingspor*)
  - (b) 2400-grit silicon carbide paper (*Company Struers*)
2. Polishing<sup>26</sup> with . . .
  - (a) 4000-grit silicium-carbide paper
  - (b)  $3\mu\text{m}$  diamond-suspension
  - (c)  $0.04\mu\text{m}$  aluminum-oxide suspension (*OPS*)
3. Soldering on a copper wire with a soft solder for the suspension on the balance:
  - (a) *Soldomol 220* (silver-tin solder; *Company ÖGUSSA*); melting point at  $T \approx 270^\circ\text{C}$
  - (b) Flux *Puradin*(*Company ÖGUSSA*)
4. Cleaning in an ultrasonic bath as mentioned before.

Since the polished silver plates consist of 925 sterling silver a not negligible influence of the 7.5 percent copper content on the contact angle may cause a systematic error of the measurements. In order to prevent these influences the polished plates were additionally coated using the method of *physical vapor deposition* (*PVD*)

<sup>24</sup>A sort of freely chosen temperature to accelerate the proceeding

<sup>25</sup>After the mentioned polishing steps the silver plates were felt nested and preserved in an seal air-tighted box during the transport from goldsmith to university.

<sup>26</sup>The following polishing steps were performed by *Ms. Rohrer* (University of Vienna; Group *Dynamics of Condensed Systems*)



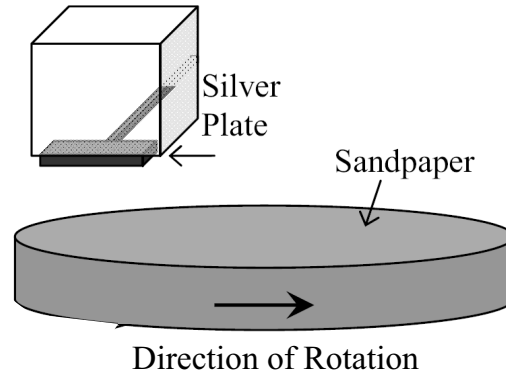


Figure 25: *Illustration of the polishing procedure performed by Ms. M. Rohrer*

which is a variety of vacuum deposition and is a general term used to describe any of a variety of methods to deposit thin films by the condensation of a vaporized form of the material onto various surfaces. As its name implies this kind of coating involves purely physical processes such as high temperature vacuum evaporation or plasma sputter bombardment. Fig. 26 shows a schematic diagram of the setup for this method: It can be seen that the vapor deposition takes place in a vacuum cloche - to be more precise under “low” vacuum at a pressure of  $\approx 10^{-5} - 10^{-4} \text{ mbar}$ .

At the beginning about  $0.02g$  of the silver powder mentioned in chapter 4.2.1; spherical, APS  $0.6 - 2\mu m$  is filled into a tungstic shuttle. Subsequently over this shuttle the solid surface to be vaporized is perpendicularly fixed. Then the material to be deposited - in this case the silver powder - is heated to a high vapor pressure by electrically resistive heating of the tungstic shuttle. Consequently a thin silver film will deposit by condensation of the vaporized powder onto the target placed above the tungstic shuttle.

Depending on the amount of vaporized solid and its elemental structure the produced film thickness amounts to  $10^{-9} - 10^{-6} m$ .

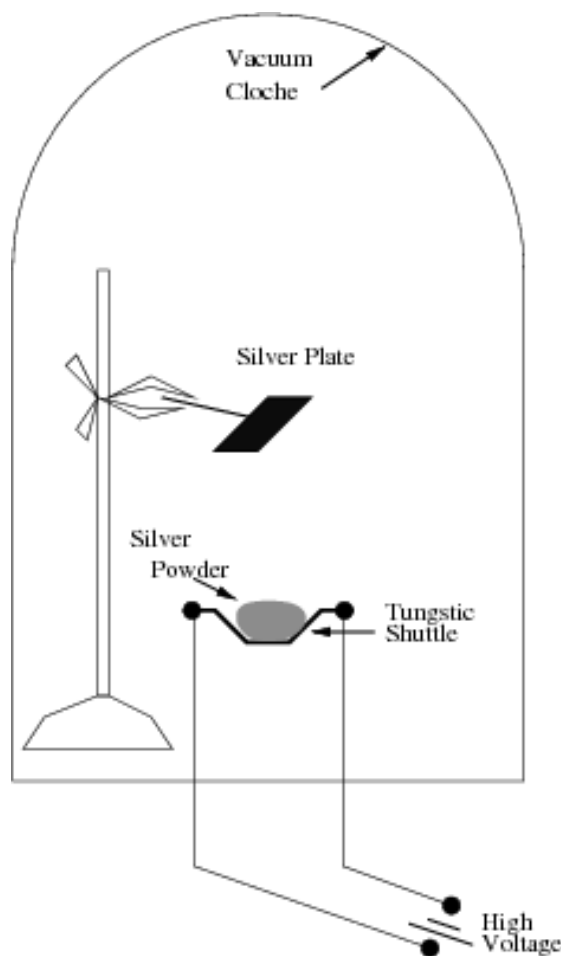


Figure 26: Scheme of PVD

## 4.4 Preparation of the Salt Plates

### 4.4.1 Polished salt crystals

The first generation of salt plates for contact angle measurements performing the dynamic *Wilhelmy* method was made out of a mechanically treated salt crystal. Potentiometric analysis<sup>27</sup> confirmed the assumption that the initial crystal consists completely of sodium chloride - except of surface impurities.

Using the same sandpapers as stated in *Preparation of the Silver Plates-Cycle 3* water as refrigerant had to be replaced by 1-propanol otherwise the crystal would have been dissolved during the polishing process. For the same reason not the diamond- and aluminumoxide- suspensions (both including water) were applied but a  $0.25\mu\text{m}$  polishing paste.

After removing paste residuals by rinsing the plates with 1-propanol the copper wires for the suspension on the balance were stuck on the plates with superglue. Since the glue spread to much on the salt plates and therefore the remaining pure salt surface would have allowed a immersion-depth of only  $1 - 2\text{mm}$  the suspensions for the next plates were not glued on anymore but stuck between copper wire.

<sup>27</sup>University of Vienna, Faculty of Chemistry

#### 4.4.2 Untreated salt crystals

Based on the same salt crystals the probational plates were this time made without modifying their natural surface. By wedging the crystal carefully salt plates of the desired shape were produced.

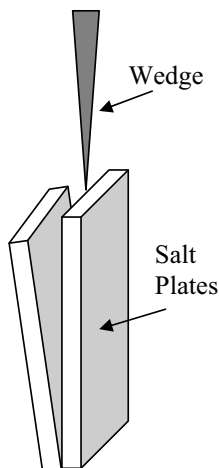


Figure 27: *Scheme of the preparation of natural shaped salt plates*

As already mentioned the advantage of this method is to preserve the natural structure particularly the positions of the surface molecules. Thus the initial surface tension related to the crystal structure will be unchanged and the measured contact angle will not be influenced by surface modifications (see chapter 1.3.1).

#### 4.4.3 Coated glass plates

The third generation of salt plates was made by *PVD*. Starting from cleaned glass plates jammed in wire as already mentioned in *Cycle1* a salt layer was deposited performing *PVD* similar to *Silver plates - Cycle 3*. Since the used salt powder mentioned in chapter 4.2.2 clearly had a lower density then the silver powder a bigger tungstic shuttle had to be applied to guarantee a complete coating of the glass plates.

The so produced salt film is very fragile because the configuration of the condensed molecules on the glass surface does not correspond to the natural ionic crystal structure of sodium chloride and therefore their intermolecular binding is lower compared to ionic bond. Even the humidity of the surrounding air may cause a destruction of the film. For that reason the salt plates were stored in argon.

### 4.5 Cleansing of the Samples During Measurements

As already mentioned in detail a basic prerequisite for convincing results of surface properties is the purity of the observed surface. The slightest contamination will lead to wrong values. Thus a thorough clean-up of the solid samples was conducted at the beginning of every individual measurement. In order to exclude a contamination of the liquids their surface tensions were controlled at 5 measurement intervals.

Plates and vessels for the liquids/solid powders were taking a cleaning as follows . . .

- At the beginning of every measuring day <sup>28</sup> the glass jar for the observed liquids were . . .
  1. degreased with Aceton p. A.,
  2. rinsed out with water p. A.,
  3. heated with a *Bunsen* burner,
  4. once again rinsed out with water p. A. and
  5. finally rinsed out with the afterwards observed liquid.
- Plates for the Wilhelmy Method
  1. As per cleaning advice [22] the platin plate<sup>29</sup> was . . .
    - (a) degreased with Aceton p. A.,
    - (b) rinsed out with water p. A. and
    - (c) finally heated with a *Bunsen* burner up to red-heat
  2. All silver plates were rinsed off with liquids in the following order. . .
    - (a) Propan-2-ol p.A
    - (b) Aceton p.A.
    - (c) Water p.A.
  3. Concerning theirs solubility the salt plates were only rinsed off with 1-Propanol
- Probes for the Washburn Method
  1. cleansing of the glass tube for the powder similar to the procedure mentioned for the glass jar
  2. applying a new filter before each measurement
  3. pouring in a weighed ( $\approx 2g$ ) amount of the natrium chloride powder mentioned in chapter 4.2.2
  4. shaking the stuffed glass tube 100 times to increase the reproducibility of the material constant

---

<sup>28</sup>Of course also when the surface tension checks indicated a contamination of the liquid

<sup>29</sup>For surface tension measurements

## 5 Temperature dependence of the contact angle for 1-propanol on silver

In order to determine the contact angle between silver and 1-propanol the *Dynamic Wilhelmy Method* was used (see chapter 2.2.2). The results will be classified according to the number of PVD steps used for coating the probes. Therefore a distinction will be made between  $0\times$ ,  $1\times$  and  $2\times$  coated plates. Additionally the results obtained for not coated plates will be differentiated according to the various polishing procedures exerted (see chapter 4.3).

Since surface contaminations of the plate by the probational liquid can only be excluded at the first time the cleaned plate is immersed (see chapter 1.3) solely  $\theta_a$  data will be evaluated to determine the desired contact angle. To be more precise each plate was cleaned like mentioned in 4.5 after immersing and withdrawing it once. All data not specified in this chapter and furthermore all not rounded values are listed below in the appendix. Therefore the respective sections will be referenced at their headlines.

### 5.1 Surface Tension during measurements (see appendix A.1)

At the beginning of every contact angle measurement apart from the wetted length the surface tension of the liquid must be determined. At this point it should be mentioned that the measured surface tensions turned out to be not only dependent on the purity of the probes but also on the depth of immersion of the plate, which consisted of a platinum-iridium alloy with and had an extent of  $19.9\text{mm} \times 0.1\text{mm}$ .

Performing surface tension measurements with various depths of immersion for water p.A and 1-propanol it turned out that an immersion depth of  $4.5\text{mm}$  is required for water whereas  $2\text{mm}$  last for 1-propanol. This difference might be explainable by the different amounts of surface tension:  $\sigma_L = 72.75 \frac{\text{mN}}{\text{m}}$  for water p. A and  $\sigma_L = 23.7 \frac{\text{mN}}{\text{m}}$  for 1-propanol p. A. at  $20^\circ\text{C}$ . Qualitatively spoken the higher the surface tension the deeper the plate must be immersed to condition the surface properly.

At the beginning and at the end of every measurement cycle<sup>30</sup> the surface tension of the liquid under study (1 – Propanol) was checked. Results are plotted in the following graph:

---

<sup>30</sup>A Cycle is meant by a series of contact angle measurements (max. 5 measurements) at constant temperature.

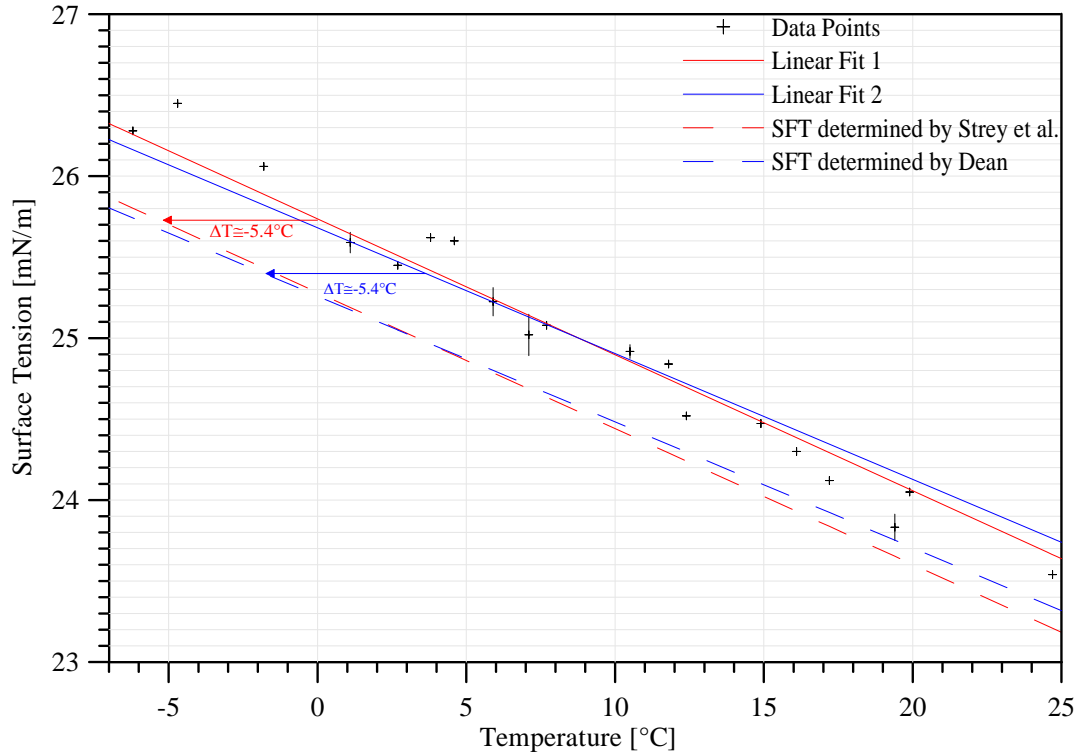


Figure 28: Experimental data for surface tension of 1-propanol compared with the curves determined by Strey [35] and by Dean [9] - Linear Fits 1 respectively 2 are chosen parallel to [35] respectively [9]

The above illustrated graph (Fig. 28 shows a comparison between the measured surface tension data (*black crosses*) and the already quoted surface tensions for 1-propanol on the one hand determined by Strey and Schmeling [35] (*dashed red line*) and on the other by Dean [9] (*dashed blue line*).

Both linear regressions through measurement data are based on the previously determined functions which are:

$$\sigma(T) = 48.21 - T(K) \cdot 0.08394 \quad (5.1)$$

for  $\sigma^{1-propanol}(T)$  stated by Strey and Schmeling [35] respectively

$$\sigma(T) = 25.26 - T(^{\circ}C) \cdot 0.0777 \quad (5.2)$$

according to Dean [9]. Considering figure 28 it turns out that the measured surface tensions obviously exceed the above mentioned functions. Thus a modification of equation 5.1 and 5.2 is necessary to fit the data.

Introducing a variable parameter  $A$  which is shifting the value of  $T(K)$  in both cases:

$$\sigma(T) = 48.21 - (T(K) + A) \cdot 0.08394 \quad (5.3)$$

$$\sigma(T) = 25.26 - (T(^{\circ}C) + A) \cdot 0.0777 \quad (5.4)$$

gives on the one hand

$$\sigma(T) = 48.21 - (T(K) - 5.4) \cdot 0.08394 \quad (5.5)$$

for linear fit 1 and on the other hand

$$\sigma(T) = 25.26 - (T(^{\circ}C) - 5.4) \cdot 0.0777 \quad (5.6)$$

for linear fit 2. The coefficient of determination for equation 5.5 amounts to  $\approx 0.97$  and for equation 5.6  $\approx 0.95$  what is indicative of a very well correlation.

Furthermore it shows that the measured surface tensions differ from those predicted by [35] as well as from the values in [9]. In either instances the amount of divergence corresponds roughly to a temperature shift of  $\Delta T \approx -5.4K$ . This mismatch might be explained by the position of the temperature sensor (see Fig. 23). Contrary to the standard placement of the sensor that is to say inside the refrigerant the temperature during measurements was metered by applying the sensor being completely surrounded by air. This placement was purposely chosen since one can assume that the plate has the temperature of the surrounding air before it comes in contact with the liquid. The temperature of this probe surrounding air is higher then the temperature of the refrigerant explainable by not complete thermal isolation against the room air. Figure 29 illustrates the difference between probe surrounding air and refrigerant. The black curve in figure 29 represents the ideal case of perfect isolation

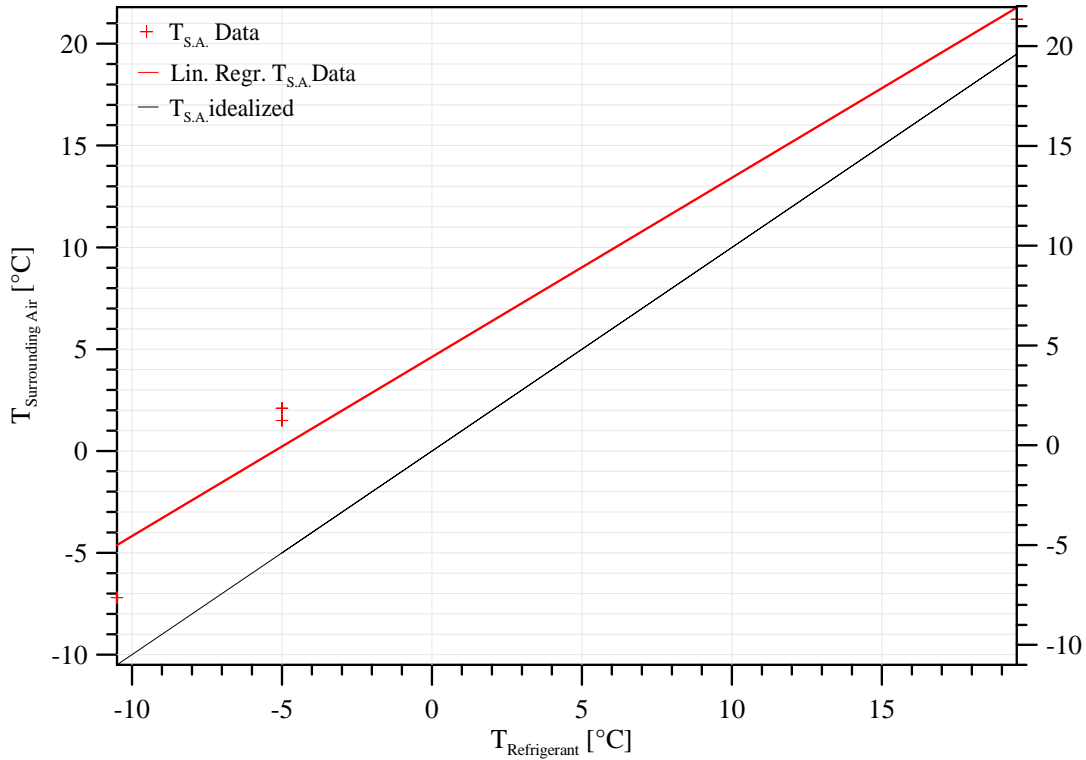


Figure 29: Surrounding air temperature as a function of refrigerant temperature

against the room temperature whereby the probe surrounding air and the refrigerant temperature are the same. It is obvious that the measurement data (*red crosses*) and therefore the linear regression (*red curve*) too vary from the ideal case. Furthermore figure 29 indicates an increase in temperature shift with approaching the room temperature ( $T_R \approx 25^{\circ}C$ ) and thus explains the mismatch illustrated in figure 28. So the temperature of the liquid surface is overestimated. Since the surface area includes both liquid as well as vapor molecules representing the transition from one

phase to the other there arises the question whether to relate the temperature of the liquid or the temperature of the surrounding air to a certain surface tension. Another indication for this assumption is the observation of a decreasing difference the more the measuring temperature converges to the room temperature ( $T_R \approx 26^\circ C$ ) just as in [12] stated.

However the following estimations show that the discrepancy between  $T_{surrounding-air}$  and  $T_{refrigerant}$  will not influence the contact angle values.

From equations 5.5 and 5.6 a constant shift in surface tension of  $\approx 0.45$  respectively  $\approx 0.42$  results. Taking the lowest surface tension value  $\sigma_{1-prop.}(34.1^\circ C) \approx 22.3 \frac{mN}{m}$  the relative error resulting from the above calculated shift amounts to  $\approx 2\%$  in either instance. The error estimation of chapter 6.4 makes clear that this systematical error will never exceed the statistical one (see equation 6.17). Consequently errors in  $\sigma$  values due to overestimation of the temperature has only negligible influence on contact angle values.



## 5.2 Not coated plates(0xPVD) (see appendix A.2)

### • Wetted lengths

Measurements were performed according to chapter 3.1 using n-hexane as liquid phase. Values indicated with \* are metered with the calliper rule<sup>31</sup>. Following average perimeters were calculated:

Preparation Type acc. to ...	$l$ [mm]	$l^*$ [mm]
<i>Roman Ortner</i>	$49.8 \pm 0.3$	50.0
<i>Josef Karoly</i> - <i>Goldsmith</i>	$51.58 \pm 0.08$	$51.6 \pm \mathbf{0.2}$
<i>Martina Rohrer</i> - <i>Expert for “<math>\mu</math>m-polishing”</i>	$50.8 \pm 0.2$	50.6

These results show very clearly that the mean values determined with the tensiometer correspond with the average perimeters metered with the calliper rule - within error bars.

In addition to it the perimeter of the plate prepared acc. to *R. Ortner* corresponds to the value represented in [19] ( $L = 50.3 \pm 0.1 \text{ mm}$ ) since the very same plate was used.

### 5.2.1 Contact Angles obtained with variously prepared but not coated 925 silver plates

As previously mentioned in (chapter 4.3) various kinds of preparation procedures were used in order to polish the plates. In the following the distinction between different preparations will be indicated with the name of the person performing it. Additionally it was possible to compare the data with values stated in [19] and [32].

---

<sup>31</sup>The sole measurement method applied with a systematical ( $\Delta l_{\text{sys.}} = 0.2 \text{ mm}$ ) exceeding the statistical one.

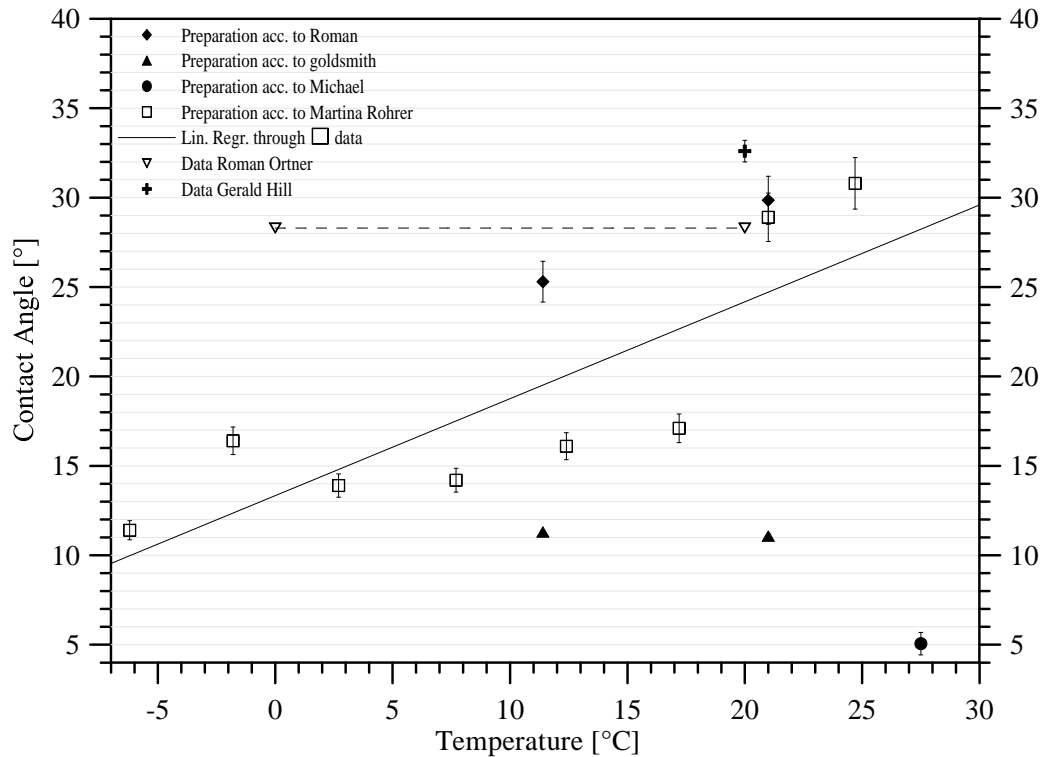


Figure 30: Contact angle of 1-propanol on not coated sterling silver - various preparation procedures by comparison

Obviously the advancing contact angle for not coated silver plates turns out to be dependent on ...

- the type of preparation,
- the cleaning procedure and
- the age of the plate.

Examining, for example, the case of contact angles at  $T \approx 20^\circ\text{C}$  ...

Preparation acc. to ...	Contact Angle [°]	Standard Deviation [°]
Roman Ortner <sup>black</sup>	30	1
Josef Karoly <sup>blue</sup>	11.1	0.1
Martina Rohrer <sup>light-green</sup>	29	1
Data R. Ortner <sup>dark-green</sup>	28.3	-
Data G. Hill <sup>pink</sup>	32.6	0.6

... following conclusions for the above listed values can be drawn on the basis of a comparison between the three parameter mentioned above:

1. Equal cleaning and surface age

Obviously contact angles received with the silver plates prepared acc. to *R. Ortner* and *M. Rohrer* agree within error bars. In addition to it they are in accord with the value stated in [32]. Concerning the three parameters it must be said that both the cleaning procedure as well as the surface age are equal thus the only variation is that different polishing steps were performed. However the conformity of the values implies that despite various preparation types the same surface conditions are on hand.

2. Equal cleaning and preparation

Providing that the error of the contact angle determined by Hill [19] is not underestimated a deviation from the already discussed values must be noticed. Although the same preparation and cleaning steps as in [32] were performed by *G. Hill* the obtained value obviously differs from the expected contact angle. This difference may be explained by the surface age and the thereby arising oxidation process. Contact angle data as a function of surface age stated in [32] provide an indication for the supposed correlation. Ortner [32] determined a contact angle increase of  $2^\circ$  for a surface age of 24 hours. Since there is no specification concerning this matter in [19] an aging of the plate surface can not be excluded.

3. Equal cleaning

The plainest drift noticeable in table 51 is the value measured with a plate prepared acc. to *J. Karoly*. Since both cleaning procedure as well as surface age were similar to the plate prepared acc. to *Ortner* the divergence may arise from a rougher surface (see chapter 3.2).

Coming back to Fig.30 the wide variance of the contact angle obtained with the silver plate prepared acc. to *Hindler* is obvious. Thereunto it must be said that primarily measurements acc. to *M. Hindler*<sup>red data point</sup> differ from all other measurements by performing goniometric analysis. Added to this the drop volume remained constant during the measurement. Consequently not the advancing but the equilibrium contact angle was measured and as already illustrated in Fig. 9  $\theta_a$  always exceeds  $\theta_e$ . In addition to it the plates were after polishing not cleaned in an ultra sonic bath but just rinsed of with acetone and water p.A. what might lead to surface contaminations of the probe. Both deviations from the otherwise applied measurements could cause the significant deviation obtained.

Since the plates prepared by *M. Rohrer* most likely conform to the requirements of smooth and uncontaminated surfaces only these plates were applied to determine the temperature dependence of the contact angle. Contrary to the results stated in [32] and indicated with the dashed black line in Fig. 30 it turned out that the contact angle is a function of temperature. The fitted linear regression makes the observed behavior more explicit:

$$\theta_a^{1-prop./925-silver}(T(^{\circ}C)) = 0.54 \times T(^{\circ}C) + 13.3 \quad ; (R^2 = 0.7)$$

... and leads to following parameters describing the contact angle as a function of temperature:

1. Contact angle at  $T = 0^\circ C$ :

$$\theta_a(0^\circ C) \cong 13.3^\circ$$

2. Change of  $\theta_a$  with increasing temperature:

$$\frac{\partial \theta_a(T)}{\partial T} \cong 0.54 \frac{deg}{^\circ C}$$

3. Contact angle at  $T = 20^\circ C$ :

$$\theta_a(20^\circ C) \cong 24^\circ$$

Respecting the inaccuracy of absolute values the result for  $\theta_a(20^\circ C)$  corresponds to the contact angle of  $28.3^\circ$  determined by Ortner [32]:

$$\Delta \theta_a(20^\circ C) = \theta_a^{Ortner} - \theta_a^{measured} \approx 4^\circ$$

However considering the contact angle at  $T = 0^\circ C$  the difference between the value received by the linear regression of measurement data and the one stated in [32] becomes significant:

$$\Delta \theta_a(0^\circ C) = \theta_a^{Ortner} - \theta_a^{measured} \approx 15^\circ$$

### 5.3 One time coated plates (1xPVD) (see appendix A.3)

- Wetted lengths

Plate marking	$l$ [mm]	$l^*$ [mm] $\delta_{l^*} = 0.2mm$
P1	$52.7 \pm 0.3$	52.6
P2	$55 \pm 1$	54.8

#### 5.3.1 Temperature dependence of the contact angle for 1-propanol on one-time coated 925 silver

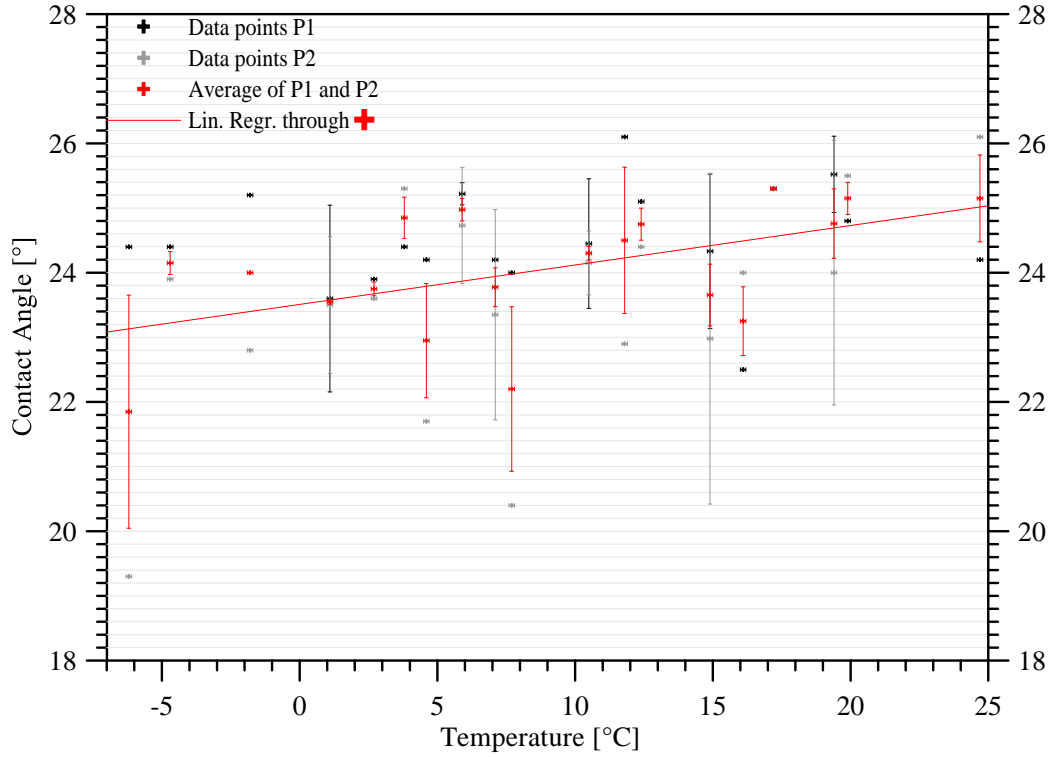


Figure 31: Contact angle of 1-propanol on one time-coated sterling silver as a function of temperature - averaging P1 and P2 data

Linear Regression fitted through the measured values(19<sup>32</sup>):

$$\theta_a^{1-prop./1 \times PVD}(T(^{\circ}C)) = 0.06 \times T(^{\circ}C) + 23.5 \quad ; (R^2 = 0.29)$$

<sup>32</sup>Number of data used for linear regression

Following parameters describing the contact angle as a function of temperature can be defined:

1. Contact angle at  $0^{\circ}C$ :

$$\theta_a(0^{\circ}C) \cong 23.5^{\circ}$$

2. Change of contact angle with increasing temperature:

$$\frac{\partial \theta_a(T)}{\partial T} \cong 0.06 \frac{deg}{^{\circ}C}$$

3. Contact angle at  $20^{\circ}C$ :

$$\theta_a(20^{\circ}C) \cong 24.7^{\circ} \tag{5.7}$$

#### 5.4 Two times coated plates(2xPVD) (see appendix A.4)

- Wetted length

Plate marking	$l$ [mm]	$l^*$ [mm] $\delta_{l^*} = 0.2mm$
P3	$52.7 \pm 0.3$	52.7

##### 5.4.1 Temperature dependence of the contact angle for 1-propanol on two-times coated 925 silver

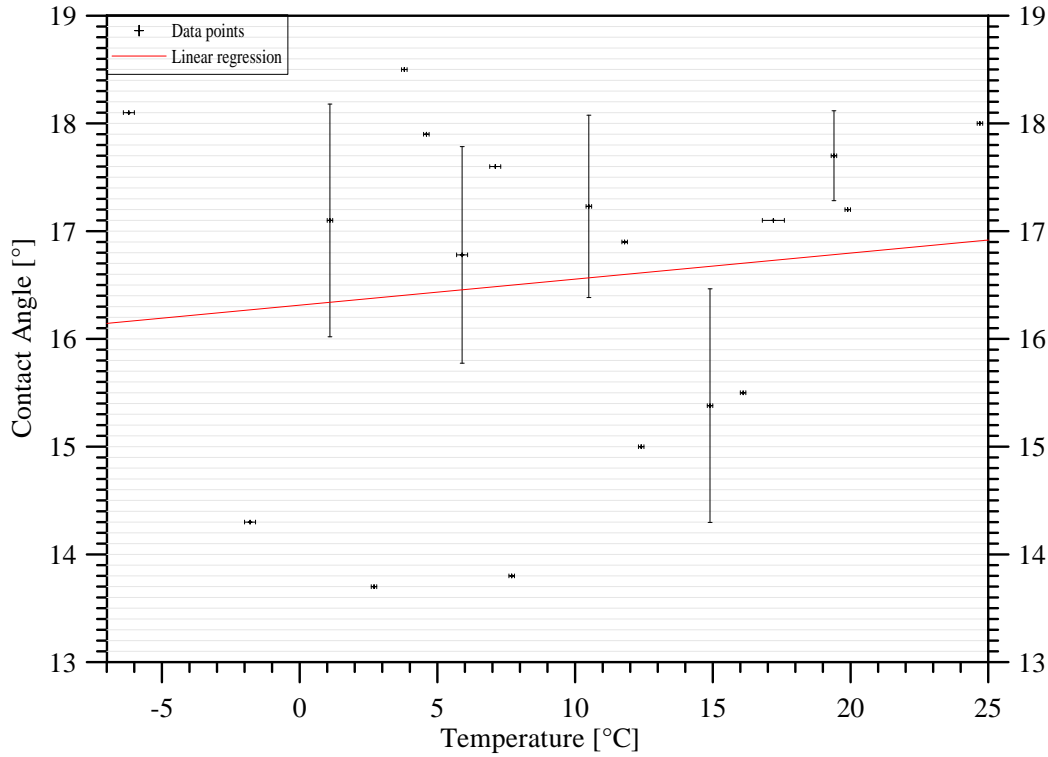


Figure 32: Contact angle of 1-propanol on two-times coated sterling silver

Linear Regression fitted through the measured values(18):

$$\theta_a^{1-prop./2 \times PVD}(T(^{\circ}C)) = 0.024 \times T(^{\circ}C) + 16.3 \quad ; (R^2 = 0.017)$$

In consideration of the errors following parameters describing the contact angle as a function of temperature can be defined:

1. Contact angle at  $0^{\circ}C$

$$\theta_a(0^{\circ}C) \cong 16.3^{\circ}$$

2. Change of contact angle with increasing temperature

$$\frac{\partial \theta_a(T)}{\partial T} \cong 0.02 \frac{deg}{^{\circ}C}$$

3. Contact angle at  $20^{\circ}C$

$$\theta_a(20^{\circ}C) \cong 16.7^{\circ}$$

### 5.5 Various often coated silver plates by comparison

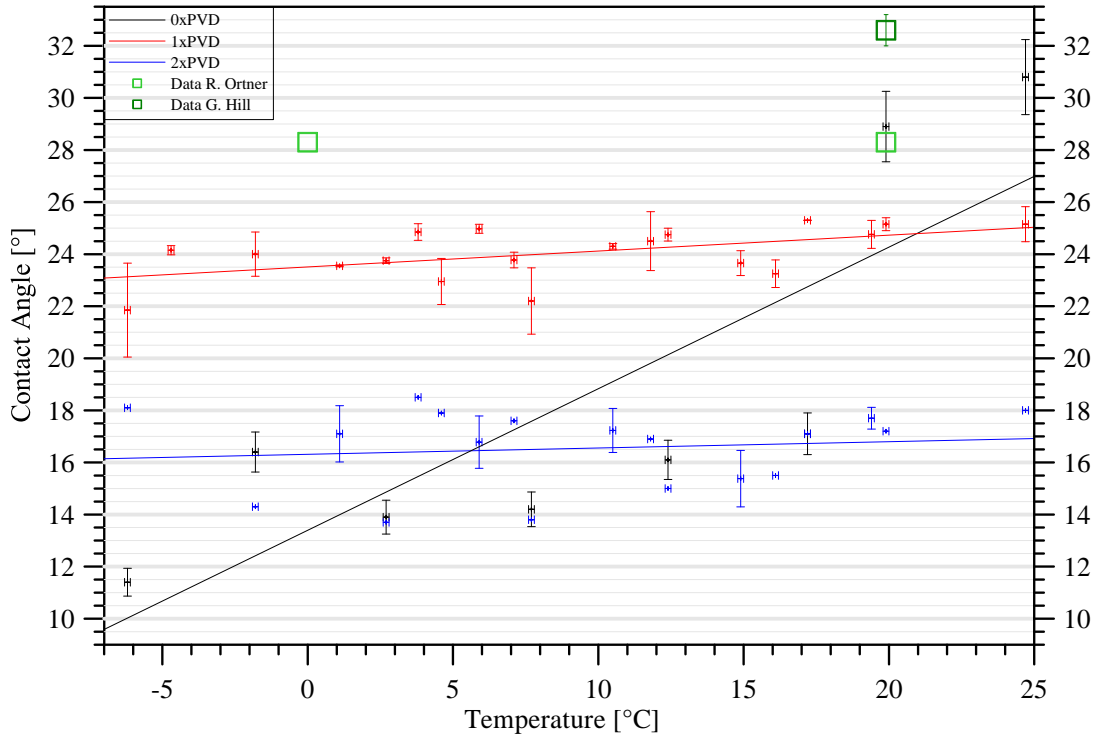


Figure 33: Temperature dependence of the contact angle for 1-propanol on silver - different numbers of PVD-steps in comparison with the values stated in [19] and [32]

$$\theta_a^{1-prop./silver}(T(^{\circ}C)) = \frac{\partial \theta}{\partial T} \times T(^{\circ}C) + \theta(0^{\circ}C) \quad (5.8)$$

	$0 \times PVD$	$1 \times PVD$	$2 \times PVD$
$\frac{\partial \theta}{\partial T} [\frac{deg}{^{\circ}C}]$	0.54	0.06	0.02
$\theta(0^{\circ}C) [^{\circ}]$	13.34	23.51	16.31
$\theta(20^{\circ}C) [^{\circ}]$	24.17	24.72	16.80

From this one can infer that not only the contact angle value but also its change with increasing temperature depend on the number of PVD-steps performed.

This result may scrap the 1-propanol/silver contact angles quoted in [?] and [19] because they must arouse suspicions that values obtained with non-coated 925 silver plates still including copper residuals ( $\approx 7.5\%$ ) don't agree with those obtained with coated plates.

Since contact angle measurements strongly depend on the surface state and purity (see chapter 1.3) one may potentially base the observed behavior on varying kinds of preparation procedures. However a comparison of the results at  $T = 20^{\circ}C \dots$



Preparation acc. to ...	$\theta_a(20^\circ C)$ [°]
<i>R. Ortnner</i>	$30 \pm 1$
<i>M. Rohrer</i>	$29 \pm 1$
<i>Data quoted in [32]</i>	28.3
... [19]	$32.6 \pm 0.6$

... disproves this hypothesis. Evidently the two different preparation procedures lead to the same surface smoothness.

Consequently it only remains to rule out the possibility surface smoothing by coating. According to [22] the macroscopic roughness of a solid surface is reflected in the contact angle hysteresis  $\theta_{hyst}$  - the difference between  $\theta_a$  and  $\theta_r$ . The bigger  $\theta_{hyst}$  the rougher the surface or in other words an increasing grade of surface smoothness results in an approximation of  $\theta_a$  and  $\theta_r$ . This equalization contains not only a decreasing  $\theta_a$  but also an increasing  $\theta_r$ . Since the measured  $\theta_r$  values did not change as a function of PVD-steps but remained generally zero also this assumption can be excluded.

It only remains to be clarified whether the varying surface age [32] may have caused the difference. In order to exclude this possibility the span of measurement time, the moment of polishing and vaporizing and the measurement procedure as a function of various temperatures need to be reviewed. In doing so it turns out that none of the mentioned parameters may cause the observed behavior. First of all the polishing and evaporation of the plates was performed inside two days an negligible stretch in comparison to the measuring period of  $\approx 3$  weeks. In addition to it attention was paid to vary the temperature after each completed series of measurements:

$$P_{0 \times PVD} \rightarrow P_{1 \times PVD} \rightarrow P_{2 \times PVD} \rightarrow P_{3_2}$$

Consequently the surface age is randomly spread over the studied temperature range but not subject to the number of PVD-steps performed. Solely the distribution of contact angle values at the same temperature may reflect an influence. However also this apparent dependency may refer to statistical dispersion and not to different physical properties due to surface age.

Now that all other possibilities could be ruled out the only explanation remaining is to attribute the observed behavior to increasing silver content with increasing number of PVD steps. Although it only amounts to 7.5% the copper content of the 925 silver plate evidently influences the contact angle. Reasonable since solely the surface of the plate influences the results and therefore even a small amount of copper may lead to a deviation from the desired silver surface.

Another point of interest is whether the temperature dependence influences the wetting behavior of 1-propanol on silver and possibly even lead to different behaviors depending on the number of coating-steps performed. Therefore the following graph will help to answer this questions.

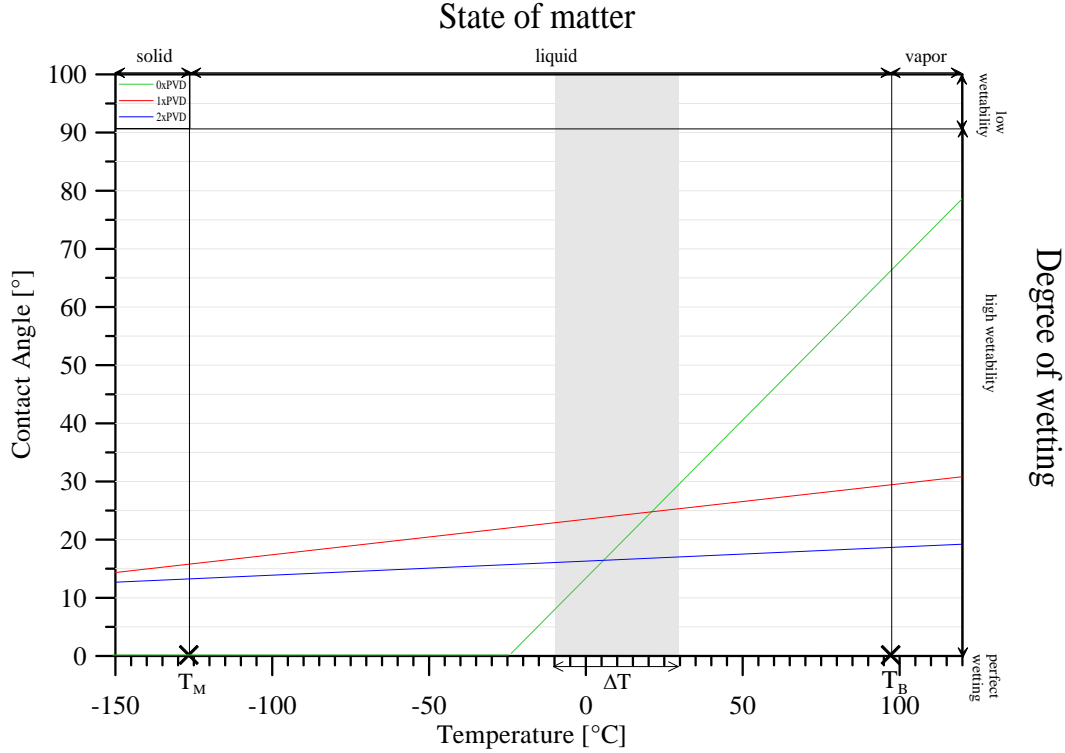


Figure 34: Temperature dependence of the contact angle for 1-propanol on silver as a function of PVD-steps - Extrapolation of the linear regressions.

As can be seen from this graph the degree of wetting for 1-propanol on silver can be classified as *highly wettable*, meaning a contact angle range from  $> 0^\circ$  to  $< 90^\circ$ , within the range where 1-propanol is determined to be liquid under atmospheric pressure. Just the not coated plate may be perfectly wetted at  $T \approx -24^\circ\text{C}$  according to the extrapolation of the linear regression fitted through data values. However within the observed temperature range  $\Delta T$  all plates are highly wetted. In addition to it one can conclude from the graph that the case of low wettability will never appear since even for the strongly rising contact angle curve of the not coated plate a temperature of  $\geq 142^\circ\text{C} \gg T_{B;1\text{-propanol}}$  may be needed to change the wettability. In spite of the unchanged wettability the measured temperature dependence of the contact angle plays an important part for heterogeneous nucleation processes (see chapter 1.4.2). Recalling equation 1.73 whose contact angle dependence is given by equations 1.74 and 1.76 the influence of  $\cos\theta$  on nucleation rate  $J$  given by 1.79 becomes evident. Thus the influence of observed temperature dependence on the nucleation rate is easily conceivable.

## 6 Temperature dependence of the contact angle for 1-propanol on NaCl

Contact angle measurements for 1-propanol on sodium chloride were conducted applying both the *Dynamic Wilhelmy Method* and the *Washburn Method*. The following results will be firstly distinguished according to the different measurement methods. Additionally contact angle data obtained with the *Dynamic Wilhelmy Method* will be divided according to the various preparation procedures mentioned in chapter 3.4.

Contrary to the silver/1-propanol data evaluation in the case of NaCl/1-prop. data additionally the receding angle  $\theta_r$  will be analyzed since they lead to unexpected negative  $\theta_{hyst} = \theta_a - \theta_r$  values(see chapter 1.3).

### 6.1 Surface Tension during measurements (see appendix B.1)

As well as for the previously discussed series of measurements the surface tension of n-propanol had to be checked at the beginning, during and at the end of every measurement cycle.

The surface tension changed as a function of temperature as shown in the following graph. . .

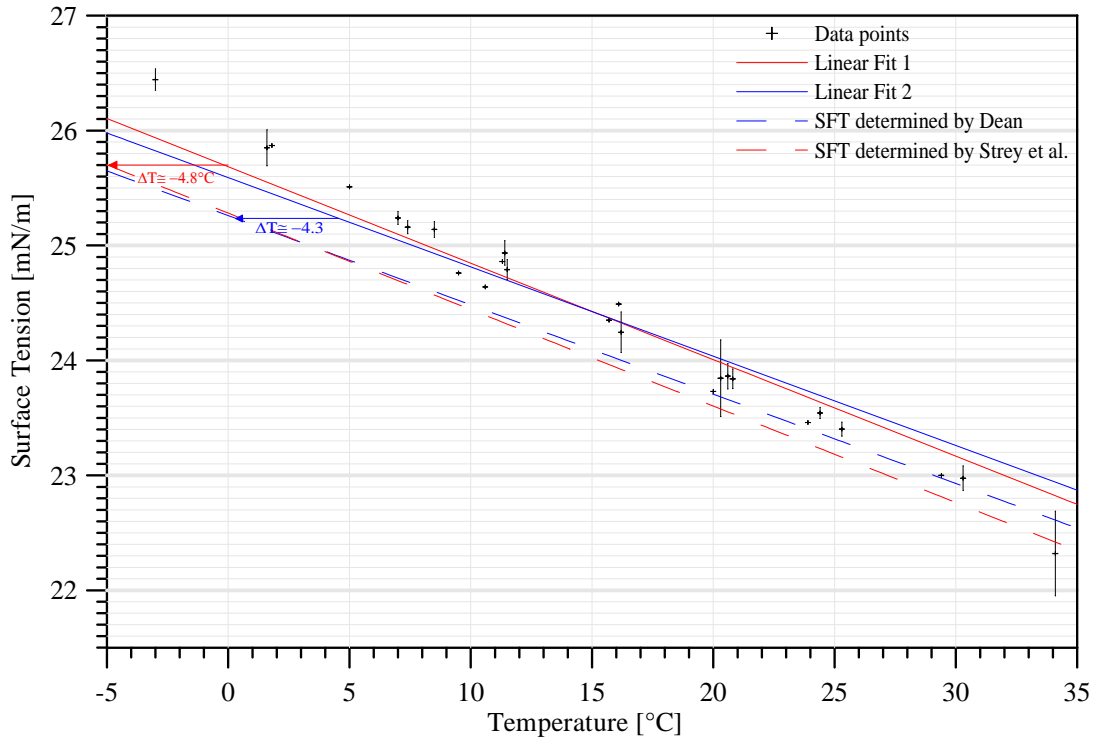


Figure 35: Experimental data for surface tension of 1-propanol compared with the curves determined by Strey [35] and by Dean [9] - Linear Fits 1 respectively 2 are chosen parallel to [35] respectively [9]

Again the linear regression fitted through the data is based on the functions

determined by [35]

$$\sigma_{1-Propanol}(T) = 48.21 - (T(K) - 4.8) \cdot 0.08394 \quad (6.1)$$

with a coefficient of determination ( $R^2$ ) of  $\approx 0.95$  K  
and by [9]

$$\sigma_{1-Propanol}(T) = 25.26 - (T(^{\circ}C) - 4.3) \cdot 0.0777$$

with a coefficient of determination ( $R^2$ ) of  $\approx 0.92$  K

Obviously the drift of temperature  $\Delta T \approx -4.8K$  resp.  $\Delta T \approx -4.3K$  is in accord with the one calculated before (see chapter 5.2) and again the linear regression according to [35] fits better then the one acc. to [9]. However this graph shows more clearly that the shift from the curve determined by [35] (red curve) increases by approaching the room temperature  $T_R$ . Reasons for the deviation from predicted values are the same as id.

## 6.2 Dynamic Wilhelmy Method

Since the *physical vapor deposition* has prove to be a suitable method for the generation of smooth surfaces in the case of silver plates it has also been used to produce a sodium chloride coat on a smooth solid surface. In order to guarantee adhesion of the salt film a glass plate was used as target. For two reasons this solid is qualified for coating with *NaCl* on the one hand its surface is already smooth and needs therefore no additional polishing and on the other hand its 14% *Na<sub>2</sub>O* content (see chapter 4.2.2) creates a good basis for the adhesion of the film.

### 6.2.1 Uncoated glass plate (see appendix B.2.1)

In order to exclude a misinterpretation of the measured contact angles due to influence of the glass subsurface comparative measurements with a pure glass plate were performed.

- Wetted lengths

Plate marking	$b$ [mm] $\pm 0.05$	$d$ [mm] $\pm 0.05$	$l$ [mm] $\pm 0.2$
<b>G</b>	20.4	2	44.8

- Temperature dependence of the contact angle for 1-propanol on glass
  - Advancing angle as a function of temperature

Measurements in a temperature range of  $(-7^{\circ}\text{C}; 34^{\circ}\text{C})$  resulted in an advancing angle of  $0^{\circ}$ . Clearly the obtained data include statistical scatter but since this uncertainty takes place in a range where  $\cos\theta_a$  is always larger than 1 it will not change the result that 1-propanol wets glass perfectly.

$$\theta_a^{1-prop./G}(T(-7^{\circ}\text{C} \rightarrow 34^{\circ}\text{C})) \equiv 0^{\circ}$$

Following figure illustrates the measured  $\cos\theta_a$  values as a function of temperature to emphasize the above stated result. Additionally a comparison with the  $\cos\theta_r$  values is diagrammed to show the unexpected ( $\theta_{hyst} < 0$ ) behavior measured.

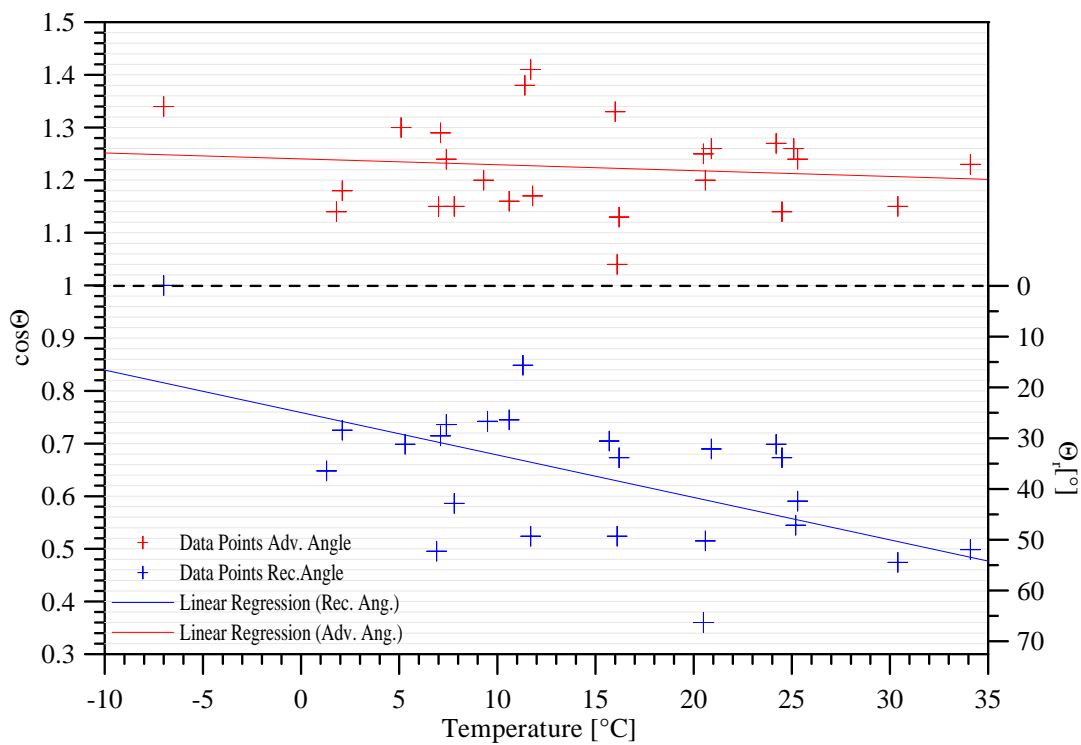


Figure 36:  $\cos\theta_a$  and  $\cos\theta_r$  data obtained with a pure glass plate as a function of temperature

– Receding angle as a function of temperature

Since the  $\cos\theta_r$  values illustrated above in fig. 36 all correspond to a finite and non-zero contact angle the following graph (fig. 37) illustrates the direct angles obtained.

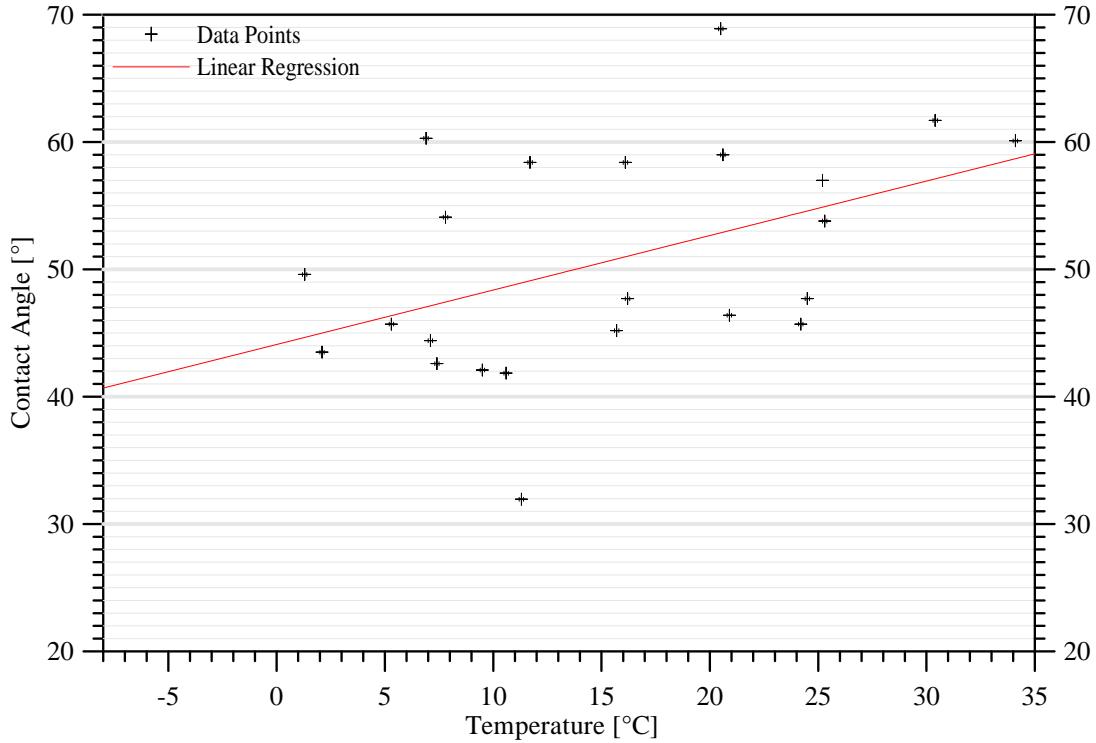


Figure 37:  $\theta_r$  data for 1-propanol on glass as a function of temperature

Linear Regression fitted through the measured values(24):

$$\theta_r^{1-prop./2 \times PVD}(T(^{\circ}C)) = 0.81 \times T(^{\circ}C) + 36.9 \quad ; (R^2 = 0.37)$$

Finally it can be stated that the contact angle between glass and 1-propanol in a temperature range from  $-7^{\circ}C$  to  $34^{\circ}C$  amounts to  $0^{\circ}$ . However the measured receding angles, which are supposed to be smaller than  $\theta_a$  (see chapter 1.3) and therefore zero too, exceed the expected values and appear to be temperature dependent. This behavior induces an increasing contact angle hysteresis with increasing temperature but it does not change the statement of perfect wetting, because propositions about the wetting behavior only depend on the advancing angle, which remains zero.

### 6.2.2 One-time coated glass plates (see appendix B.2.1)

Two glass plates were coated with a sodium chloride film as described in chapter 4.4.3. It was clearly visible that the so produced coats were rougher than the silver films although in both cases the method of PVD was performed to generate the thin films. An explanation for the difference in surface roughness is stated in 4.4.3. In order to exclude destruction of the sensitive surface coats the plates were stored in argon atmosphere between measurements. During measurements the salt film may be destroyed by bringing in contact with the probational liquid. For that reason the liquid was firstly saturated with sodium chloride powder in an ultra sonic bath so that a sediment of salt was visible. Fortunately surface tension measurements of this solution resulted in the same values as though using 1-propanol p. A. and thus surface modifications due to solid-liquid contact can be excluded.

- Wetted lengths

Unlike the determination of the silver plate perimeter, in the case considered here wetted length measurements can only be performed applying a calliper rule ( $l = 2 \times (b + d)$ ). Otherwise due to the solubility of salt in n-hexan the probational plates would have been destroyed.

Plate marking	$b$ [mm] $\pm 0.05$	$d$ [mm] $\pm 0.05$	$l$ [mm] $\pm 0.2$
S1	20	2	44
S2	20.70	2.00	45.4

- Temperature dependence of the contact angle for 1-propanol on sodium chloride (1xPVD)
  - Advancing contact angle

Contact angle measurements between 1-propanol and one time coated glass plates yield also to a vanishing advancing angle. Thus it can be concluded that the liquid under study wets the sensitive salt film perfectly too.

$$\theta_a^{1-prop./S1;2}(T(-3^\circ C \text{ to } 34^\circ C)) \equiv 0^\circ$$



Again a graph of the obtained  $\cos\theta_a$  data is illustrated to elucidate that although statistical scatter of the values exists the resulting advancing angles never exceed  $0^\circ$ . The comparison with the  $\cos\theta_r$  data leads again to a behavior contradicting theoretical assumptions. Obviously both the glass as well as the one time coated

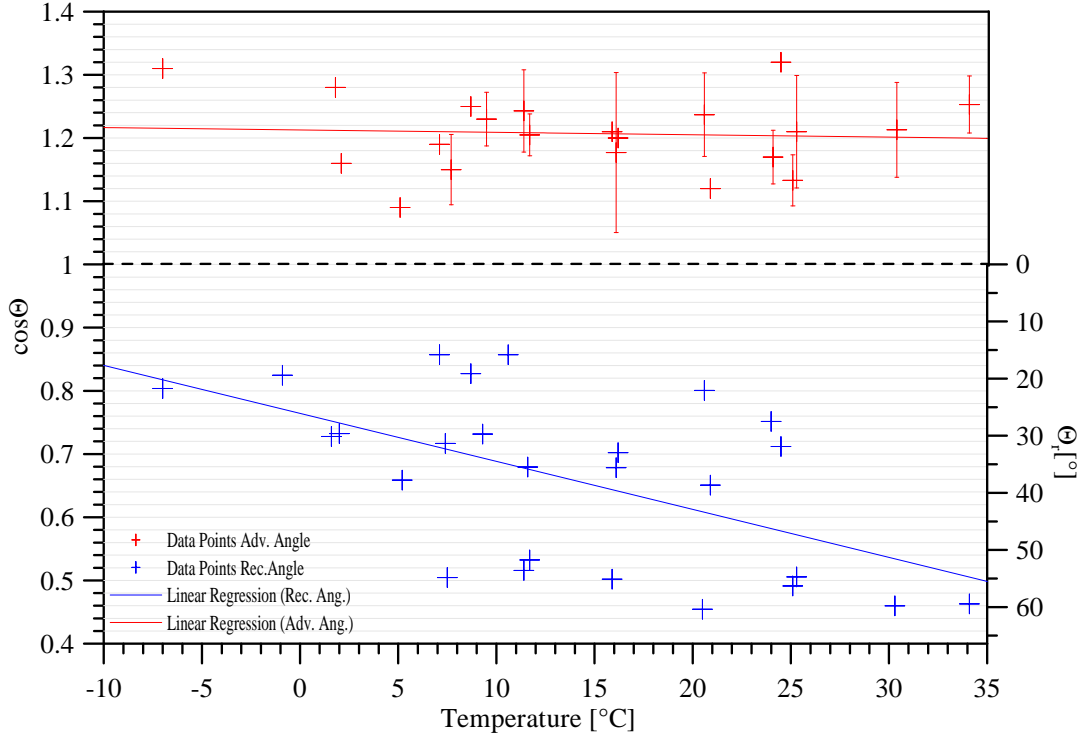


Figure 38:  $\cos\theta_a$  and  $\cos\theta_r$  data obtained with one time coated plates as a function of temperature

plate behave in the same way by coming into contact with 1-propanol. It might be that the sodium chloride is too thin and therefore the glass subsurface influences the data. However the later quoted results of two and three times coated plates disagree with this statement since primarily the receding angle turns out to be influenced by the number of coating processes and not the advancing angle. Though the impact of glass should most notably affect the advancing angle analogously to the change in advancing angle determined for the silver plates. Against this a change in receding angle related to the number of salt coats rather indicates a variation of surface roughness.

– Receding contact angle

Once more a negative contact angle hysteresis  $\theta_{hyst} = \theta_a - \theta_r$  is observed. Values for  $\theta_r$  are illustrated below in figure 39.

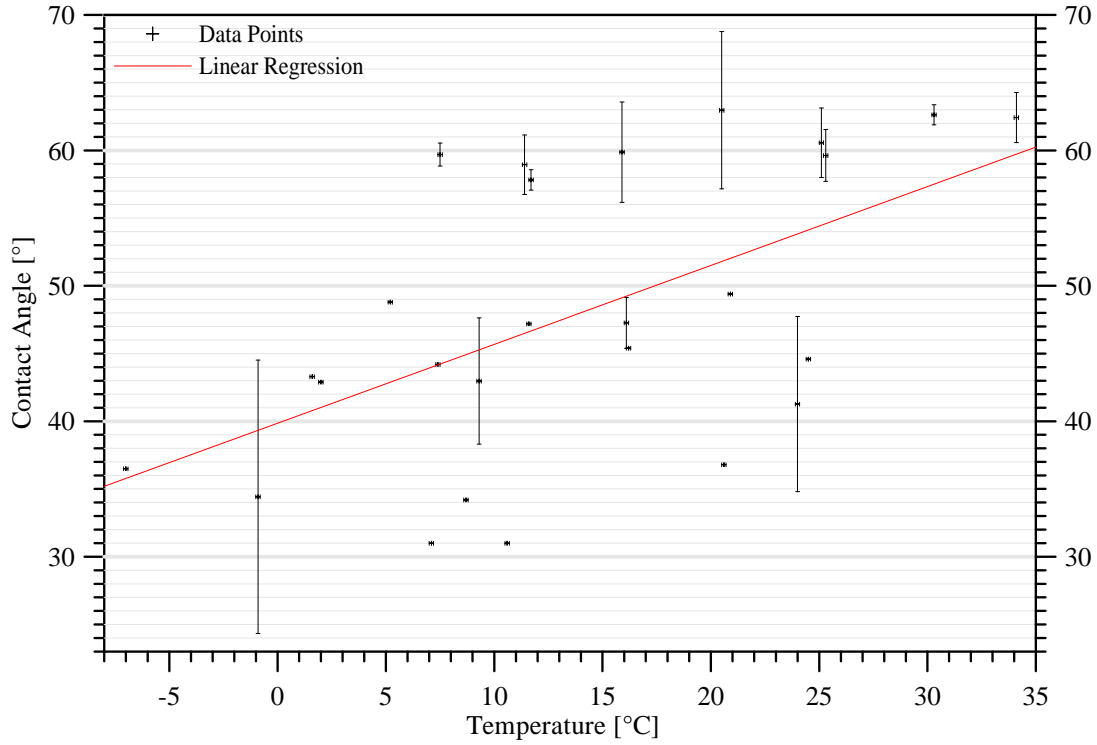


Figure 39:  $\theta_r$  data for 1-propanol on one time coated glass as a function of temperature

Linear Regression fitted through the measured values(26):

$$\theta_r^{1-prop./2 \times PVD}(T(^{\circ}C)) = 0.58 \times T(^{\circ}C) + 39.9 \quad ; (R^2 = 0.31)$$

Again the errors of  $\theta_r$  data exceeds the those arising out of  $\theta_a$  measurements. However a comparison with the receding angles of the polished salt plates (see figure 6.2.5 shows that a relative error of 60% clearly exceeds the maximum relative error occurring in this case  $\approx 15\%$ .

### 6.2.3 Two-times coated glass plates (see appendix B.2.1)

The second coat of sodium chloride was under similar conditions produced. That is to say, that both the distance between tungstic shuttle and target as well as the amount of *NaCl* powder were retained. Consequently it's safe to assume that layer thickness is twice as large as for the one time coated plate.

- Wetted lengths

Plate marking	$b$ [mm] $\pm 0.05$	$d$ [mm] $\pm 0.05$	$l$ [mm] $\pm 0.2$
S3	20.37	2.00	44.7
S4	19.98	2.00	44.0

- Temperature dependence of the contact angle for 1-propanol on sodium chloride (2xPVD)
  - Advancing Angle

As already well-known from the glass and the one time coated plate contact angle measurements with two times coated plates result again in an unexpected negative  $\theta_{hyst}$  behavior. Figure 40 shows the measured  $\cos\theta_a$  and  $\cos\theta_r$  data.

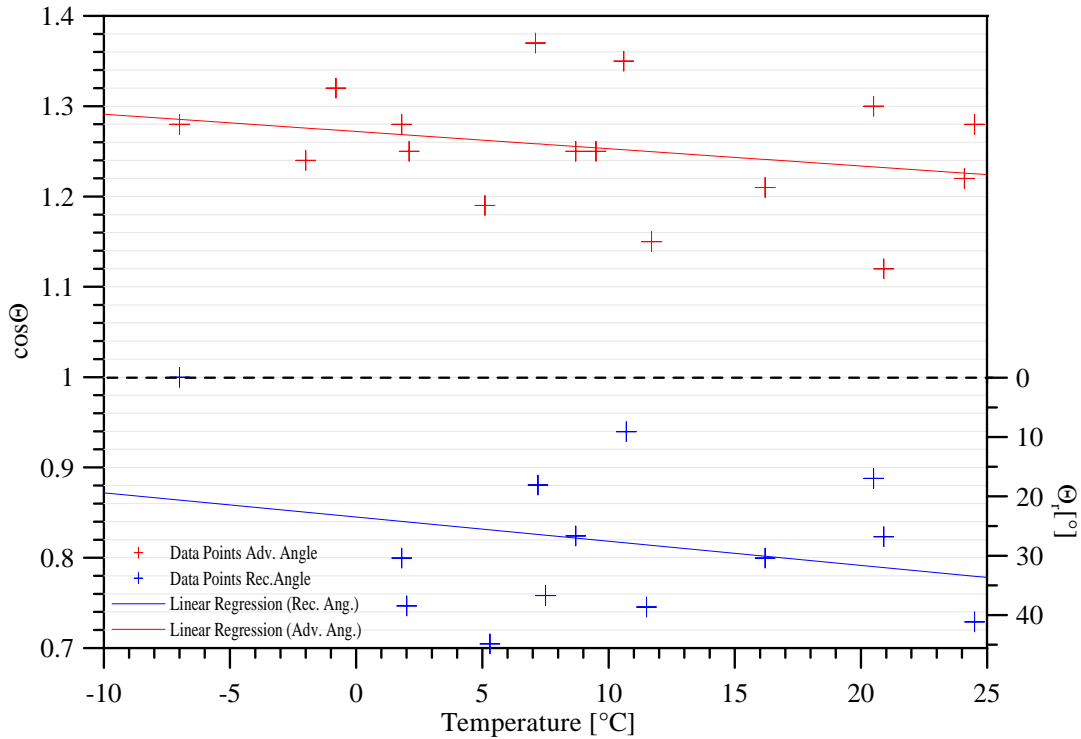


Figure 40:  $\cos\theta_a$  and  $\cos\theta_r$  data obtained with two times coated plates as a function of temperature

As already broached before the results for  $\cos\theta_a$  values remain in the same range of values as in the case of glass and one time coated plates. Thus again the perfect wetting of 1-propanol on two times coated plates can be deduced. The fact that the  $\cos\theta_a$  values remain unchanged indicates that not the glass subsurface causes a contact angle of  $0^\circ$  but rather both glass as well as sodium chloride are perfectly wetted by 1-propanol.

$$\theta_a^{1-prop./S3;4}(T(-3^\circ C \text{ to } 34^\circ C)) \equiv 0^\circ$$

- Receding Angle

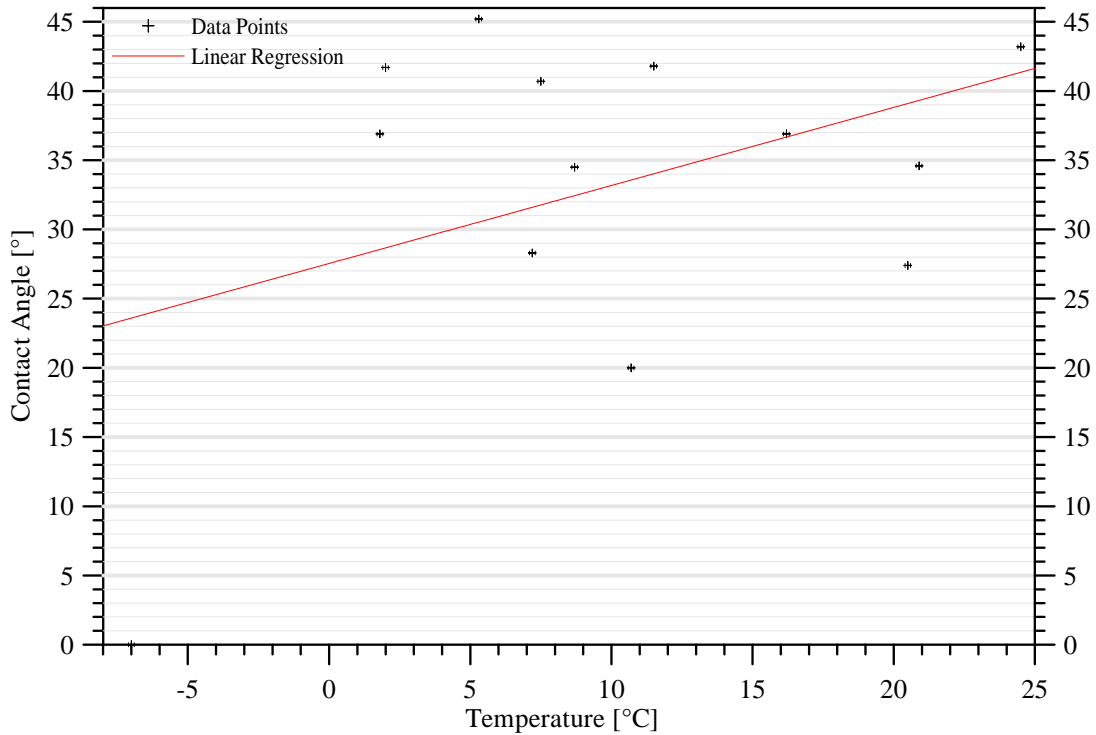


Figure 41:  $\theta_r$  data for 1-propanol on two times coated glass as a function of temperature

Linear Regression fitted through the measured values(13):

$$\theta_r^{1-prop./2 \times PVD}(T(^{\circ}C)) = 0.56 \times T(^{\circ}C) + 27.5 \quad ; (R^2 = 0.16)$$

Obviously the measured receding angles are smaller than in former cases. This result leads to the assumption that surface of a twice coated plate is smoother.

### 6.2.4 Three-times coated glass plates (see appendix B.2.1)

For the very same reasons stated above one can assume that the layer of a three times coated plate is three times as thick as the coat of the one time coated plate. Respecting the short range of surface forces the influence of the glass plate on contact angle measurements can a priori be excluded through layer thickness.

- Wetted length

Plate marking	$b$ [mm] $\pm 0.05$	$d$ [mm] $\pm 0.05$	$l$ [mm] $\pm 0.2$
S5	20.32	2.00	44.6

- Temperature dependence of the contact angle for 1-propanol on sodium chloride (3xPVD)

Just as with the less often respectively non coated plates the contact angle hysteresis turns out to be negative and the advancing angle amounts to  $0^\circ$  in the whole temperature range observed. The measured  $\cos\theta_a$  data not only result in a contact angle of zero but they are also located in the same range of values as shown in the following graph.

– Advancing Angle

$$\theta_a^{1-prop./S5}(T(-3^\circ C \text{ to } 34^\circ C)) \equiv 0^\circ$$

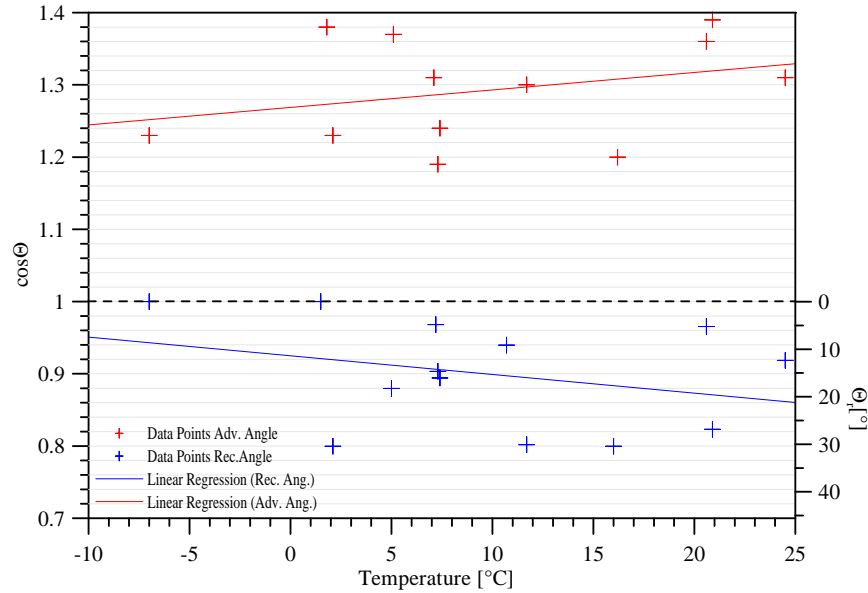


Figure 42:  $\cos\theta_a$  and  $\cos\theta_r$  data obtained with three times coated plates as a function of temperature

– Receding Angle

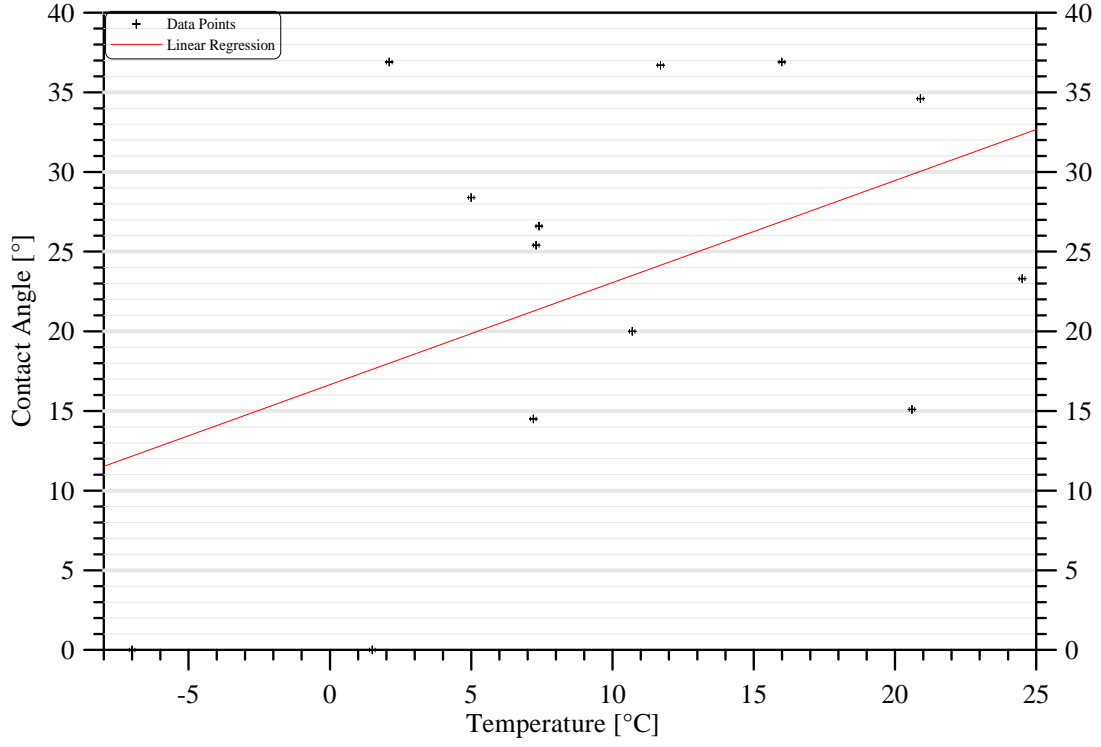


Figure 43:  $\theta_r$  data for 1-propanol on three times coated glass as a function of temperature

Linear Regression fitted through the measured values(13):

$$\theta_r^{1-prop./2 \times PVD}(T(^{\circ}C)) = 0.64 \times T(^{\circ}C) + 16.7 \quad ; (R^2 = 0.20)$$

Considering the receding angles it turns out that their values decrease once more just as observed above. This change in absolute values can again be interpreted as a property of surface roughness.

Following conclusions can be drawn from the measurements with *NaCl*-coated glass plates:

1. The advancing angle, which describes the wetting behavior of a liquid on a solid surface, is always zero. That is to say, that the glass as well as the salt-coated plates were perfectly wetted by 1-propanol in the whole temperature range observed.

$$\theta_a^i(T) \equiv 0^\circ \quad \forall \quad T \in (-7^\circ C; 34^\circ C)$$

i=glass;1xPVD;2xPVD or 3xPVD

2. The statistical scatter of  $\cos\theta_a$  values is not large enough that a contact angle unequal  $0^\circ$  could be deduced from it.
3. All receding angles exceed the advancing ones. Therefore the contact angle hysteresis defined as  $\theta_{hyst} = \theta_a - \theta_r$  is always negative and thus contradicts the theoretical expected positive value.
4. The measured  $\theta_r$  values decrease with increasing number coating steps. Since receding angles just allow statements about the surface roughness it can be concluded that with increasing layer thickness the surface becomes smoother.
5. Just a comparison between the  $\frac{\partial\theta_r}{\partial T}$  calculated for the various plates:

	$\frac{\partial\theta_r}{\partial T} [\frac{deg}{^\circ C}]$
Glass	0.81
1xPVD	0.58
2xPVD	0.56
3xPVD	0.64

might possibly be interpreted as a difference in contact angle behavior between glass and sodium chloride by means of a different  $\theta_{hyst}$  increase with increasing temperature.

### 6.2.5 Polished Salt Crystals (see appendix B.2.2)

Besides the salt-coated glass plates probes were also made out of a sodium chloride crystals. This has the advantage that no additional coating is necessary and the influence of a different substances below the surface coat can be excluded<sup>33</sup>. On the other hand its more difficult to realize a smooth surface with sodium chloride than with glass. Consequently some of the split off plates had to be polished additionally.(see chapter 4.4.1) How the polishing influences the contact angel will become clear in the following.

Since no sensitive film was deposited on the solid surface the plates were stored in room air just like all silver plates. Also a saturation of the probational liquid with sodium chloride powder was not necessary what simplified the test sequence.

The following contact angles will be divided into those obtained with polished sodium chloride crystals and those measured with salt plates, which were innately smooth and therefore required no additional preparation.

- Wetted lengths

Plate marking	$b$ [mm] $\pm 0.05$	$d$ [mm] $\pm 0.05$	$l$ [mm] $\pm 0.2$
<b>N1</b>	15.48	2.9	26.8
<b>N2</b>	14.04	1.6	31.3
<b>N3</b>	11.35	2.4	27.5
<b>N4</b>	7.81	2.56	20.7
<b>N5</b>	9.54	3.71	26.5
<b>N6</b>	13.94	1.7	31.28

- Temperature dependence of the contact angle for 1-propanol on polished salt crystals

Just like in the former case of coated glass plates contact angle measurements with polished salt crystals resulted in a negative contact angle hysteresis.

---

<sup>33</sup>the purity of the sodium chloride crystal was tested as mentioned in chapter 4.4.1



– Advancing angle as a function of temperature

The results for  $\cos\theta_a$  imply again, that the advancing angle is  $0^\circ$  in the whole temperature range as illustrated in figure 44.

$$\theta_a^{1-prop./N_1-6}(T(-3^\circ C \rightarrow 34^\circ C)) \equiv 0^\circ$$

Clearly also these advancing angle measurements include statistical variation. However the variations never lead to a  $\cos\theta_a < 1$  and therefore they don't change the zero contact angle.

Although the range of  $\cos\theta_a$  values is the same as for the case of coated glass plates

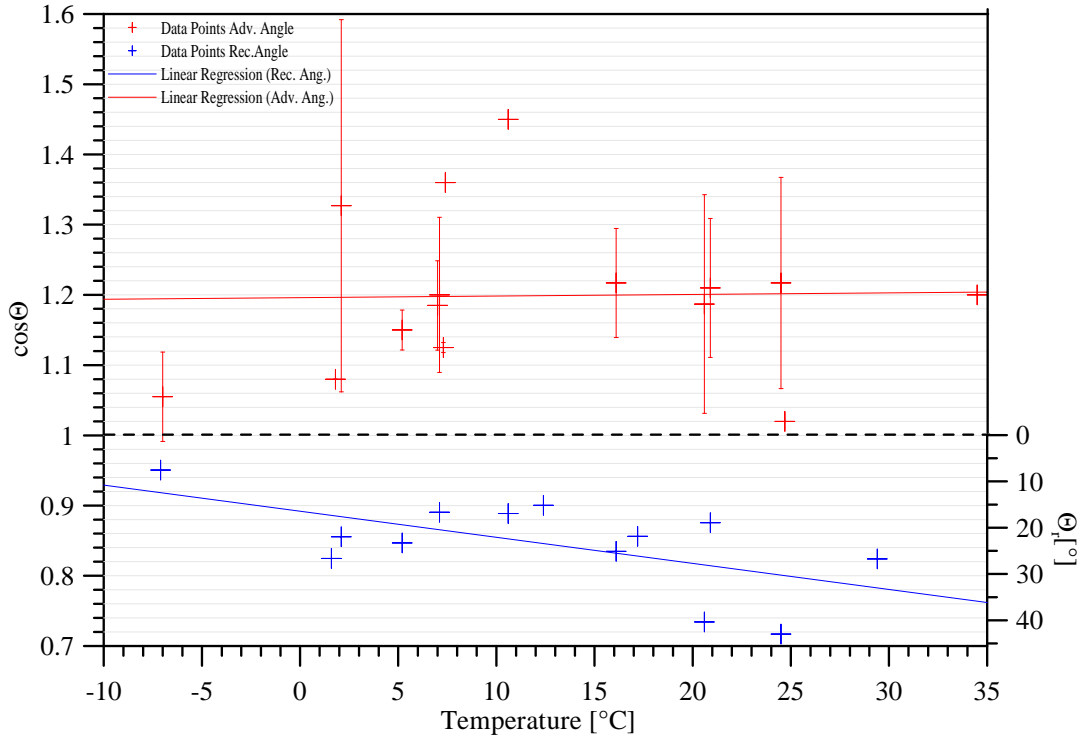


Figure 44:  $\cos\theta_a$  and  $\cos\theta_r$  data obtained with polished salt crystals as a function of temperature

the larger error bars indicate, that the surface quality is lower. That is to say the smoother a surface the better reproducible the measurements and the smaller the errors. That's also the reason why errors for receding angles always exceed the ones for advancing angles.

– Receding angle as a function of temperature

Contrary to the advancing angles the measured receding angles differ from zero as shown below and lead to the already mentioned negative contact angle hysteresis.

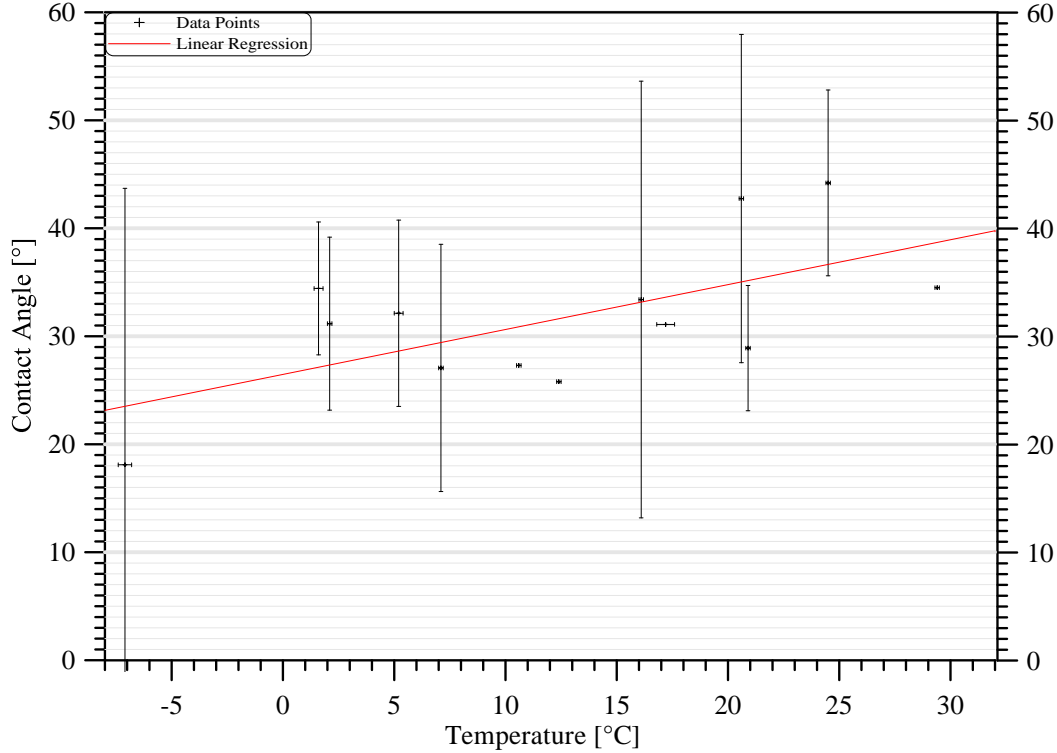


Figure 45:  $\theta_r$  data for 1-propanol on polished salt crystals as a function of temperature

Linear Regression fitted through the measured values(13):

$$\theta_r^{1-prop./N_{1-6}}(T(^{\circ}C)) = 0.42 \times T(^{\circ}C) + 26.47 \quad ; (R^2 = 0.40)$$

Re-emphasising the occurring errors a comparison between the uncertainties of  $\cos\theta_a$  (fig.44) and  $\theta_r$  (fig. 6.2.5) demonstrates the difference in reproducibility between advancing and receding angles. As already mentioned in chapter 1.3  $\theta_r$  is less reproducible than  $\theta_a$  and therefore  $\theta_r$  values exhibit bigger scattering. E. g. the maximum relative error for the advancing angle amounts to  $\approx 23\%$  (fig.44) whereas the relative error of the above plotted receding angles (fig. 6.2.5) amounts up to  $\approx 60\%$ .

### 6.2.6 Untreated salt plate (see appendix B.2.3)

The untreated salt plate turned out to have the most qualified surface for contact angle measurements. In contrast to all the other plates mentioned above this probe neither includes other materials nor is it modified by polishing. Therefore the surface molecules are located in energetically favorable positions. The following results will confirm this statement.

- Wetted length

Plate marking	$\bar{b}$ [mm]	$\bar{d}$ [mm]	$\bar{l}$ [mm]
N	$8.1 \pm 0.05$	$0.8 \pm 0.05$	$17.8 \pm 0.2$

- Temperature dependence of the contact angle for 1-propanol on untreated sodium chloride

Measurements with untreated plates resulted in a contact angle of  $0^\circ$  for both the advancing as well as the receding angle. Following graph illustrates the measured  $\cos\theta_{a/r}$  data in the observed temperature range.

$$\theta_{a\&r}^{1-prop./N}(T) \equiv 0^\circ \quad \forall \quad T \in (-3^\circ C; 35^\circ C)$$

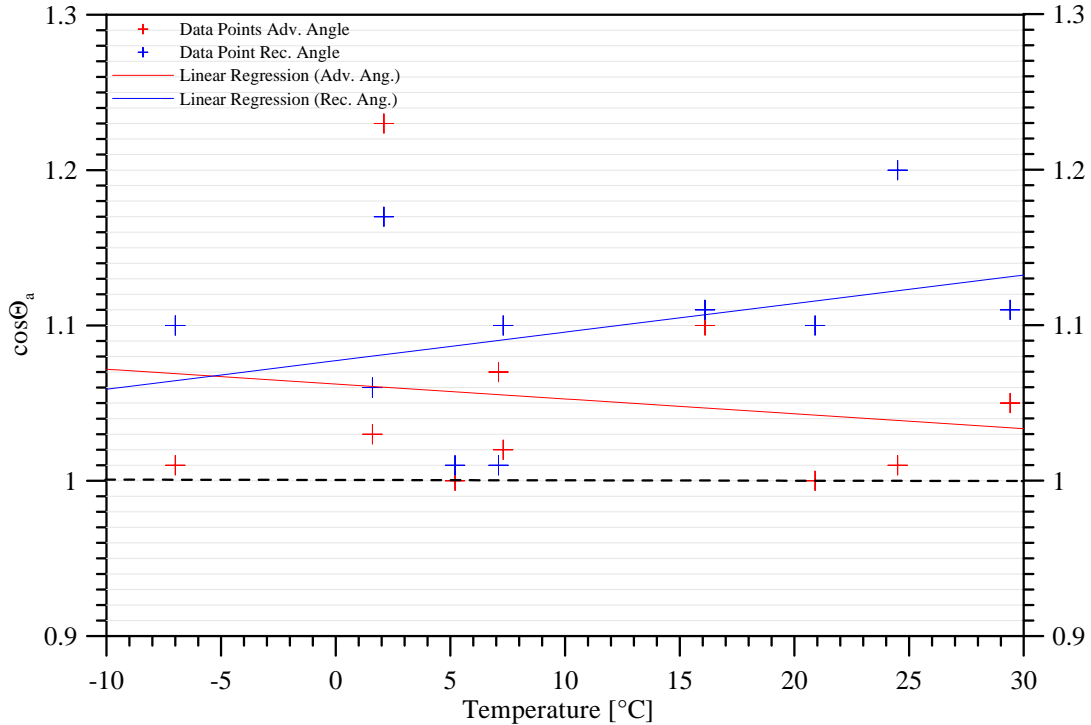


Figure 46:  $\cos\theta_a$  and  $\cos\theta_r$  data obtained with untreated salt crystals as a function of temperature

It shows that on the one hand the  $\cos\theta_a$  values increase compared to the previous cases and on the other hand the receding angle increases so much that it becomes  $0^\circ$

too. In addition to it solely for the untreated plate the “indirect” contact angle hysteresis  $\theta_{hyst}$  is positive and thus accords to theoretical expectations. The expression “indirect” points out that not the usual definition of  $\theta_{hyst} = \theta_a - \theta_r$ , which would lead to  $\theta_{hyst} \equiv 0^\circ$  since both  $\theta_a$  and  $\theta_r$  are zero, is meant. But rather the difference between forces acting on the plate by immersing ( $F_a$ ) respectively withdrawing ( $F_r$ ) it (see figure 19). That is to say that as already mentioned in chapter 2.2.2 the recorded force given by equation 2.6 is proportional to  $\cos\theta$  and therefore leads to  $\cos\theta_r$  values exceeding the  $\cos\theta_a$  ones if  $\theta_a > \theta_r$ .

The crossing of the linear regressions might be misleading since the  $\cos\theta_r$  values always exceed the  $\cos\theta_a$  values. Since the correlation coefficients of the linear regressions amount to 0.02 for  $\cos\theta_a$  data respectively 0.12 for  $\cos\theta_r$  data one should not pay particular attention on an interpretation of this behavior.

## 6.2.7 Various prepared plates by comparison

- Advancing Angles

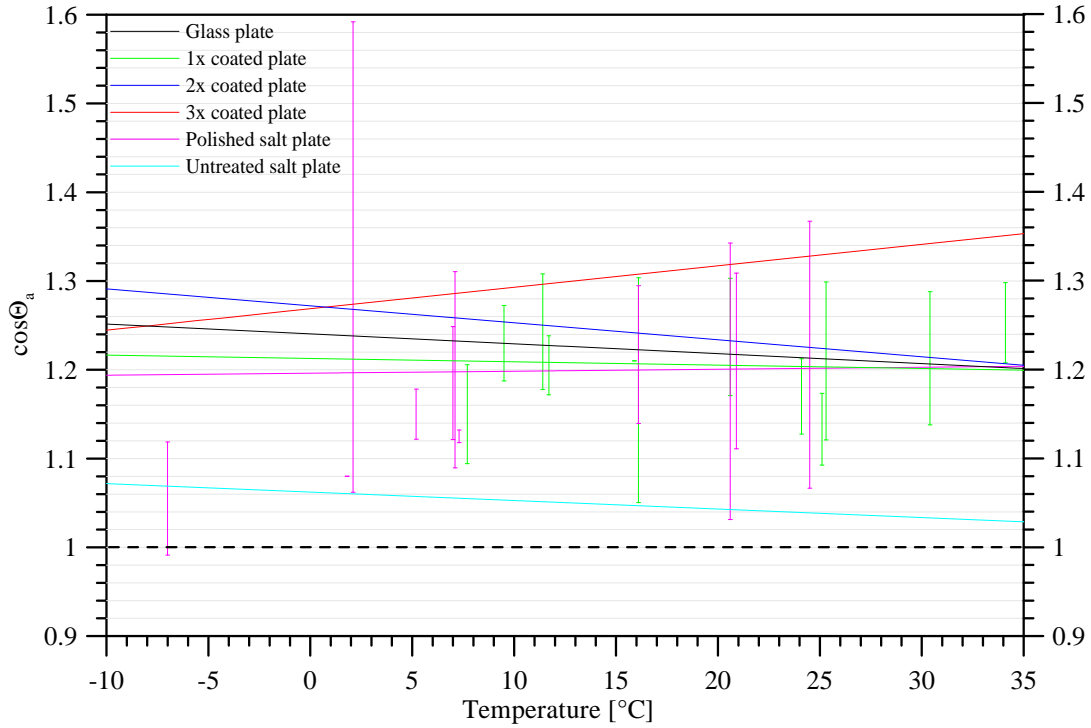


Figure 47:  $\cos\theta_a$  values obtained with variously prepared plates as a function of temperature by comparison.

The comparison between all  $\cos\theta_a$  values measured with variously prepared plate shows very plainly that the advancing angles always amount  $0^\circ$  and thus 1-propanol perfectly wets sodium chloride. Except data obtained with the untreated salt plate all results for the advancing angle can broadly be classified into the same range of values that is to say:

$$\cos\theta_a \in (1.2; 1.4) \quad (6.3)$$

The fact that the  $\cos\theta_a$  data of the untreated salt plate do not correspond with the others is needs an explanation since it can not be reasoned with surface roughness. The usual argumentation of surface roughness 1.3.1 as reason for contact angle hysteresis and therefore change of both the advancing as well as the receding angle would imply a  $\cos\theta_a$  value of the untreated plate exceeding all the others. Since the difference between  $\cos\theta_a$  and  $\cos\theta_r$  values is minimal for the untreated plate it can be inferred that the surface quality is the best and therefore the force acting on this plate is supposed to exceed the other recorded forces.

A quite tentative interpretation of the observed unusual behavior includes indeed surface quality too but the consequent change in contact angle is different.

Starting from the formation process of the salt surface one must consider that contrary to the metallic bond between silver molecules the sodium chloride molecules interact by ionic bonds. This fundamental difference in intermolecular correlation

leads to different crystal structure and has therefore also consequences for the coat produces by PVD. Whereas the silver vapor forms a homogeneous film due to the strong metallic bond the sodium chloride particles condense in patches and may therefore leave uncoated areas on the plate. Consequently a cavity-riddled surface appears and it interacts like a porous solid. Since the contact angle of 1-propanol on sodium chloride is smaller than  $90^\circ$  this “bundle of capillaries” (see chapter 1.2.3) on the plate surface leads to capillary adhesion of the liquid. Thus the pores are filled up by 1-propanol when getting in contact with the liquid.

Performing the *Wilhelmy* method this liquid adsorption influences the recorded force by immersing the plate into the probational liquid. As soon as the plate comes in contact with the liquid under study not only the expected force due to  $\sigma_L$  and  $\theta_{SL}$ :

$$F_{rec} = \frac{\cos\theta_a}{\sigma_{1.prop.l}} \quad (6.4)$$

whereas  $a$  indicates that it's a matter of advancing angle, act on the plate but also an additional weight force caused by capillary adhesion might effect an increase in weight. Thus the recorded force  $F_a$  correlated to  $\cos\theta_a$  obtained with a porous surface exceeds the one measured with a smooth surface.

The following graph should help to get an idea how the obtained  $\cos\theta_a$  values might influence the wetting behavior of 1-propanol on sodium chloride within the possible temperature range from  $T_M = -126^\circ C$  to  $T_B = 97^\circ C$ . Therefore the calculated linear regressions for the  $\cos\theta_a$  data obtained with variously prepared plates are extrapolated. Since all correlation coefficient are far beneath 1 (see appendix B.2)

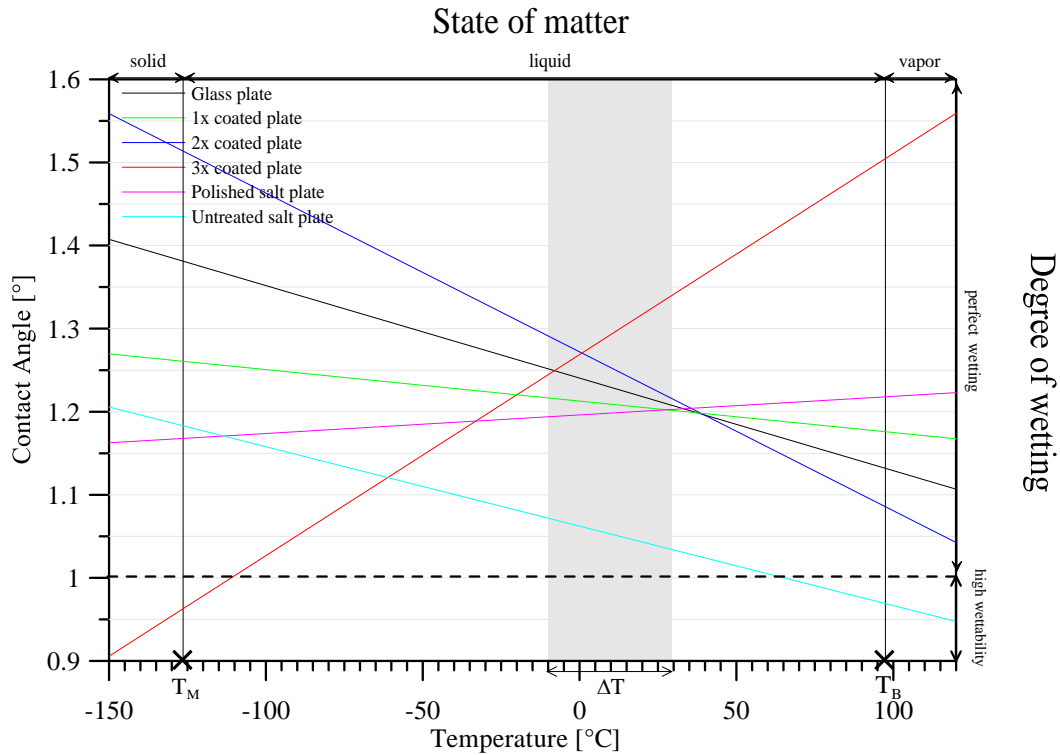


Figure 48: Temperature dependence of  $\cos\theta_a$  for 1-propanol on sodium chloride - Extrapolation of the linear regressions

what indicates a rather low correlation between data points and fitted graphs the above illustrated graph is rather supposed to show, that the wetting behavior of 1-propanol will not change than to compare the various slopes. As already noticed in figure 46 the slopes of the linear regressions are rather less expressive.

- Receding Angles

Coming now to the measured receding angles and a tentative interpretation of the unexpected behavior. As already mentioned for the particular cases except for the untreated salt plate all contact angle measurements resulted in a negative contact angle hysteresis. The corresponding  $\theta_r$  values are compared in the following graph:

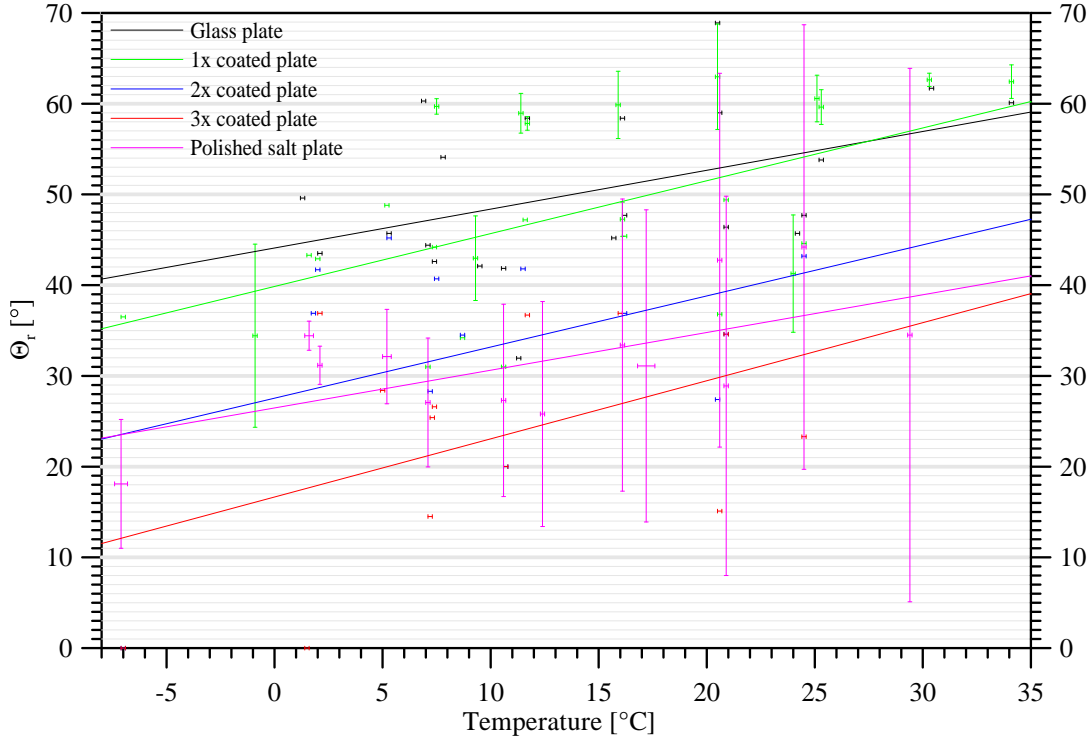


Figure 49:  $\theta_r$  values obtained with variously prepared plates as a function of temperature by comparison.

From the associated linear regressions:

$$\theta_r^{1-prop./i}(T(^{\circ}C)) = \frac{\partial \theta}{\partial T} \times T(^{\circ}C) + \theta(0^{\circ}C) \quad (6.5)$$

following contact angle specific quantities can be deduced:

	$\frac{\partial \theta}{\partial T} [\frac{deg}{^{\circ}C}]$	$\theta(0^{\circ}C) [^{\circ}]$	$\theta(20^{\circ}C) [^{\circ}]$
Glass	0.81	36.9	53.0
1XPVD	0.81	39.9	51.5
2xPVD	0.56	27.5	38.8
3xPVD	0.64	16.7	29.5
Polished crystal	0.42	26.5	34.8

Clearly also in the case of sodium chloride the contact angle and its temperature dependence changes with the number of PVD-steps performed. Since the evaluated contact angles are receding angles the above stated parameters should not be over-estimated. The reasons of the occurring differences have to be reduced on surface



quality only. Therefore an interpretation of the stated values should always be related to the corresponding  $\theta_a$  resp.  $\cos\theta_a$  value in order to calculate the contact angle hysteresis out of it.

Thus examining the contact angle hysteresis the correlation between forces acting on the plate and consequent contact angles reads as follows (for the expected behavior of  $\theta_{hyst} > 0$ :

$$\begin{array}{ccc} \theta_a > \theta_r & \rightarrow & \cos\theta_a < \cos\theta_r \\ \cos\theta = \frac{F}{\sigma_{1-prop,l}} & \rightarrow & F = \sigma_{1-prop}l\cos\theta \end{array} \quad (6.6)$$


---


$$\Rightarrow F_a < F_r$$

whereas  $a$  indicates advancing and  $r$  receding angle. Accordingly the force recorded by withdrawing the plate from the liquid is supposed to be larger than the one by immersing the plate. Obviously the the results are counter to expectations. Based on the above made assumption of porous surfaces a tentative interpretation of the unexpected behavior will be given in the following.

As already mentioned it is assumed that the pores are filled up with 1-propanol as soon as the plate gets in contact with the liquid. Based on the results of chapter 6.3 it's safe to assume that wetting proceeds fast and the pores will be filled up soon after the first contact. Thus further immersing and withdrawing will not lead to additional weight due to padding of pores. But as soon as some wetted areas of the plate is long enough out of the liquid the 1-propanol in the pores will start to evaporate, probably faster the the buoyant force decreases. This evaporation would entails a decrease in recorded force.

Finally both the overestimation of the force by immersing the plate as well as the underestimation of the force by withdrawing it perhaps lead to a negative contact angle hysteresis just as measured.

### 6.3 Washburn Method (see appendix B.3)

#### 6.3.1 Determination of the material constant $c$

As already mentioned in chapter 2.2.3 it is initially required to obtain knowledge of the solid specific material constant  $c$  before determining contact angles by means the *Washburn* method. Performing this “*premeasurements*” one receives not only the required constant  $c$  but in the course of a measurement cycle also the capillary rise velocity  $v$  of the liquid. This additional parameter provides information about the wetting velocity and is therefore the main parameter determining the contact angle.

Based on equation (2.9) the tensiometer software calculates  $c$  from recorded  $\frac{(\Delta m)^2}{t}$  data by applying the following equation ...

$$c = \frac{\Delta m^2}{t} \frac{\eta}{\rho^2 \sigma_L} \quad (6.7)$$

According to this equation perfect wetting ( $\theta_a = 0^\circ$ ) of the probational liquid on the tested powder is presupposed and therefore n-hexane was applied as recommended in [22].

The previously mentioned rise velocity is proportional to the recorded  $\frac{\Delta m^2}{t}$  data:

$$v^2 = \frac{l^2}{t} \propto \frac{\Delta m^2}{t} \cdot t \quad (6.8)$$

whereas  $l$  indicates the capillary rise - approximately the height of the lifted liquid volume (see 1.2.3). Thus in what follows  $\frac{\Delta m^2}{t}$  will be termed  $v'$  keeping in mind that actually the mass increase per unit time is meant.

In order to calculate the just reviewed constants following liquid specific parameters were additionally required to calculate firstly  $c$  and afterwards the wanted contact angle  $\theta_a$  out of  $c$  and  $v'$  data ...

Probational Liquid		N-Hexane p.A.	1-Propanol p.A.
Surface tension $\sigma_L$	$\left[\frac{mN}{m}\right]$	$18.6 \pm 0.1$	$23.7 \pm 0.1$
Viscosity $\eta$	$\left[\frac{g}{ms}\right]$	0.32	2.2227
Density $\rho$	$\left[\frac{g}{ml}\right]$	0.68	0.8034
Substance specific constant $a = \frac{\eta}{\rho^2 \sigma_L}$	$\left[\frac{sm^2}{g^2m}\right]$	$3.7206533 \cdot 10^{-2}$	$1.4530108 \cdot 10^{-1}$

The above defined constant  $a$  is a solely liquid specific property and related to  $v'$ ,  $c$  and  $\theta$  as follows ...

$$\theta_a \begin{cases} = 0^\circ & \rightarrow c = av' \\ > 0^\circ & \rightarrow \cos\theta_a = a \frac{v'}{c} \end{cases}$$

- $c$  and  $v$  results for n-hexane on sodium chloride powder

Measurements were performed at a temperature of  $\approx 20.2^\circ\text{C} \pm 0.3^\circ\text{C}$ .

	$c$	$[cm^5]$	$v'$	$[\frac{g^2}{s}]$
1.	$3.2643 \cdot 10^{-6}$		$8,755 \cdot 10^{-5}$	
2.	$3.8632 \cdot 10^{-6}$		$1.037 \cdot 10^{-4}$	
3.	$5.7210 \cdot 10^{-6}$		$1.536 \cdot 10^{-4}$	
4.	$3.2168 \cdot 10^{-6}$		$8.636 \cdot 10^{-5}$	
5.	$3.5846 \cdot 10^{-6}$		$9.614 \cdot 10^{-5}$	
6.	$3.7266 \cdot 10^{-6}$		$9.9941 \cdot 10^{-5}$	
7.	$3.4376 \cdot 10^{-6}$		$9.294 \cdot 10^{-5}$	
8.	$5.2034 \cdot 10^{-6}$		$1.396 \cdot 10^{-4}$	
9.	$3.2238 \cdot 10^{-6}$		$8.669 \cdot 10^{-5}$	
10.	$3.6915 \cdot 10^{-6}$		$8.058 \cdot 10^{-5}$	
11.	$2.9966 \cdot 10^{-6}$		$1.15 \cdot 10^{-4}$	
12.	$4.5461 \cdot 10^{-6}$		$1.229 \cdot 10^{-4}$	
13.	$3.6002 \cdot 10^{-6}$		$9.666 \cdot 10^{-5}$	
<b>Mean</b>	$(3.9 \pm 0.9) \cdot 10^{-6}$		$(1.1 \pm 0.2) \cdot 10^{-4}$	

### 6.3.2 Contact angle for 1-propanol on sodium chloride

Not until after the determination of  $c$  the proper contact angle measurement was performed. Based on the assumption of a unchanged material constant and a finite contact angle equation 6.7 becomes:

$$\cos\theta_a = v' \frac{a}{c} \quad (6.9)$$

Obviously the contact angle depends on the capillary rise velocity:

$$\theta_a \begin{cases} \in (0^\circ; 90^\circ) & \text{if } v' < \frac{c}{a} \\ \equiv 0^\circ & \text{if } v' \geq \frac{c}{a} \end{cases}$$

Complying with the probe preparation instructions listed in chapter 3.4. the contact angle for 1-propanol on sodium chloride at  $T = 20^\circ\text{C} \pm 0.1$  was determined as ...

$$\theta_a \equiv 0^\circ \quad (6.10)$$

In order to elucidate how strong the wetting behavior of 1-propanol is the comparison between  $v'$  data obtained for n-hexane and 1-propanol turns out to be most helpful. In doing so the corresponding physical property compared is the rise velocity (see equ.6.9).

- $v'$  obtained for 1-propanol on sodium chloride

	$v'$ $\left[\frac{g^2}{s}\right]$
1.	$9.88 \cdot 10^{-3}$
2.	$1.1655 \cdot 10^{-2}$
3.	$1.8606 \cdot 10^{-2}$
<b>Mean</b>	$(1.3 \pm 0.5)10^{-2}$

Following graph illustrates the contact angle as a function of  $v'$  comparing 1-propanol results with those obtained for n-hexane.

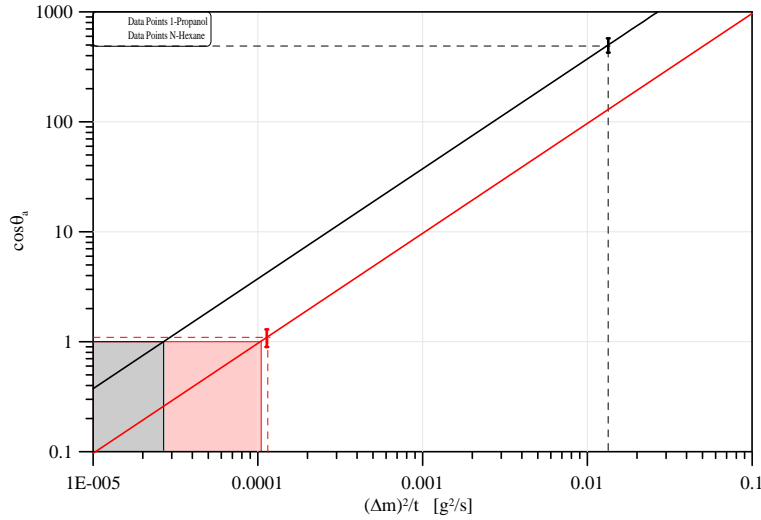


Figure 50: Comparison of the contact angle as a function of  $v'$  obtained with 1-propanol and n-hexane

Noticing the logarithmic scale the “magnitude” of perfect wetting determined for 1-propanol on sodium chloride becomes explicit.

Quantitatively examined the  $v'$  ratio of n-hexane to 1-propanol gives...

$$\frac{v'_{1-prop.}}{v'_{n-hex.}} = \frac{1.3 \cdot 10^{-2}}{1.1 \cdot 10^{-4}} \approx 10^2 \quad (6.11)$$

thus the only parameter left for a non zero contact angle of 1-propanol on sodium chloride is the substance specific constant  $a_{1-propanol}$ . Just in case of  $\frac{a_{1-prop.}}{a_{n-hex.}} \ll 10^{-2}$  the contact angle will differ from zero. However the comparison between liquid specific constants results in...

$$\frac{a_{1-prop.}}{a_{n-hex.}} = \frac{1.4530108 \cdot 10^{-1}}{3.7206533 \cdot 10^{-2}} \approx 4 \gg 10^{-2} \quad (6.12)$$

It shows clearly that  $\frac{a_{1-prop.}}{a_{n-hex.}} \gg 10^{-2} \propto \frac{1}{\frac{v'_{1-prop.}}{v'_{n-hex.}}}$  and thus it's safe to assume that the contact angle (advancing angle  $\theta_a$ ) for 1-propanol on sodium chloride is zero:

$$\theta_a(T \approx 20^\circ C) \equiv 0^\circ \quad (6.13)$$

Even n-hexane, which is supposed to wet all solids perfectly and therefor always recommended as probational liquid when perfect wetting is required, wets the sodium chloride powder slower than 1-propanol. Since the wetting velocity is directly proportional to  $\cos\theta_a$  the measured difference in  $v'$  shows very clearly how “perfect” 1-propanol wets sodium chloride.

In the course of the presented thesis it was unfortunately not possible to apply the *Washburn* methods in a wider range of temperature. However the realized sorption measurements confirm the contact angle results obtained with the *Wilhelmy* method.

All contact angle measurements resulted in an advancing angle of  $0^\circ$  within the observed temperature range.

#### 6.4 Errors of the measurement data

In the following a detailed error analysis is presented.

Following parameters were required to calculate the contact angle...

	Mean	$\delta_{stat.}$	$\delta_{syst.}$
<b><math>l[mm]</math></b>	52.7	$\pm 0.3$	$\pm 0.001$
$\sigma_L \left[ \frac{mN}{m} \right]$	25.52	0.1	0.1
$\left[ \frac{F}{a_{acc.}} \right] [mg]$	121.6	0.2	0.1

wheres the statistical errors result from 4 measurements (conditions being equal). According to propagation of uncertainty the error of  $\theta = \arccos(\frac{F}{\sigma l})$  is given by ...

$$\begin{aligned}
 \Delta\theta &= \left( \frac{\partial\theta}{\partial F} \right) \cdot \Delta F + \left( \frac{\partial\theta}{\partial l} \right) \cdot \Delta l + \left( \frac{\partial\theta}{\partial \sigma} \right) \cdot \Delta\sigma \\
 &= \left( -\frac{1}{\sqrt{1 - \left(\frac{F}{\sigma l}\right)^2}} \frac{1}{\sigma l} \right) \cdot \Delta F + \left( \frac{1}{\sqrt{1 - \left(\frac{F}{\sigma l}\right)^2}} \frac{F}{\sigma l^2} \right) \cdot \Delta l + \\
 &\quad + \left( \frac{1}{\sqrt{1 - \left(\frac{F}{\sigma l}\right)^2}} \frac{F}{\sigma^2 l} \right) \cdot \Delta F \sigma
 \end{aligned} \tag{6.14}$$

Consequent the systematical error of the contact angle results in ...

$$\Delta\theta \approx 0.003^\circ \tag{6.15}$$

as against the statistical error ...

$$\Delta\theta \approx 0.2^\circ \tag{6.16}$$

Thus the statistical error due to random distribution of measurement values exceeds the systematical one significantly:

$$\frac{\Delta\theta_{syst.}}{\Delta\theta_{stat.}} \approx 1.5\% \tag{6.17}$$

Based on this estimate all errors for surface tensions, contact angles and material constants stated are statistical nature. Solely the systematical error of one wetted lengths metered with the gauge ( $\pm 0.2mm$ ) exceeds - specifically marked by bold font - and is therefore adopted for further calculations.

## 7 Conclusions

Following conclusions for the temperature dependence of the contact angle for 1-propanol on silver and on sodium chloride can be deduced from the measurements performed in the course of the presented thesis:

- Contact angle between silver and 1-propanol as a function of temperature
  1. Applying the *Dynamic Wilhelmy method* it turns out that depending on the type of preparation, the cleaning procedure and the age of the plate the contact angle between 1-propanol and sterling silver varies from  $11^\circ \pm 0.1^\circ$  to  $32.6^\circ \pm 0.6^\circ$  at  $T \approx 20^\circ C$ .
  2. In coating the smoothest sterling silver plate with silver p.A. via PVD it transpires that the 7.5% copper content in the original probe influences the contact angle and its temperature dependence. Thus measurements using a sterling silver plate are not representative for the contact angle between silver and 1-propanol.
  3. The more often a plate is coated the more decreases the contact angle and its temperature dependence. The contact angle obtained with an uncoated plate increases from  $11.4^\circ \pm 0.5$  at  $T = -6.2 \pm 0.1^\circ C$  to  $31^\circ \pm 1$  at  $T = 24.7 \pm 0.1^\circ C$  what corresponds to a  $\Delta\theta_a$  of  $\approx 20^\circ$  at a temperature increase of  $\approx 30^\circ C$ . In contrast measurements using a one time coated plate result in an advancing angle increasing from  $22^\circ \pm 3$  at  $-6.2 \pm 0.1^\circ C$  to  $25^\circ \pm 1$  at  $24.7 \pm 0.1^\circ C$  and thus correspond to a  $\Delta\theta_a$  of  $\approx 3^\circ$  within the observed temperature range. Finally the usage of a two times coated plates leads to a contact angle increasing from  $17.1^\circ \pm 1$  at  $-6.2^\circ C \pm 0.1$  to  $18.0^\circ \pm 0.4$  at  $24.7 \pm 0.1^\circ C$ . Considering the statistical errors of single measurements the contact angles obtained with two times coated plates can also be interpreted as remaining  $17^\circ \pm 1^\circ$  within the whole temperature range.
  4. A correlation between surface roughness and change in contact angle for the similarly prepared but variously often coated plates can be excluded since no change in receding angle was noticed. If the plate surface would have become smoother with increasing number of silver layers not only the advancing angles would decrease but also the receding angles should be increasing as a consequence. However the receding angles in the main remained  $0^\circ$  independent of the used plate.
- Contact angle between sodium chloride and 1-propanol as a function of temperature
  1. Contact angle measurements using both the *Dynamic Wilhelmy method* as well as the *Washburn method* resulted in an advancing angle of  $0^\circ$  for 1-propanol on sodium chloride. Thus no temperature dependence of the contact angle was observed.

2. The *Dynamic Wilhelmy method* was applied at temperatures from  $\approx -7^\circ\text{C}$  to  $\approx 35^\circ\text{C}$  using on the one hand sodium chloride plates and on the other hand via PVD *NaCl*-coated glass plates. Solely measurements with the untreated salt plate resulted in  $0^\circ$  for the receding angle as well. Contrary to expectations the receding angles obtained with all the other plates always exceeded the advancing angles, what might be referred to surface roughness and therewith associated adsorption of the liquid under study at the surface of the plates.
  3. Although the advancing angle remains  $0^\circ$  statistical scatter of  $\cos\theta_a$  values exist. However these errors never lead to a  $\cos\theta_a$  value smaller than 1 and thus a variation of the contact angle due to statistical errors can be excluded.
  4. Solely the untreated salt plate complies with theoretical expectations of  $\theta_{hyst} > 0$ . Although all  $\cos\theta$  values exceed 1 a comparison between the forces recorded by immersing respectively withdrawing the plate accord to expectations. Considering that the the recorded forces are proportional to  $\cos\theta_a$  respectively  $\cos\theta_r$  a positive contact angle hysteresis corresponds to  $\cos\theta_a < \cos\theta_r$ .
  5. Examining the sodium chloride-coated glass plates the decrease in  $\theta_r$  values with increasing number of coats indicates an increasing surface quality. That is to say, that the more salt layers are placed on the glass surface the smaller the “pore” size becomes and thus the less liquid is adsorbed by the surface of the plate.
  6. The polishing of the salt crystal obviously changes the surface properties and leads to inapplicable probes what is reflected in large statistical errors.
  7. Measurements using the *Washburn method* were performed at a temperature of  $\approx 20^\circ\text{C}$  and confirmed the results obtained with the *Dynamic Wilhelmy method*. How fast the perfect wetting of 1-propanol on sodium chloride progresses elucidates a comparison between the capillary rise velocity of 1-propanol and n-hexane. Due to its low surface tension ( $18.4 \frac{\text{mN}}{\text{m}}$ ) n-hexane is supposed to perfectly wet every probational solid and thus it is always applied when calibration measurements require a contact angle of  $0^\circ$ . However 1-propanol wets sodium chloride 100 times faster than n-hexane. Considering that the wetting velocity is proportional to  $\cos\theta_a$  the factor 100 shows clearly how “perfect” *NaCl* is wetted by 1-propanol.
- The strange temperature dependence for the nucleation process of n-propanol vapour on NaCl is not explainable by a temperature dependent macroscopic contact angle.



## Bibliography

- [1] **Adamson, A.W.**; *Physical Chemistry of Surfaces, 5th ed.* (1990) , Wiley-Interscience N.Y.
- [2] **Bangham D. H. and Razouk R. I.**; *Trans. Faraday Soc.* **(33)** 1459 , (1937)
- [3] **Bermann, Schäfer**; *Lehrbuch der Experimentalphysik -Bd.1* , (1998)
- [4] **Brandon S. and Marmur A.**; *Simulation of Contact Angle Hysteresis on Chemically Heterogeneous Surfaces; J. Coll. Int. Sci* **(183)** 351-355 , (1996)
- [5] **Bronstein I. N., Semendjajew K. A., Musiol G. and Mühlig H.**; *Taschenbuch der Mathematik* (2001) , Verlag Harri Deutsch
- [6] **Cassie A. B. D.**; *Disc. Faraday Soc.* **(3)** 11 , (1948)
- [7] **Chen W. and McCarthy T. J.**; *Macromolecules* **(30)** 78 , (1997)
- [8] **Cubaud T. and Fermigier M.**; *Advancing Contact Lines on Chemically Patterned Surfaces; J. Coll. Int. Sci.* **(269)** 171-177 , (2004)
- [9] **Dean J.**; *Lange's Handbook of Chemistry*, **(15)**, New York (1999)
- [10] **Fadeev A. Y. and McCarthy T. J.**; *Langmuir* **(15)** 3759 , (1999)
- [11] **Fletcher, N. H.**; *Size Effect in Heterogeneous Nucleation; J. Chem. Phy.* **(29)**, (1958)
- [12] **Gaman A. I. and Napari I. et al.**; *J. Chem. Phy.*, **(123)**, 244502 (2005)
- [13] **Decker E. L. and Garoff S.**; *Langmuir* **(12)** 2100 , (1996) and *Langmuir* **(13)** 6321 , (1997)
- [14] **Germer L. H. and McRae A. U.**; *J. Appl. Phys.* **(33)** 2923 , (1962)
- [15] **Gibbs J. W.**; *Collected Works of J. W. Gibbs* **(1)** , (1928) ; Yale University Press
- [16] **Gibbs J. W.**; *Collected Works of J. W. Gibbs* p.322 , (1931); Longmans Green; New York
- [17] **Neumann A. W. and Good R. J.**; *Techniques of Measuring Contact Angles, Surface and Colloid Science (Vol. II)* , (1979) ; New York
- [18] **Harkins W. D. and Livingston H. K.**; *J. Chem. Phys.* **(10)** 342 , (1942)
- [19] **Hill, G.**; *Experimentelle Bestimmung von Oberflächenspannungen organischer Flüssigkeiten sowie von deren Kontaktwinkeln bezüglich poröser und nicht poröser Substrate mit Hilfe der Methoden nach Washburn und nach Wilhelmy* (2007) , Diplomarbeit; Universität Wien
- [20] **Hinds, W. C.**; *Aerosol Technology* (1982) , John Wiley and Sons
- [21] **Kirkwood J. G. and Buff F. P.**; *The Statistical Mechanical Theory of Surface Tension; J. Chem. Phy.* **(17)** 338-343 , (1948)

- [22] **Fa. Krüss GmbH**; *Seminar zu Tensiometrie und Kontaktwinkelmessung* , (2008)
- [23] **Tensiometer K12 - Manual**; *KRÜSS GmbH. Wissenschaftliche Laborgeräte*; (1996)
- [24] **Lam C. N. C., Neumann A. W. et al**; *Dynamic Cycling Contact Angle Measurements: Study of Advancing and Receding Contact Angles*; *J. Coll. Int. Sci.* (**243**) 208-218 , (2001)
- [25] **London F.**; *z. Phys. Chem.*(**B11**) 222 , (1930)
- [26] **Miller C. A.**; *Interfacial phenomena*; *Surf. Sci. Ser. vol 17* , Marcel Dekker Inc., New York, (1985)
- [27] **Brezesinski G. and Mögel Hans-Jörg**; *Grenzflächen und Kolloide* (1993) , Spektrum Akademischer Verlag; Heidelberg
- [28] **Neumann A. W., Spelt J. K.**; *Applied Surface Thermodynamics; Surfactant Science Series* (**63**) , (1996)
- [29] **Neumann A. W. and Renzow D.**; *Z. Phys. Chemie Neue Folge* (**68**) 11 , (1969)
- [30] **Cain J. B. and Neumann A. W.**; *J. Col. Int. Sci* (**94**) 123 , (1983)
- [31] **Noüy, L. du**; *A New Apparatus for Measuring Surface Tension*, *J. gen. Physio.* (**1**) 521-524 , (1919)
- [32] **Ortner, R.**; *Experimentelle Bestimmung von Kontaktwinkeln unärer und binärer Flüssigkeiten bezüglich verschiedener Substrate und Vergleich der Wilhelmy-Methode mit dem goniometrischen Verfahren* (2000) , Diplomarbeit; Universität Wien
- [33] **Schobesberger S.**; *Strange Temperature Dependence Observed For Heterogeneous Nucleation of n-Propanol Vapor On NaCl Particles* (2008) , Diplomathesis at University of Vienna.
- [34] **Sedev R. V., Petrov J. G. and Neumann A. W.**; *J. Coll. Int. Sci* (**180**) 36 , (1996)
- [35] **Strey R. and Schmeling T.**; *Ber. Bunsenges. Phys. Chem.*, (**87**), 423-327 (1983)
- [36] **Wagner P. E.**; *Kondensationsvorgänge, Vorlesungsmitschrift* (2009) ; Wien
- [37] **Washburn E. W.**; *Phys. Rev. Ser. 2* (**17**) 273 , (1921)
- [38] **Washburn E. W.**; *The dynamics of capillary flow*; *Phys. Rev.* (**17**) 273-283 , (1921)
- [39] **Wegener P. P.**; *J. Phys. Chem.* (**91**) 2479 , (1987)
- [40] **Wegener P. P.**; *Naturwissenschaften* (**74**) 111 , (1987)
- [41] **Wenzel R. N.**; *Ind. Eng. Chem.* (**28**) 988 , (1936)
- [42] **Wenzel R. N.**; *J. Phys. Coll. Chem.* (**53**) 1466 , (1949)

- [43] **Wulff G.**; *Z. Krist.* **(34)** 449 , (1901)
- [44] **Youngblood J. P. and McCarthy T. J.**; *Macromolecules* **(32)** 6800 , (1999)
- [45] **Zettlemoyer A. C.**; *Ind. Eng. Chem.* **(57)** 27 , (1965)
- [46] **biade.itrust.de**
- [47] **[www.unicorns-garden.com/info.html](http://www.unicorns-garden.com/info.html)**
- [48] **[www.azom.com/Details.asp?ArticleID=3473](http://www.azom.com/Details.asp?ArticleID=3473)**

## List of Figures

1	<i>Interfacial profile in molecular dimensions [3]</i> . . . . .	1
2	<i>Density profile across a deformable liquid-vapor interface showing the placement of the dividing surface and the regions of the density profile which contribute to the final value of the surface density.[28]</i> . . . . .	3
3	<i>Schematic diagram showing the intermolecular forces acting across the surface [3]</i> . . . . .	6
4	<i>Circumscription of the interface region - <math>S_S</math> is orthogonal to <math>S_\sigma, S_\alpha</math> and <math>S_\beta</math> [26]</i> . . . . .	6
5	<i>Condition for mechanical equilibrium for an arbitrarily curved surface[28]</i> . . . . .	9
6	<i>Lennard-Jones potential showing the intermolecular correlation as a function of molecule distance[1]</i> . . . . .	10
7	<i>Draft of the 3 forces action on the contact line[36]</i> . . . . .	12
8	<i>Work of adhesion and work of cohesion[1]</i> . . . . .	13
9	<i>Illustration of the difference between <math>\theta_a</math>, <math>\theta_e</math> and <math>\theta_r</math></i> . . . . .	16
10	<i>Idealized rough surface showing the difference between apparent and real contact angle[19]</i> . . . . .	17
11	<i>Change of the contact angle on a rough surface[22]</i> . . . . .	17
12	<i>Illustration of an idealized heterogeneous surface [19]</i> . . . . .	18
13	<i>Free energy <math>\Delta G</math> as a function of droplet radius <math>r</math> at different saturation ratios <math>S = \frac{p}{p_s(T)}</math>[36]</i> . . . . .	22
14	<i>Draft of a cluster on the surface of an insoluble solid particle[32]</i> . . .	24
15	<i>Schematic profile of the slide method[22]</i> . . . . .	29
16	<i>Illustration of both applicabilities by performing the sessile drop method - liquid density decreases with increasing lightness</i> . . . . .	30
17	<i>Neumann's method for contact angle measurement [1]</i> . . . . .	31
18	<i>Illustration of the occurring contact angles as a function of the plate's direction of movement in comaprison with the contact angle occurring by holding the plate constant on liquid surface level</i> . . . . .	32
19	<i>Idealized measurement log of the dynamic Wilhelmy method [22]</i> . . .	32
20	<i>Illustration of the forces acting on a plate by performing the dynamic Wilhelmy method</i> . . . . .	33
21	<i>Scheme of the Washburn method[22]</i> . . . . .	34
22	<i>Draft of the measuring setup</i> . . . . .	36
23	<i>Profile of the measurement chamber</i> . . . . .	37
24	<i>Illustration of the polishing procedure showing the position of the plate in right coordination with the direction of rotation</i> . . . . .	40
25	<i>Illustration of the polishing procedure performed by Ms. M. Rohrer</i> . .	42
26	<i>Scheme of PVD</i> . . . . .	43
27	<i>Scheme of the preparation of natural shaped salt plates</i> . . . . .	44
28	<i>Experimental data for surface tension of 1-propanol compared with the curves determined by Strey [35] and by Dean [9] - Linear Fits 1 respectively 2 are chosen parallel to [35] respectively[9]</i> . . . . .	47
29	<i>Surrounding air temperature as a function of refrigerant temperature</i>	48
30	<i>Contact angle of 1-propanol on not coated sterling silver - various preparation procedures by comparison</i> . . . . .	51

31	Contact angle of 1-propanol on one time-coated sterling silver as a function of temperature - averaging P1 and P2 data . . . . .	54
32	Contact angle of 1-propanol on two-times coated sterling silver . . . .	56
33	Temperature dependence of the contact angle for 1-propanol on silver - different numbers of PVD-steps in comparison with the values stated in [19] and [32] . . . . .	57
34	Temperature dependence of the contact angle for 1-propanol on silver as a function of PVD-steps - Extrapolation of the linear regressions. .	59
35	Experimental data for surface tension of 1-propanol compared with the curves determined by Strey [35] and by Dean [9] - Linear Fits 1 respectively 2 are chosen parallel to [35] respectively [9] . . . . .	60
36	$\cos\theta_a$ and $\cos\theta_r$ data obtained with a pure glass plate as a function of temperature . . . . .	63
37	$\theta_r$ data for 1-propanol on glass as a function of temperature . . . . .	64
38	$\cos\theta_a$ and $\cos\theta_r$ data obtained with one time coated plates as a function of temperature . . . . .	66
39	$\theta_r$ data for 1-propanol on one time coated glass as a function of temperature . . . . .	67
40	$\cos\theta_a$ and $\cos\theta_r$ data obtained with two times coated plates as a function of temperature . . . . .	68
41	$\theta_r$ data for 1-propanol on two times coated glass as a function of temperature . . . . .	69
42	$\cos\theta_a$ and $\cos\theta_r$ data obtained with three times coated plates as a function of temperature . . . . .	70
43	$\theta_r$ data for 1-propanol on three times coated glass as a function of temperature . . . . .	71
44	$\cos\theta_a$ and $\cos\theta_r$ data obtained with polished salt crystals as a function of temperature . . . . .	74
45	$\theta_r$ data for 1-propanol on polished salt crystals as a function of temperature . . . . .	75
46	$\cos\theta_a$ and $\cos\theta_r$ data obtained with untreated salt crystals as a function of temperature . . . . .	76
47	$\cos\theta_a$ values obtained with variously prepared plates as a function of temperature by comparison. . . . .	78
48	Temperature dependence of $\cos\theta_a$ for 1-propanol on sodium chloride - Extrapolation of the linear regressions . . . . .	79
49	$\theta_r$ values obtained with variously prepared plates as a function of temperature by comparison. . . . .	81
50	Comparison of the contact angle as a function of $v'$ obtained with 1-propanol and n-hexane . . . . .	85
51	Mean of P1 data . . . . .	99
52	Results for Cycle 1 with P1 . . . . .	100
53	Results for Cycle 2 with P1 . . . . .	101
54	Results for Cycle 3 with P1 . . . . .	102
55	Results for Cycle 4 with P1 . . . . .	103
56	Mean of P2 data . . . . .	105
57	Results for Cycle 1 with P2 . . . . .	106
58	Results for Cycle 2 with P2 . . . . .	107
59	Results for Cycle 3 with P2 . . . . .	108

60 Results of Cycle 4 with P2 . . . . . 109

61 Results for Cycle 1 with P3 . . . . . 112

62 Results for Cycle 2 with P3 . . . . . 113

63 Results for Cycle 3 with P3 . . . . . 114

64 Results for Cycle 4 with P3 . . . . . 115

## A Data for silver/1-propanol contact angle measurements

### A.1 Surface Tension during measurements

- Surface tension data

$T$ [°C]	$\sigma$ [ $\frac{mN}{m}$ ]	$\delta_\sigma$ [ $\frac{mN}{m}$ ]	$T$	$\sigma$	$\delta_\sigma$
34.1	22.3	0.4	11.5	24.79	0.09
30.3	22.9	0.1	11.4	24.9	0.1
29.4	23	-	11.3	24.86	-
25.3	23.40	0.06	10.6	24.64	-
24.4	23.54	0.05	9.5	24.76	-
23.9	23.46	-	8.5	25.14	0.07
20.8	23.84	0.08	7.4	25.16	0.06
20.6	23.9	0.1	7	25.24	0.06
20.3	23.8	0.3	5	25.51	0.01
20	23.73	-	1.8	25.87	-
16.2	24.2	0.2	1.6	25.9	0.2
16.1	24.49	-	-3	26.44	0.09
15.7	24.35	-			

- Linear Regression 1

$$\sigma(T) = 48.21 - (T(K) - 5.417607788) \cdot 0.08394$$

$$R^2 = 0.965439$$

- Linear Regression2

$$\sigma(T) = 25.26 - (T(^{\circ}C) - 5.426821857) \cdot 0.0777$$

$$R^2 = 0.946197$$

**A.2 Uncoated 925 sterling silver - 0xPVD**

- Wetted lengths

Prep. acc. to ...	$l$ [mm]	$b^*$ [mm]	$d^*$ [mm]	$l^*$ [mm]
R. Ortner	50.465	24.50	0.10	49.2
	47.950	25.00	0.10	50.2
<b>Mean</b>	$49.8 \pm 0.3$	$24.75 \pm 0.05$	$0.10 \pm 0.05$	$50.0 \pm 0.2$
J. Karoly	51.436	25.40	0.50	51.8
	51.411	25.40	0.50	51.8
	51.432	25.25	0.50	51.5
	51.554	25.20	0.50	51.4
<b>Mean</b>	$51.58 \pm 0.08$	$25.28 \pm 0.05$	$0.50 \pm 0.05$	$51.6 \pm 0.2$
M. Rohrer	50.879	24.70	0.50	50.4
	50.602	24.70	0.50	50.4
	50.470	24.85	0.50	50.7
<b>Mean</b>	$50.8 \pm 0.2$	$24.75 \pm 0.05$	$0.50 \pm 0.05$	$50.6 \pm 0.2$

- Contact angle data

Prep. acc. to ...	$T$ [°C]	$\theta_a$	$\theta_r$
R. Ortner	21	30.8	12.1
		29.5	7.8
		28.9	7.4
		$29.85 \pm 1.34(4.5\%)$	
	11.4	25.3	14.3
J. Karoly	21	10.8	5.2
		11	3.3
		11	3
		11.5	3.2
		$11.075 \pm 0.13(1.2\%)$	
	11.4	11.6	5.5
		11.3	3.8
		11.1	0
		11.2	3.5
		$11.3 \pm 0.09(0.8\%)$	
M. Hindler	27.5	5.1	-
		5.51	-
		4.16	-
		5.46	-
		$5.06 \pm 0.63(12.4\%)$	
M. Rohrer	24.7	31	4.5
	21	28.9	0
	17.2	17.1	0
	12.4	16.1	0
	7.1	14.2	0
	2.7	13.9	0
	-1.8	16.4	0
	-6.2	11.4	0



- Linear Regression

$$\theta_a^{1-prop./925-silver}(T(^{\circ}C)) = 0.54 \times T(^{\circ}C) + 13.34$$

$$R^2 = 0.69$$

### A.3 One-time coated sterling silver - 1xPVD

- Wetted lengths

Plate marking	$l$ [mm]	$b^*$ [mm]	$d^*$ [mm]	$l^*$ [mm]
P1	52.414	25.55	0.50	52.1
	52.938	25.60	0.50	52.2
	52.866	25.55	0.50	52.1
Mean	$52.7 \pm 0.3$	$25.57 \pm 0.05$	$0.50 \pm 0.05$	$52.6 \pm 0.2$
P2	54.729	26.80	0.50	54.6
	55.631	26.75	0.50	54.5
	53.394	26.90	0.50	54.8
Mean	$55 \pm 1$	$26.82 \pm 0.05$	$0.50 \pm 0.05$	$54.8 \pm 0.2$

- Contact angle data P1

$T[^{\circ}C]$	Cycle 1		Cycle 2		Cycle 3		Cycle 4	
	$\theta_a$	$\theta_r$	$\theta_a$	$\theta_r$	$\theta_a$	$\theta_r$	$\theta_a$	$\theta_r$
24.7	24.2	0	-	-	-	-	-	-
19.9	24.8	31.8	-	-	-	-	-	-
19.4	25.1	4.3	26.4	0	25.3	0	25.3	0
	$25.5 \pm 0.6(2.3\%)$							
14.9	24.6	0	23.3	30.7	25.9	0	23.5	0
	$24 \pm 1(4.9\%)$							
12.4	25.1	0	-	-	-	-	-	-
11.8	26.1	0	-	-	-	-	-	-
10.5	24.7	34.9	24.8	34.3	25.3	0	23	0
	$24 \pm 1(4.1\%)$							
7.7	24	32.4	-	-	-	-	-	-
7.1	24.2	0	24.7	0	-	-	-	-
	$24.5 \pm 0.2(0.7\%)$							
5.9	25.4	0	25.2	0	25.3	0	25	0
	$25.2 \pm 0.2(0.7\%)$							
4.6	24.2	0	-	-	-	-	-	-
3.8	24.4	0	-	-	-	-	-	-
2.7	23.9	0	-	-	-	-	-	-
1.1	22.2	0	25.4	0	22.7	0	24.1	0
	$24 \pm 1(6.0\%)$							
-1.8	25.2	12.1	-	-	-	-	-	-
-4.7	24.4	0	-	-	-	-	-	-
-6.2	24.4	33.0	-	-	-	-	-	-

- Temperature dependence of the contact angle for 1-propanol on P1

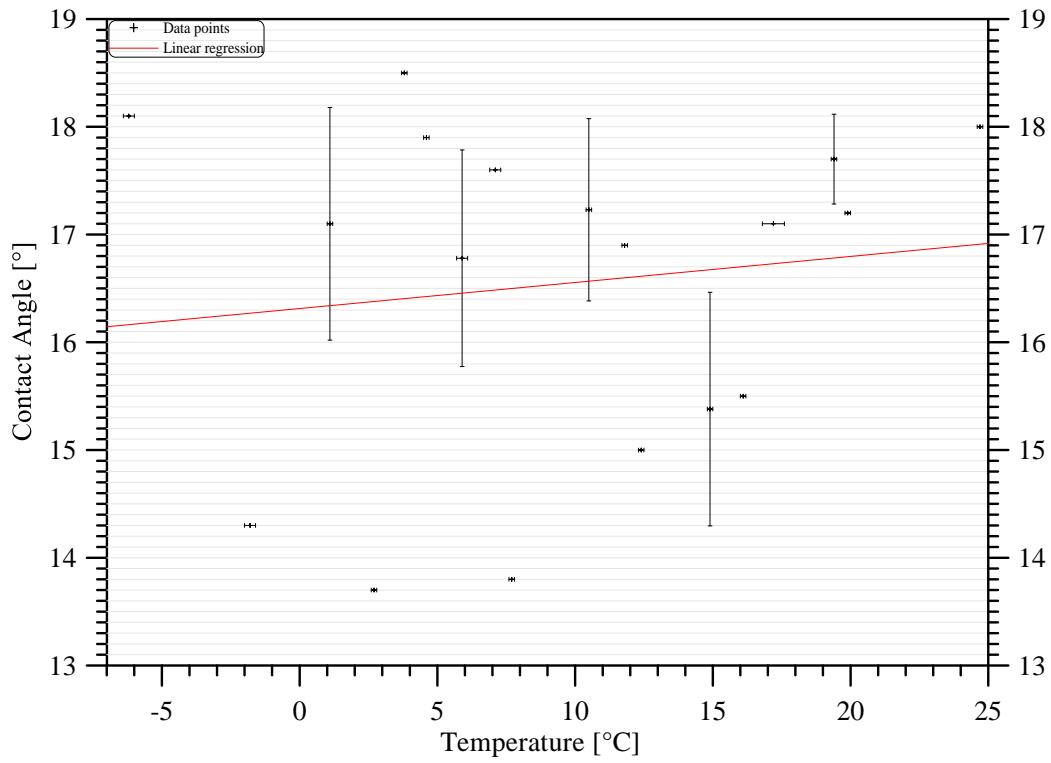


Figure 51: Mean of P1 data

- Linear Regression P1

$$\theta_a^{1-prop./P1}(T(^{\circ}C)) = 0.01 \times T(^{\circ}C) + 24.42$$

$$R^2 = 0.01$$

– Data Plot P1 - Cycle 1

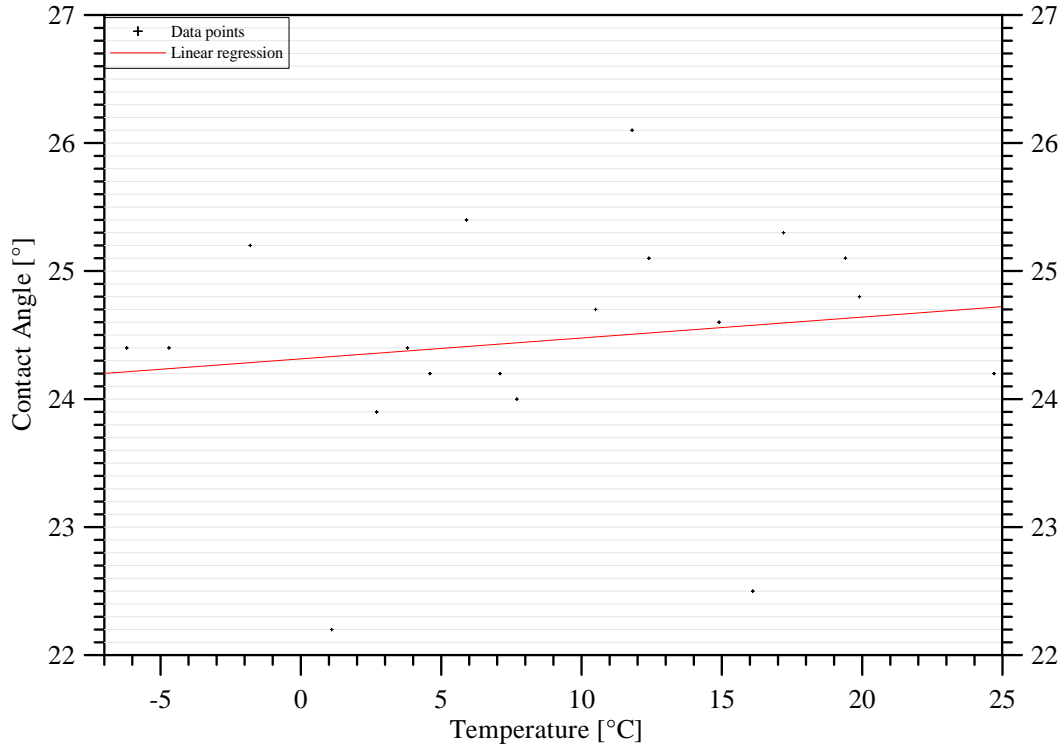


Figure 52: Results for Cycle 1 with P1

Linear Regression fitted through the measured values(19):

$$\theta_a^{1-prop./P1}(T(^{\circ}C)) = 0.02 \times T(^{\circ}C) + 24.31 \quad (\text{A.1})$$

Coef of determination, R-squared = 0.02

– Data Plot P1 - Cycle 2

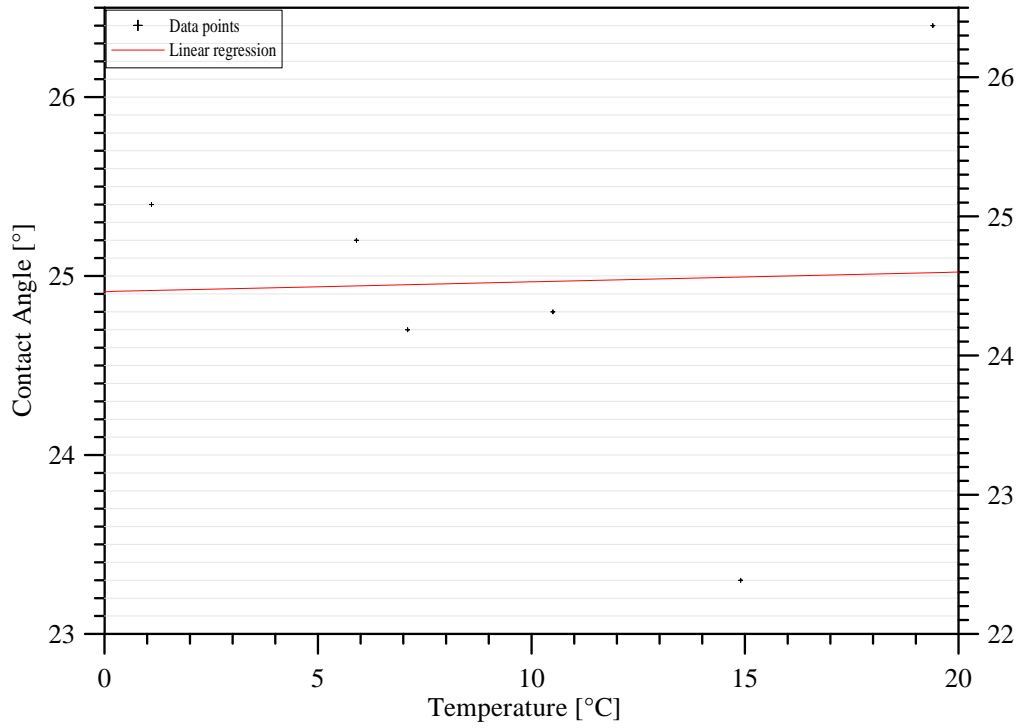


Figure 53: Results for Cycle 2 with P1

Linear Regression fitted through the measured values(6):

$$\theta_a^{1-prop./P1}(T(^{\circ}C)) = 0.005 \times T(^{\circ}C) + 24.91 \quad (\text{A.2})$$

Coef of determination, R-squared = 0.001

– Data Plot P1 - Cycle 3

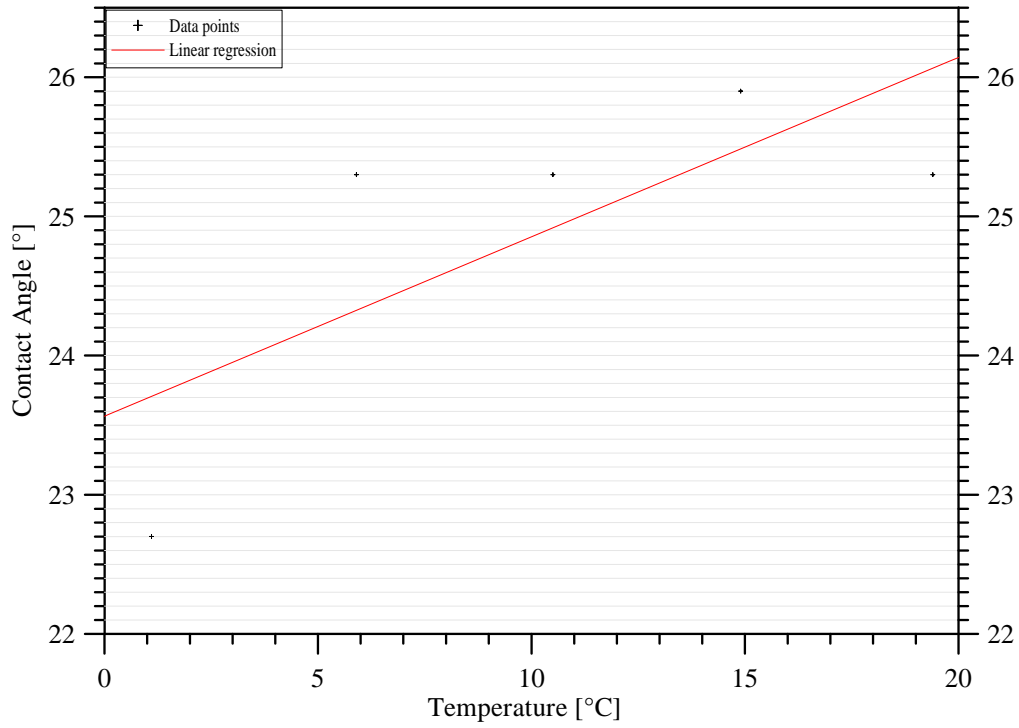


Figure 54: Results for Cycle 3 with P1

Linear Regression fitted through the measured values(5):

$$\theta_a^{1-prop./P1}(T(^{\circ}C)) = 0.13 \times T(^{\circ}C) + 23.57 \quad (\text{A.3})$$

Coef of determination, R-squared = 0.55

– Data Plot P1 - Cycle 4

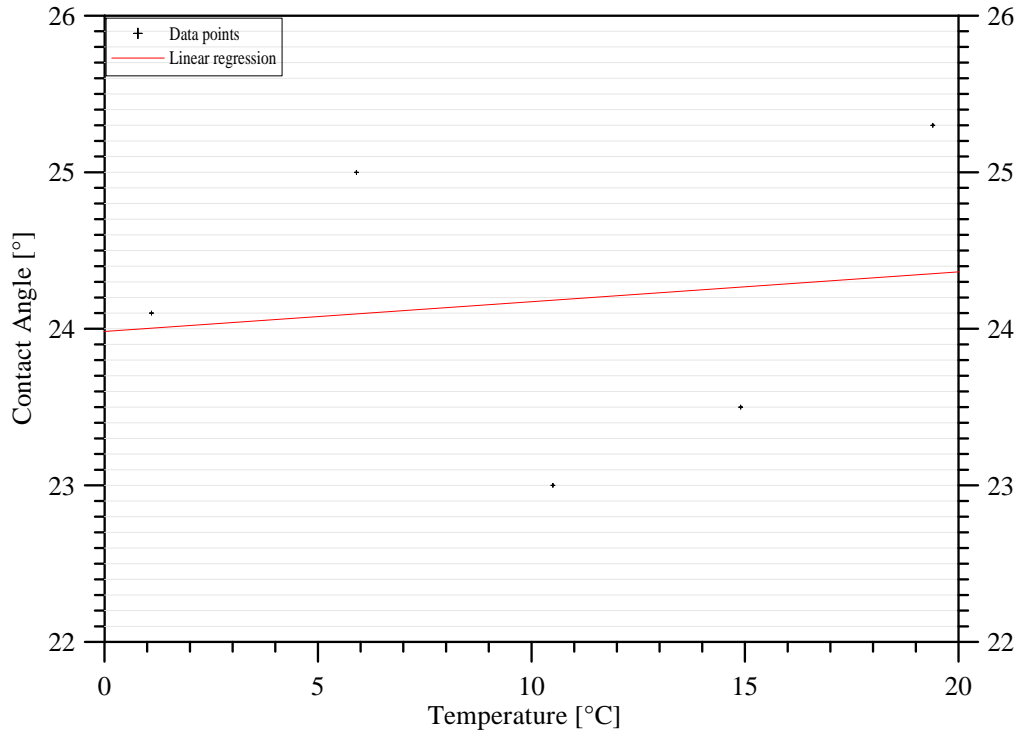


Figure 55: Results for Cycle 4 with P1

Linear Regression fitted through the measured values(5):

$$\theta_a^{1-prop./P1}(T(^{\circ}C)) = 0.02 \times T(^{\circ}C) + 23.98 \quad (\text{A.4})$$

Coef of determination, R-squared = 0.02

– Comparison of  $\frac{\partial\theta}{\partial T}$  and  $\theta(0)$  data between the 4 cycles of P1

	$\frac{\partial\theta}{\partial T}$	$\theta(0)$
1.	0.02	24.31
2.	0.005	24.91
3.	0.13	23.57
4.	0.02	23.98
<b>Average</b>	0.04	24.19
<i>Standard deviation</i>	0.06 $\hat{=}$ 136%	0.57 $\hat{=}$ 2%

- Contact angle data P2

$T[^\circ C]$	Cycle 1		Cycle 2		Cycle 3		Cycle 4	
	$\theta_a$	$\theta_r$	$\theta_a$	$\theta_r$	$\theta_a$	$\theta_r$	$\theta_a$	$\theta_r$
24.7	26.1	-	-	-	-	-	-	-
19.9	25.5	-	-	-	-	-	-	-
19.4	21.2 $24 \pm 2(8.5\%)$	-	25.8	-	23.8	-	25.2	-
17.2	25.3	-	-	-	-	-	-	-
16.1	24	-	-	-	-	-	-	-
14.9	23.6 $23 \pm 3(11.1\%)$	-	24.4	-	24.7	-	19.2	-
12.4	24.4	-	-	-	-	-	-	-
11.8	22.9	-	-	-	-	-	-	-
10.5	3.6 $24.2 \pm 0.5(1.0\%)$	-	24.4	-	24.7	-	23.9	-
7.7	20.4	-	-	-	-	-	-	-
7.1	24.5 $23 \pm 2(7.0\%)$	-	22.2	-	-	-	-	-
5.9	24.7 $24.7 \pm 0.9(3.6\%)$	-	24.2	-	24	-	26	-
4.6	21.7	-	-	-	-	-	-	-
3.8	25.3	-	-	-	-	-	-	-
2.7	23.6	-	-	-	-	-	-	-
1.1	22.1 $24 \pm 1(4.5\%)$	-	23.3	-	24.1	-	24.5	-
-1.8	22.8	-	-	-	-	-	-	-
-4.7	23.9	-	-	-	-	-	-	-
-6.2	19.3	-	-	-	-	-	-	-

- Temperature dependence of the contact angle for 1-propanol on P2

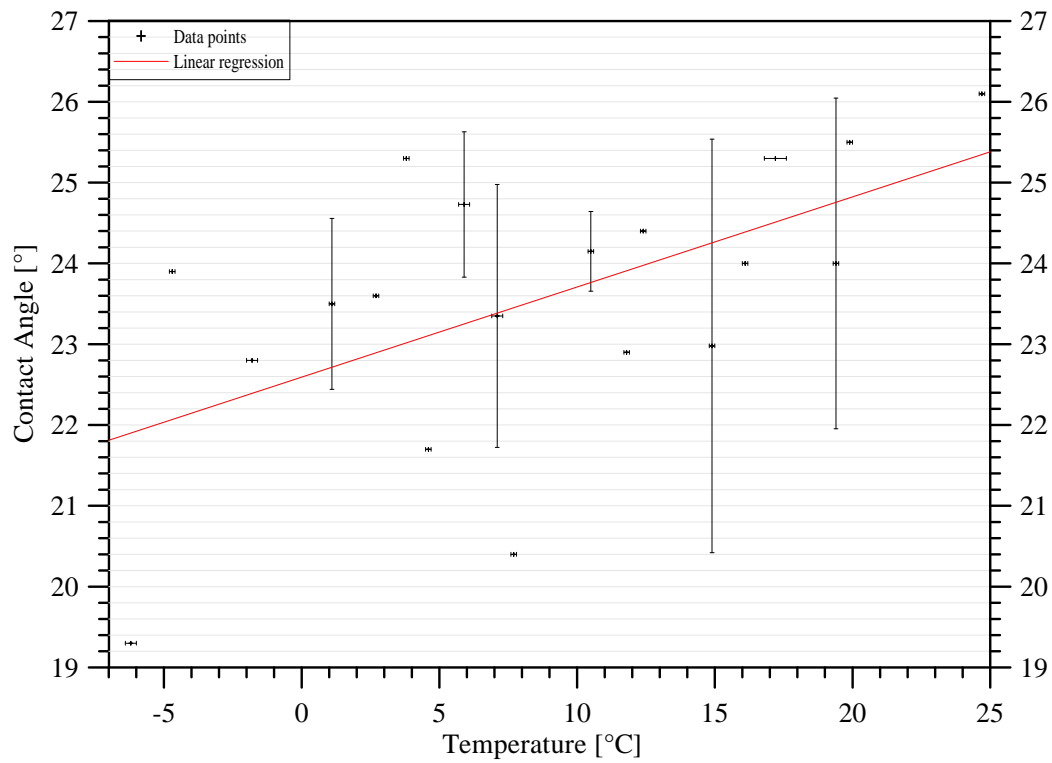


Figure 56: Mean of P2 data

- Linear Regression P2

$$\theta_a^{1-prop./P2}(T(^{\circ}C)) = 0.11 \times T(^{\circ}C) + 22.59 \quad R^2 = 0.32$$



– Data plot P2 - Cycle 1

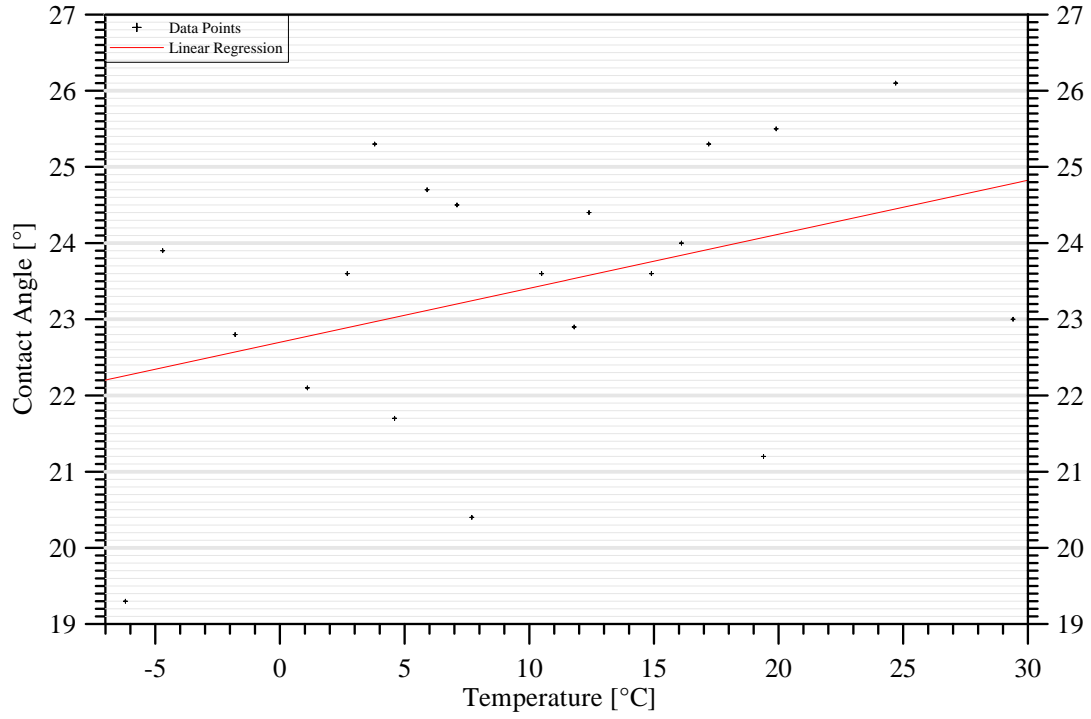


Figure 57: Results for Cycle 1 with P2

Linear Regression fitted through the measured values(20):

$$\theta_a^{1-prop./P2}(T(^{\circ}C)) = 0.07 \times T(^{\circ}C) + 22.70 \quad (\text{A.5})$$

Coef of determination, R-squared = 0.15

– Data plot P2 - Cycle 2

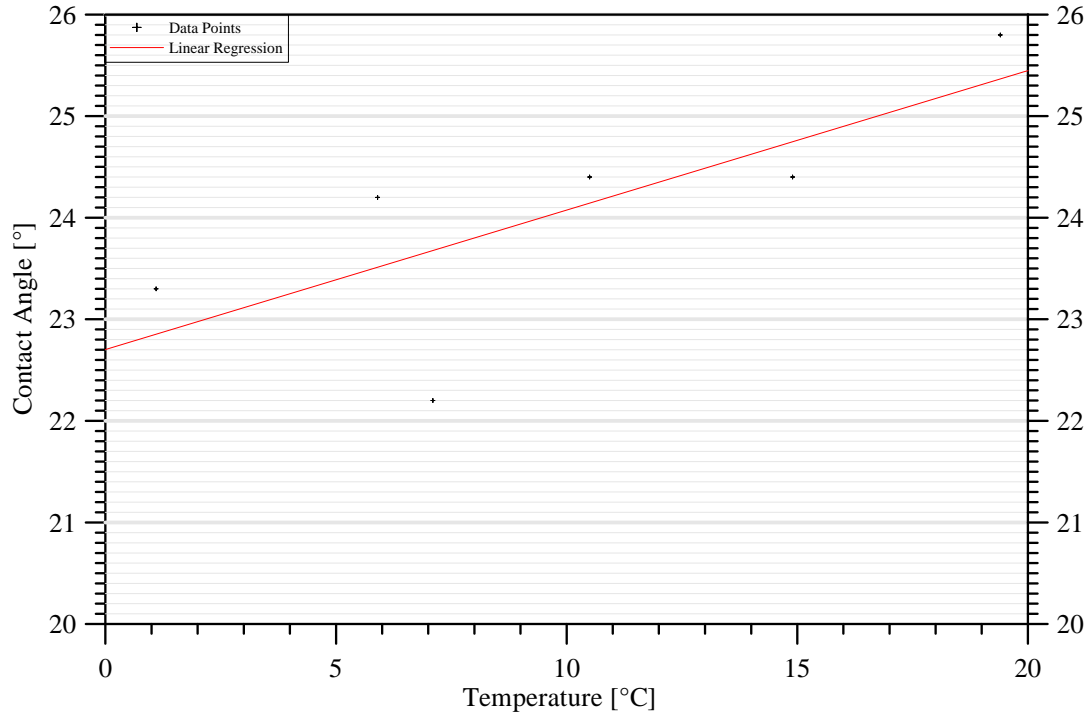


Figure 58: Results for Cycle 2 with P2

Linear Regression fitted through the measured values(6):

$$\theta_a^{1-prop./P2}(T(^{\circ}C)) = 0.14 \times T(^{\circ}C) + 22.70 \quad (\text{A.6})$$

Coef of determination, R-squared = 0.56

– Data plot P2 - Cycle 3

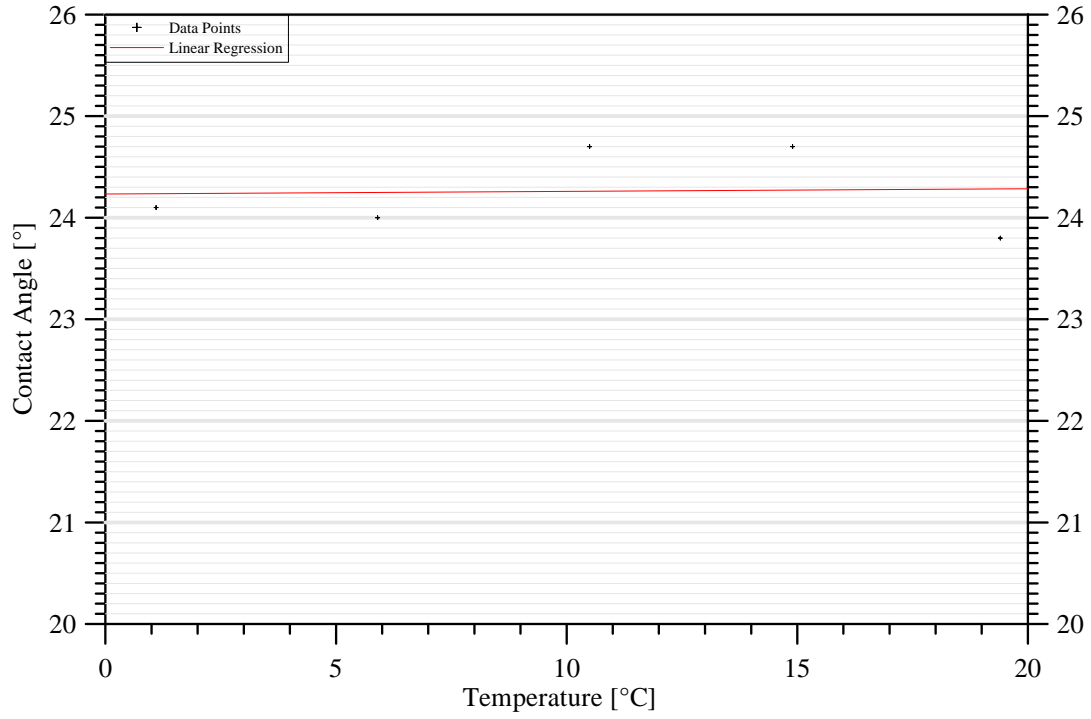


Figure 59: Results for Cycle 3 with P2

Linear Regression fitted through the measured values(6):

$$\theta_a^{1-prop./P2}(T(^{\circ}C)) = 0.003 \times T(^{\circ}C) + 24.23 \quad (\text{A.7})$$

Coef of determination, R-squared = 0.002

– Data plot P2 - Cycle 4

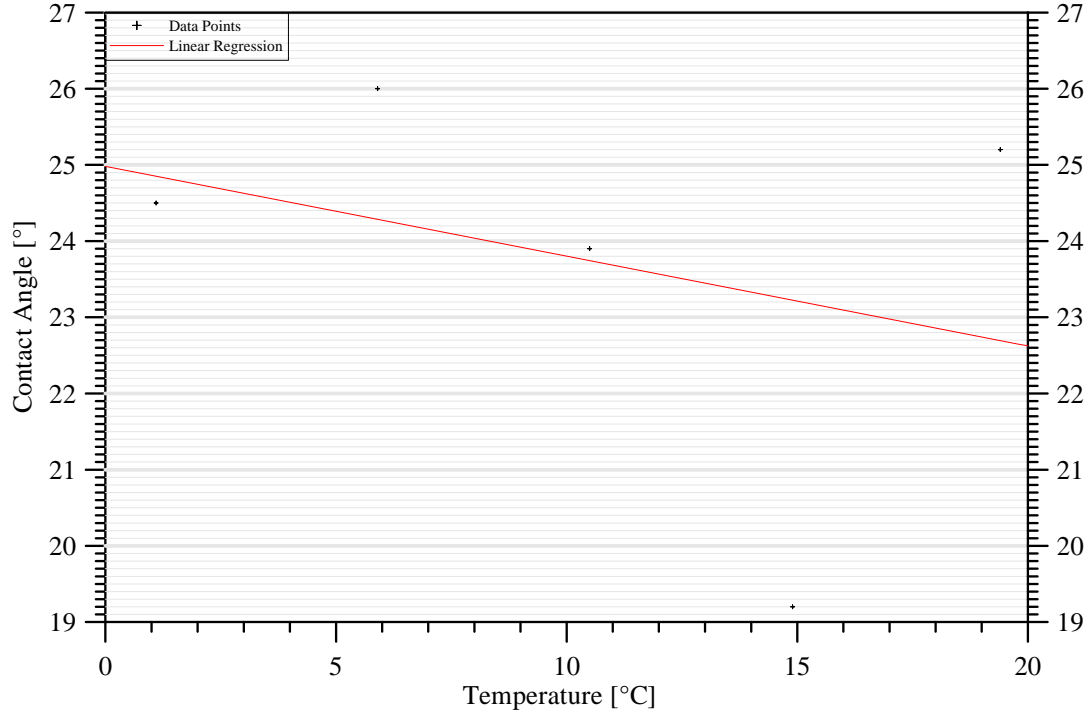


Figure 60: Results of Cycle 4 with P2

Linear Regression fitted through the measured values(6):

$$\theta_a^{1-prop./P2}(T(^{\circ}C)) = -0.12 \times T(^{\circ}C) + 24.98 \quad (\text{A.8})$$

Coef of determination, R-squared = 0.10

– Comparison of  $\frac{\partial\theta}{\partial T}$  and  $\theta(0)$  data between the 4 cycles of P2

	$\frac{\partial\theta}{\partial T}$	$\theta(0)$
1.	0.07	22.70
2.	0.14	22.70
3.	0.003	24.23
4.	-0.12	24.98
<b>Average</b>	0.023	23.65
<i>Standard deviation</i>	0.1 $\hat{=}$ 469%	1.14 $\hat{=}$ 5%

- Averaging P1 and P2 data

$T[^\circ\text{C}]$	$\bar{\theta}_a$	$\delta_{\bar{\theta}_a}$	$\frac{\delta_{\bar{\theta}_a}}{\bar{\theta}_a}$
24.7	25.2	0.7	2.7%
19.9	25.2	0.2	1.0%
19.4	24.8	0.5	2.1%
17.2	25.3	0	0
16.1	23.3	0.5	2.3%
14.9	23.7	0.5	2.0%
12.4	24.8	0.2	1.0%
11.8	25	1	4.6%
10.5	24.3	0.1	0.4%
7.7	22	1	5.7%
7.1	23.8	0.3	1.3%
5.9	25.0	0.2	0.7%
4.6	23.0	0.9	3.9%
3.8	24.9	0.3	1.3%
2.7	23.8	0.1	0.4%
1.1	23.55	0.04	0.2%
-1.8	24.0	0.8	3.5%
-4.7	24.2	0.2	0.7%
-6.2	22	2	8.3%

- Linear Regression P1/P2

$$\theta_a^{1-prop./1 \times PVD}(T(^{\circ}\text{C})) = 0.06 \times T(^{\circ}\text{C}) + 23.51$$

$$R^2 = 0.29$$

## A.4 Two-times coated sterling silver - 2xPVD

- Wetted lengths

Plate Marking	$l$ [mm]	$b^*$ [mm]	$d^*$ [mm]	$l^*$ [mm]
P3	53.038	25.70	0.50	52.4
	52.769	25.90	0.50	52.8
	52.442	25.85	0.50	52.7
<b>Mean</b>	$52.7 \pm 0.3$	$25.82 \pm 0.05$	$0.50 \pm 0.05$	$52.6 \pm 0.1$

- Contact angle data

$T[^\circ C]$	Cycle 1		Cycle 2		Cycle 3		Cycle 4	
	$\theta_a$	$\theta_r$	$\theta_a$	$\theta_r$	$\theta_a$	$\theta_r$	$\theta_a$	$\theta_r$
24.7	18	-	-	-	-	-	-	-
19.9	17.2	-	-	-	-	-	-	-
19.4	17.6 $17.7 \pm 0.4(2.4\%)$	-	17.2	-	17.8	-	18.2	-
17.2	17.1	-	-	-	-	-	-	-
16.1	15.5	-	-	-	-	-	-	-
14.9	15.7 $15 \pm 1(7.0\%)$	-	14	-	15.2	-	16.6	-
12.4	15	-	-	-	-	-	-	-
11.8	16.9	-	-	-	-	-	-	-
10.5	18.3 $17.2 \pm 0.8(4.9\%)$	-	16.5	-	17.5	-	16.6	-
7.7	13.8	-	-	-	-	-	-	-
7.1	17.6	-	-	-	-	-	-	-
5.9	18.2 $17 \pm 1(6.0\%)$	-	16.3	-	16.7	-	15.9	-
4.6	17.9	-	-	-	-	-	-	-
3.8	18.5	-	-	-	-	-	-	-
2.7	13.7	-	-	-	-	-	-	-
1.1	15.9 $17 \pm 1(6.3\%)$	-	17.2	-	16.8	-	18.5	-
-1.8	14.3	-	-	-	-	-	-	-
-6.2	18.1	-	-	-	-	-	-	-

- Linear Regression P3

$$\theta_a^{1-prop./2 \times PVD}(T(^{\circ}C)) = 0.02 \times T(^{\circ}C) + 16.31$$

$$R^2 = 0.02$$

– Data plot P3 - Cycle 1

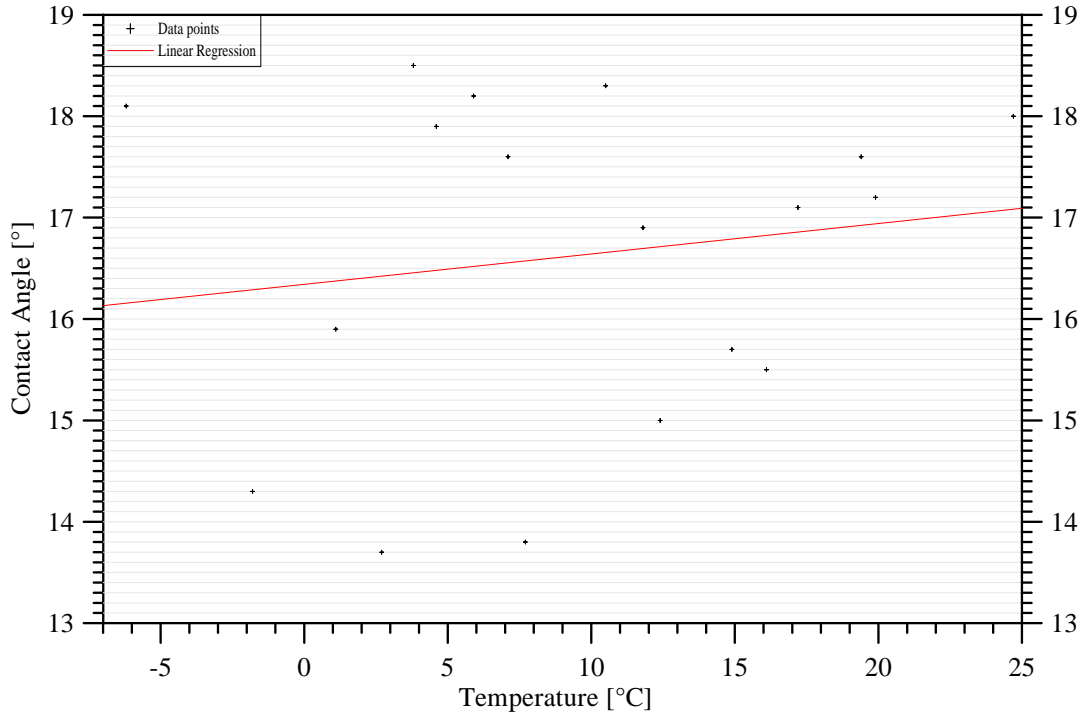


Figure 61: Results for Cycle 1 with P3

Linear Regression fitted through the measured values(18):

$$\theta_a^{1-prop./P3}(T(^{\circ}C)) = 0.03 \times T(^{\circ}C) + 16.34 \quad (\text{A.9})$$

Coef of determination, R-squared = 0.02

– Data plot P3 - Cycle 2

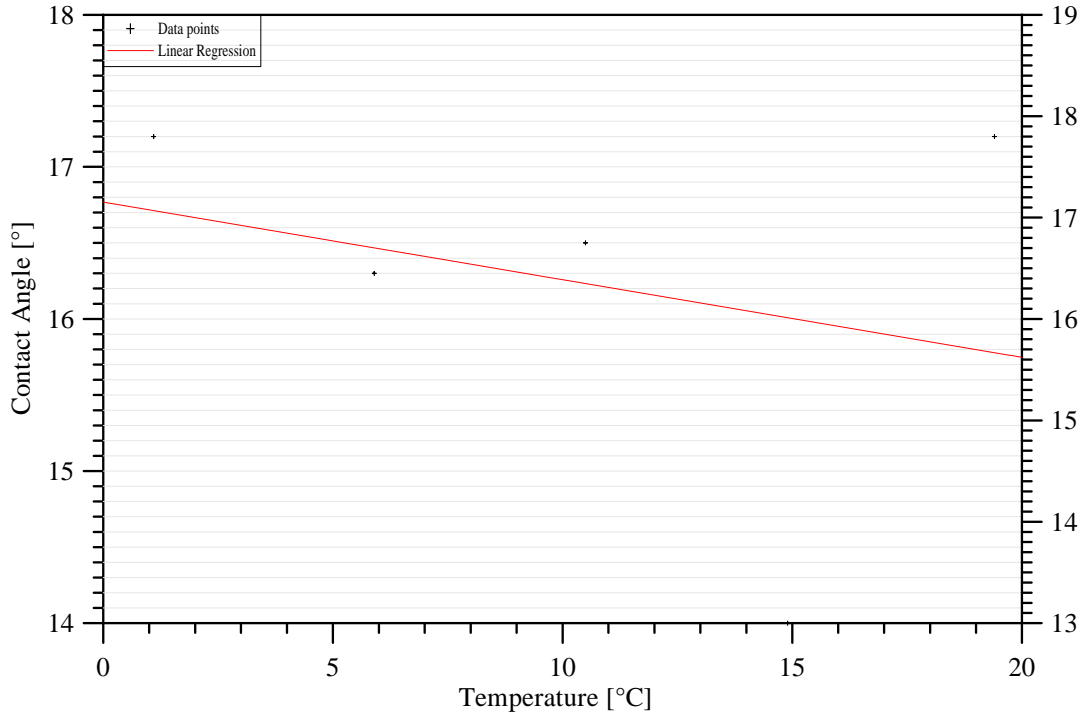


Figure 62: Results for Cycle 2 with P3

Linear Regression fitted through the measured values(5):

$$\theta_a^{1-prop./P3}(T(^{\circ}C)) = -0.05 \times T(^{\circ}C) + 16.77 \quad (\text{A.10})$$

Coef of determination, R-squared = 0.08



– Data plot P3 - Cycle 3

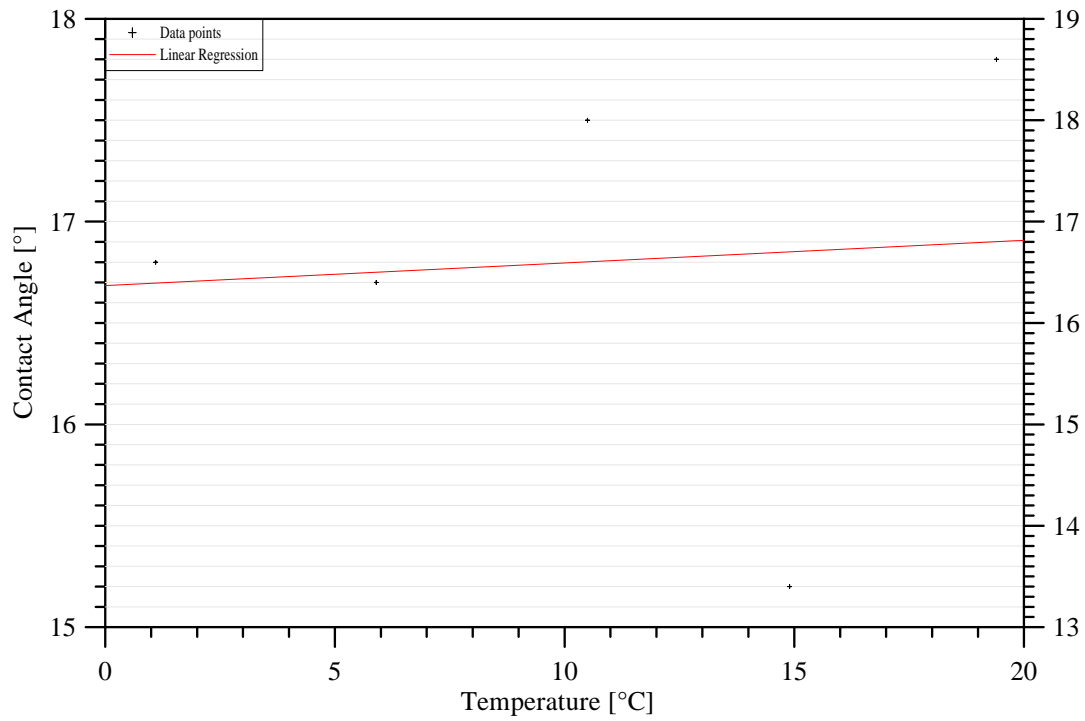


Figure 63: Results for Cycle 3 with P3

Linear Regression fitted through the measured values(5):

$$\theta_a^{1-prop./P3}(T(^{\circ}C)) = 0.01 \times T(^{\circ}C) + 16.68 \quad (\text{A.11})$$

Coef of determination, R-squared = 0.006

– Data plot P3 - Cycle 4

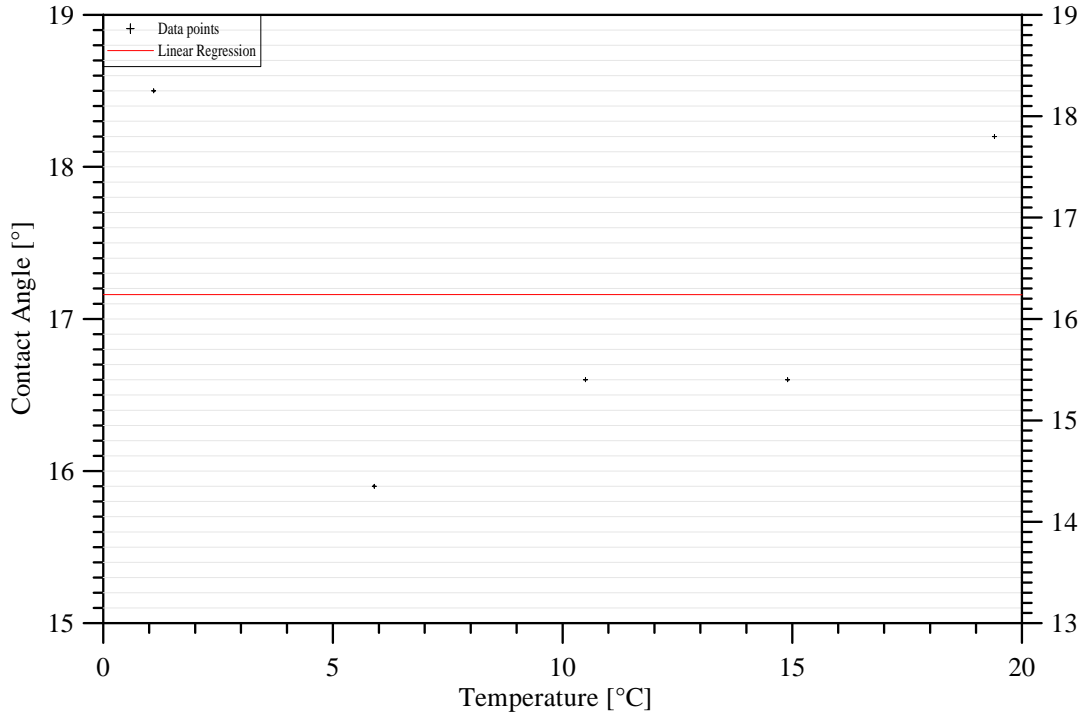


Figure 64: Results for Cycle 4 with P3

Linear Regression fitted through the measured values(5):

$$\theta_a^{1-prop./P3}(T(^{\circ}C)) = -3.85 \cdot 10^{-5} \times T(^{\circ}C) + 17.16 \quad (\text{A.12})$$

Coef of determination, R-squared =  $6 \cdot 10^{-8}$

– Comparison of  $\frac{\partial \theta}{\partial T}$  and  $\theta(0)$  data between the 4 cycles of P3

	$\frac{\partial \theta}{\partial T}$	$\theta(0)$
1.	0.03	16.34
2.	-0.05	16.77
3.	0.01	16.68
4.	$-3.85 \cdot 10^{-5}$	17.16
<b>Average</b>	-0.002	16.74
<i>Standard deviation</i>	0.03 $\hat{=}$ 1399%	0.34 $\hat{=}$ 2%

## B Data for NaCl/1-propanol contact angle measurements

### B.1 Surface tension during measurements

$T$	$[^{\circ}C]$	$\sigma$	$[\frac{mN}{m}]$	$\delta_{\sigma}$	$[\frac{mN}{m}]$	$T$	$\sigma$	$\delta_{\sigma}$
34.1		22.3		0.4		11.5	24.79	0.09
30.3		22.9		0.1		11.4	24.9	0.1
29.4		23				11.3	24.86	
25.3		23.40		0.06		10.6	24.64	
24.4		23.54		0.05		9.5	24.76	
23.9		23.46				8.5	25.14	0.07
20.8		23.84		0.08		7.4	25.16	0.06
20.6		23.9		0.1		7	25.24	0.06
20.3		23.8		0.3		5	25.51	0.01
20		23.73				1.8	25.87	
16.2		24.2		0.2		1.6	25.9	0.2
16.1		24.49				-3	26.44	0.09
15.7		24.35						

- Linear Regression 1

$$\sigma_{1-Propanol}(T) = 48.21 - (T(K) - 4.8) \cdot 0.08394$$

$$R^2 = 0.95$$

- Linear Regression 2

$$\sigma_{1-Propanol}(T) = -0.0777 \times (T(^{\circ}C) - 4.3) + 25.26$$

$$R^2 = 0.92$$

## B.2 Dynamic Wilhelmy method

### B.2.1 Coated glass plates

- Glass plate - 0xPVD
  - Wetted lengths

Plate Number	$b^*$ [mm]	$d^*$ [mm]	$l^*$ [mm]
G	20.40	2.00	44.8
	20.40	2.00	44.8
	20.40	2.00	44.8
Mean	$20.40 \pm 0.05$	$2.00 \pm 0.05$	$44.8 \pm 0.2$

- Contact angle data

$T[^\circ C]$	$\theta_a$	$\cos\theta_a$	$\theta_r$
34.1	0	1.23	60.1
30.4	0	1.15	61.7
25.3	0	1.24	53.8
25.2	0		57
24.5	0	1.14	47.7
24.2	0	1.27	45.7
20.9	0	1.26	46.4
20.6	0	1.2	59
20.5	0	1.25	68.9
16.2	0	1.13	47.7
16.1	0	1.04	58.4
15.7	0	1.33	45.2
11.7	0	1.41	58.4
11.3	0	1.38	31.95
10.6	0	1.16	41.85
9.5	0	1.2	42.1
7.8	0	1.15	54.1
7.4	0	1.24	42.6
7.1	0	1.29	44.4
6.9	0	1.15	60.3
5.3	0	1.13	45.7
2.1	0	1.18	43.5
1.3	0	1.14	49.6
-7	0	1.34	0

- Linear Regression through  $\cos\theta_a$  values:

$$\cos\theta_a = -0.001 \times T(^{\circ}C) + 1.24 \quad (\text{B.1})$$

Coef of determination, R-squared = 0.02

- Linear Regression through  $\theta_r$  values:

$$\theta_r^{1-prop./glass}(T(^{\circ}C)) = 0.81 \times T(^{\circ}C) + 36.88$$

$$R^2 = 0.37$$

- 1xPVD

– Wetted lengths

Plate Number	$b^*$ [mm]	$d^*$ [mm]	$l^*$ [mm]
S1	20.00	2.00	44.0
	20.05	2.00	44.1
	20.00	2.00	44.0
Mean	$20.02 \pm 0.05$	$2.00 \pm 0.05$	$44.0 \pm 0.2$
S2	20.8	2.00	45.6
	20.65	2.00	45.3
	20.65	2.00	45.3
Mean	$20.70 \pm 0.05$	$2.00 \pm 0.05$	$45.4 \pm 0.2$

– Contact angle data

$T[^\circ C]$	$\theta_a$	$\cos\theta_a$	$\theta_r$
34.1	0	1.25	63.6
	0	1.21	63.4
	0	1.3	60.3
	0	$1.25 \pm 0.04$	$62.43 \pm 1.85$
30.3	0	1.29	62.9
	0	1.14	61.8
	0	1.21	63.2
	0	$1.21 \pm 0.08$	$62.63 \pm 0.7371$
25.3	0	1.31	57.5
	0	1.14	60.2
	0	1.18	61.2
	0	$1.21 \pm 0.9$	$59.63 \pm 1.914$
25.1	0	1.09	59.9
	0	1.14	58.4
	0	1.17	63.4
	0	$1.13 \pm 0.04$	$60.57 \pm 2.566$
24.5	0	1.32	44.6
24	0	1.2	43.9
	0	1.14	46.0
	0	1.16	33.9
	0	$1.17 \pm 0.4$	$41.27 \pm 6.466$

Continued on the next page ...

$T[^\circ\text{C}]$	$\theta_a$	$\cos\theta_a$	$\theta_r$
20.9	0	1.12	49.4
20.6	0	1.31	36.8
20.5	0	1.25	61.7
	0	1.24	57.3
	0	1.15	62.7
	0	$1.24 \pm 0.07$	$62.97 \pm 5.805$
16.2	0	1.2	45.4
16.1	0	1.32	45.1
	0	1.08	48.2
	0	1.13	48.5
	0	$1.2 \pm 0.1$	$47.27 \pm 1.882$
15.9	0	1.21	55.7
	0	1.21	62.8
	0	1.21	61.1
	0	$1.21 \pm 0$	$59.87 \pm 3.707$
11.7	0	1.21	58.6
	0	1.18	57.8
	0	1.18	57.1
	0	$1.21 \pm 0.3$	$57.83 \pm 0.7506$
11.6	0	1.25	47.2
11.4	0	1.24	60.5
	0	1.18	57.4
	0	$1.24 \pm 0.07$	$58.95 \pm 2.192$
10.6	1.31	0	31
9.3	0	1.26	41.8
	0	1.2	39
	0	1.18	48.1
	0	$1.23 \pm 0.4$	$42.97 \pm 4.661$
8.7	0	1.25	34.2
7.5	0	1.21	59.1
	0	1.1	60.3
	0	$1.15 \pm 0.06$	$59.7 \pm 0.8485$
7.4	0	1.14	44.2
7.1	0	1.19	31
5.2	0	1.09	48.8
2	0	1.16	42.9
1.6	0	1.28	43.3
-0.9	0		42.1
	0		38.2
	0		23.0
	0		$34.43 \pm 10.09$
-7	0	1.31	36.5

- Linear Regression through  $\cos\theta_a$  values:

$$\cos\theta_a = -0.0004 \times T(^{\circ}C) + 1.21 \quad (\text{B.2})$$

Coef of determination, R-squared = 0.004

- Linear Regression through  $\theta_r$  values:

$$\begin{aligned} \theta_r^{1-prop./2 \times PVD}(T(^{\circ}C)) &= 0.58 \times T(^{\circ}C) + 39.86 \\ R^2 &= 0.3 \end{aligned}$$

- 2xPVD

– Wetted lengths

Plate Number	$b^*$ [mm]	$d^*$ [mm]	$l^*$ [mm]
S3	20.40	2.00	44.8
	20.40	2.00	44.8
	20.30	2.00	44.6
Mean	$20.37 \pm 0.05$	$2.00 \pm 0.05$	$44.7 \pm 0.2$
S4	20.00	2.00	44.0
	20.00	2.00	44.0
	19.95	2.00	43.9
Mean	$19.98 \pm 0.05$	$2.00 \pm 0.05$	$44.0 \pm 0.2$

– Contact angle data

$T[^\circ C]$	$\theta_a$	$\cos\theta_a$	$\theta_r$
24.5	0	1.28	43.2
20.9	0	1.22	34.6
20.5	0	1.3	27.4
16.2	0	1.21	36.9
11.5	0	1.15	41.8
10.7	0	1.35	20
8.7	0	1.25	34.5
7.5	0	1.37	40.7
7.2	0	1.35	28.3
5.3	0	1.19	45.2
2	0	1.25	41.7
1.8	0	1.28	36.9
-0.8	0	1.32	
-2	0	1.24	
-7	0	1.28	0

- Linear Regression through  $\cos\theta_a$  values:

$$\cos\theta_a = -0.002 \times T(^{\circ}C) + 1.27 \quad (\text{B.3})$$

Coef of determination, R-squared = 0.08

- Linear Regression through  $\theta_r$  values:

$$\theta_r^{1-prop./2 \times PVD}(T(^{\circ}C)) = 0.56 \times T(^{\circ}C) + 27.54$$

$$R^2 = 0.16$$



- 3xPVD

– Wetted length

Plate Number	$b^*$ [mm]	$d^*$ [mm]	$l^*$ [mm]
S5	20.40	2.00	44.8
	20.30	2.00	44.6
	20.25	2.00	44.5
Mean	$20.32 \pm 0.05$	$2.00 \pm 0.05$	$44.6 \pm 0.2$

– Contact angle data

$T[^\circ C]$	$\theta_a$	$\cos\theta_a$	$\theta_r$
24.5	0	1.31	23.3
20.9	0	1.39	34.6
20.6	0	1.36	15.1
16	0	1.2	36.9
11.7	0	1.3	36.7
10.7	0		20
7.4	0	1.24	26.6
7.3	0	1.19	25.4
7.2	0	1.31	14.5
5	0	1.37	28.4
2.1	0	1.23	36.9
1.5	0	1.38	0
-7	0	1.23	0

- Linear Regression through  $\cos\theta_a$  values:

$$\cos\theta_a = 0.002T(^{\circ}C) + 1.27 \quad (\text{B.4})$$

Coef of determination, R-squared = 0.10

- Linear Regression through  $\theta_r$  values:

$$\theta_r^{1-prop./2 \times PVD}(T(^{\circ}C)) = 0.64 \times T(^{\circ}C) + 16.65$$

$$R^2 = 0.20$$

**B.2.2 Polished salt plates**

- Wetted lengths

Plate marking	$b^*$ [mm]	$d^*$ [mm]	$l^*$ [mm]
N1	15.4	2.9	36.6
	15.5	2.9	36.8
	15.5	2.9	36.8
	15.5	2.9	36.8
Mean	$15.48 \pm 0.05$	$2.9 \pm 0.05$	$36.8 \pm 0.2$
N2	14.05	1.6	31.3
	14.1	1.6	31.4
	14.0	1.6	31.2
	14.0	1.6	31.2
Mean	$14.04 \pm 0.05$	$1.6 \pm 0.05$	$31.3 \pm 0.2$
N3	11.25	2.4	27.3
	11.35	2.4	27.5
	11.40	2.4	27.6
	11.40	2.4	27.6
Mean	$11.35 \pm 0.05$	$2.4 \pm 0.05$	$27.5 \pm 0.2$
N4	7.90	2.55	20.9
	7.70	2.55	20.5
	7.75	2.55	20.6
	7.90	2.55	20.9
Mean	$7.81 \pm 0.05$	$2.55 \pm 0.05$	$20.7 \pm 0.2$
N5	9.50	3.75	26.5
	9.55	3.70	26.5
	9.60	3.55	26.3
	9.50	3.90	26.8
Mean	$9.54 \pm 0.05$	$3.71 \pm 0.05$	$26.5 \pm 0.2$
N6	13.85	1.70	31.1
	13.90	1.70	31.2
	13.90	1.70	31.2
	14.10	1.70	31.6
Mean	$13.94 \pm 0.05$	$1.70 \pm 0.05$	$31.3 \pm 0.2$

• Contact Angle data

$T[^\circ C]$	$\theta_a$	$\cos\theta_a$	$\theta_r$
29.4	0	1.2	34.5
24.5	0	1.12	35.1
	0	1.14	52.5
	0	1.39	45.3
	0	$1.2 \pm 0.2$	$44.2 \pm 8.603$
20.9	0	1.14	24.8
	0	1.28	33.0
	0	$1.21 \pm 0.9$	$28.9 \pm 5.798$
20.6	0	1.35	32
	0	1.04	53.5
	0	$1.2 \pm 0.2$	$42.75 \pm 15.2$
17.2	0	1.17	31.1
16.1	0	1.13	19.1
	0	1.28	47.7
	0	$1.22 \pm 0.08$	$33.4 \pm 20.22$
12.4	0	1.24	25.8
10.6	0	1.45	27.3
7.1	0	1.2	33.3
	0	1.33	22.6
	0	1.21	11.1
	0	1.06	14.5
	0	1.14	35.2
	0	1.23	30.3
	0	1.20	42.5
	0	$1.2 \pm 0.1$	$27.0 \pm 11.45$
5.2	0	1.17	35.7
	0	1.13	22.3
	0	1.15	38.4
	0	$1.15 \pm 0.03$	$32.13 \pm 8.622$
2.1	0	1.63	27.0
	0	1.14	26.1
	0	1.21	40.4
	0	$1.3 \pm 0.3$	$31.17 \pm 8.009$
1.6	0	1.08	37.1
	0	1.08	27.4
	0	1.08	38.8
	0	$1.08 \pm 0$	$34.43 \pm 6.15$
-7.1	0	1.1	36.2
	0	1.01	0
	0	$1.06 \pm 0.06$	$18.1 \pm 25.6$

- Linear Regression through  $\cos\theta_a$  values

$$\cos\theta_a = 0.0002 \times T(^{\circ}C) + 1.20 \quad (\text{B.5})$$

Coef of determination, R-squared = 0.0005

- Linear Regression through  $\theta_r$  values

$$\begin{aligned} \theta_a^{1-prop./N_{1-6}}(T(^{\circ}C)) &= 0.42 \times T(^{\circ}C) + 26.47 \\ R^2 &= 0.4 \end{aligned}$$

**B.2.3 Naturally split salt plates**

- Wetted length

Plate	$b^*$ [mm]	$d^*$ [mm]	$l^*$ [mm]
N	8.1	0.8	17.8
	8.1	0.75	17.7
	8.1	0.8	17.8
Mean	$8.1 \pm 0.05$	$0.78 \pm 0.05$	$17.8 \pm 0.2$

- Contact angle data

$T[^\circ C]$	$\theta_a$	$\cos\theta_a$	$\theta_r$	$\cos\theta_r$
29.4	0	1.05	0	1.11
24.5	0	1.01	0	1.2
20.9	0	1	0	1.1
16.1	0	1.1	0	1.11
7.3	0	1.02	0	1.1
7.1	0	1.07	0	1.01
5.2	0	1	0	1.01
2.1	0	1.23	0	1.17
1.6	0	1.03	0	1.06
-7.1	0	1.01	0	1.1

Linear Regression through  $\cos\theta_a$  values:

$$\cos\theta_a = -0.0010 \times T(^{\circ}C) + 1.06 \quad (\text{B.6})$$

Coef of determination, R-squared = 0.02

Linear Regression through  $\cos\theta_r$  values:

$$\cos\theta_r = 0.002 \times T(^{\circ}C) + 1.08 \quad (\text{B.7})$$

Coef of determination, R-squared= 0.1

### B.3 Washburn method

- Surface tension during measurements

Preliminary to each measurement the surface tension of the probational liquid was checked. Consequently the stated values are averages of 13 (for n-hexane) resp 3(for 1-propanol) measurements.

Probational liquid	$T[^\circ C]$			$\sigma_L[\frac{mN}{m}]$		
<b>N-Hexane</b>	20.3	$\pm$	0.4	18.58	$\pm$	0.05
<b>1-Propanol</b>	20.4	$\pm$	0.3	23.8	$\pm$	0.2

- $\bar{c}, \frac{\Delta \bar{m}^2}{t}$  and  $\cos \bar{\theta}_a$  values for n-hexane

$\bar{c}$	$[cm^{-5}]$	$3.88495 \cdot 10^{-6}$
$\delta_{\bar{c}}$	$[cm^{-5}]$	$9.35007 \cdot 10^{-7}$
$\frac{\Delta \bar{m}^2}{t}$	$[\frac{g^2}{s}]$	$1.06176 \cdot 10^{-4}$
$\delta_{\frac{\Delta \bar{m}^2}{t}}$	$[\frac{g^2}{s}]$	$2.24879 \cdot 10^{-5}$
$\cos \bar{\theta}_a$		1.1
$\delta_{\cos \bar{\theta}_a}$		0.2

- $\cos \bar{\theta}_a$  and  $\frac{\Delta \bar{m}^2}{t}$  values for 1-propanol

$\cos \bar{\theta}_a$		480
$\delta_{\cos \bar{\theta}_a}$		70
$\frac{\Delta \bar{m}^2}{t}$	$[\frac{g^2}{s}]$	$1.33803 \cdot 10^{-2}$
$\delta_{\frac{\Delta \bar{m}^2}{t}}$	$[\frac{g^2}{s}]$	$4.61176 \cdot 10^{-3}$

## LEBENS LAUF

### PERSÖNLICHE DATEN

*Geburtsdatum*      25. Februar 1986  
*Geburtsort*        Wien  
*Adresse*            Simmeringer Hauptstraße 68/1/17  
                         1110 Wien

### AUSBILDUNG

*1992 – 1996*        Volksschule Sacré – Coeur in Wien  
*1996 – 2004*        Gymnasium Sacré – Coeur in Wien  
*September-  
Februar 2004*      Teilnahme an einem Rhetorik- und  
                         Projektmanagementseminar  
*Oktober 2004*      Beginn des Diplomstudiums Physik an der Universität Wien  
*Jänner 2007*        Seminarvortrag zum Thema „*Cloud Microphysics and  
Climate*“  
*Februar 2008*        Mitarbeit bei Untersuchungen zur „*Partikelemission von  
Laserdruckern*“ unter der Leitung von Prof. Georg Reischl  
*März 2008*          Beginn des Lehramtsstudiums Physik und Mathematik an der  
                         Universität Wien  
*September 2008*    Teilnahme am Tensiometrie- und  
                         Kontaktwinkelmessungsseminar der Firma Krüss  
*Oktober 2008*      Seminarvortrag zum Thema „*Tenisometrie und  
Kontaktwinkelmessung*“